

# **Design and Manufacture of a Universal Mechanical Human Joint Simulator**

**A thesis submitted for the degree of  
Doctor of Philosophy**

by  
**Nawaf Alhaifi**

**School of Engineering and Design  
Brunel University  
London  
June 2011**

---

## **Abstract**

The work performed in this thesis involves the study of human hip joint kinematics and load analysis. Such analyses are very useful for investigating mobility and natural functionality as well as the variation in motion due to replacement implants. The objective of this study is to design, build and testing of a universal human joint simulator that is configurable to hold several human joints and easily programmable to create the required motion. This was performed by creating a Stewart Platform, which is capable of moving in all six degrees of freedom; the maximum number needed by any human joint.

Many specific human joint simulators are available on the market for simulating all major human limbs. These are used for wear testing replacement joints by using high load repetitive motion. These systems have a predetermined limit degree of movement and are very expensive; if one wanted to emulate another joint, one would have to purchase a whole new system.

This novel system comprises of a three-phase power supply, Control Area Network with six actuators and drivers, a force reading clamp with strain gauges and data logger. A user friendly computer program was developed that is able to derive joint movement data from two inputs and replicating the movement by driving the platform, as well as recording force and displacement data from the joint. The product would be marketed towards biomechanical researchers and implant designers.

Verification of this system was performed by simulating the human hip joint. A known combination of kinematic and force data were inputted into the system for nine different types of activities. The resultant force and joint centre displacement was then compared to see how well the system perform in comparison to the inputted data from a previous study.

The outcome of this project is a fully functional machine and configurable program that can create movement data at varying speeds and body weights; which is also able to drive the human joint simulator. The design also costs a fraction of any industrial joint simulator.

It is hoped that the simulator will allow easier study of both the kinematics and load analysis within the human joints, with the intent on aiding investigation into mobility and functionality; as well as variation in motion caused by a replacement implant.

---

## **Copyright**

Copyright © 2011 Nawaf Alhaifi. All rights reserved.

The copyright of this thesis rests with the Author. Copies (by any means) either in full, or of extracts, may not be made without prior written consent from the Author.

---

**To my Father and Mother**



---

## Table of Contents

Chapter 1. Introduction .....	1
1.1 Overview .....	1
1.2 Motivation .....	4
1.3 Objectives.....	4
1.4 Product design specifications .....	5
1.5 Significance of the study.....	5
1.6 Thesis outline .....	7
Chapter 2. Literature Review .....	10
2.1 Human Musculoskeletal System .....	10
2.1.1 Body Frame, Bones .....	10
2.1.2 Muscles, Ligaments and Tendons .....	12
2.1.3 Joints .....	13
2.1.4 Joint Replacement .....	15
2.1.5 Musculoskeletal Structure of the Hip Joint.....	17
2.1.5.1 Hip Joint, Muscle, Ligaments and Tendons .....	17
2.1.5.2 Prosthesis Hip Replacement .....	18
2.2 Joint Biomechanical Analysis .....	20
2.2.1 Hip Joint: Kinematics .....	22
2.2.2 Hip Joint: Kinetics.....	29
2.2.3 Theoretical Studies .....	31

---

2.2.4	Experimental and Clinical Studies .....	38
2.3	Joint simulators.....	40
Chapter 3.	Theory of Stewart Platform.....	52
3.1	Geometric Analysis of Stewart Platform .....	54
3.1.1	The Inverse Problem: lengths as a function of position .....	56
3.2	Calculate motion geometry by markers .....	62
3.3	Force Feedback Motion .....	69
Chapter 4.	Software Development .....	72
4.1	Introduction .....	72
4.2	Software Design Specification .....	73
4.3	Simulation Data Generator and Stewart Platform Driver .....	74
4.4	Experiment Runtime and Data Logging .....	82
Chapter 5.	Design and Manufacturing of the Stewart Platform Simulator.....	84
5.1	Introduction .....	84
5.2	Product Design specification.....	86
5.2.1	Base Plate.....	88
5.2.2	Top Plate .....	88
5.2.3	Top of the Arch .....	89
5.2.4	Stationary Bone Attachment .....	89
5.2.5	Fixing Pole .....	89
5.2.6	Pelvic Clamp .....	90
5.2.7	Actuator Holder .....	90
5.2.8	Rod Attachment.....	91
5.2.9	Bearing Attachment .....	92

---

5.2.10	Femur Attachment .....	92
5.2.11	Assembly and exploded view of the test rig .....	93
5.3	Strain Gauges .....	95
5.3.1	Calibration of strain gauge .....	96
5.4	Experimental Set Up .....	100
5.4.1	Equipment .....	100
5.4.2	Connections .....	111
5.4.3	Assembling.....	120
Chapter 6.	Experiment Procedure and Results.....	122
6.1	Introduction .....	122
6.2	Experiment Procedure.....	124
6.3	Experimental Outcome: .....	130
6.3.1	Force .....	136
6.3.2	Displacement.....	143
Chapter 7.	Evaluation of Results.....	150
7.1	Force .....	155
7.2	Displacement.....	161
Chapter 8.	Conclusion .....	165
8.1	Introduction .....	165
8.2	Recommendation for Future Study.....	167
References	.....	168
Appendix 1 – Force Data used in Experiment .....		177
Appendix 2 – Data used in Creating Generic Movement Model for the Software .....		179
Appendix 3 – CAD Plans of Stewart Platform.....		184

---

Appendix 4 – Parts and Equipments used.....	190
Appendix 5 – Strain Gauges.....	196
Appendix 6 – Visual Basic Code for Kinematic Simulation .....	202

---

## Table of Figures

Figure 2.1 Load versus Deformation of a bone specimen under compression (KidsHealth.org) .....	11
Figure 2.2 Muscles, Ligaments and Tendons (MedlinePlus 2009) .....	12
Figure 2.3 Hip Joint Labelled (Drake, 2010) .....	17
Figure 2.4 Hip joint replacement (Physiotherapy 2010).....	18
Figure 2.5 Body showing all three-axes and planes (Kapandji, 1987).....	22
Figure 2.6 Hip Movements A) Flexion/Extension, B) Adduction/ Abduction, .....	23
Figure 2.7 Maximum pathway of motion for the hip (Kapandji, 1987).....	25
Figure 2.8 Range of motion during one cycle of normal walking (Bergmann et al., 2001) .....	28
Figure 2.9 Free body force diagram of hip .....	29
Figure 2.10 Resultant hip joint force versus a time curve (Bergmann et al., 2001).....	31
Figure 3.1 General Stewart Platform. (Fong, 1990) .....	54
Figure 3.2 General Stewart Platform (Azevedo et al., 2008).....	55
Figure 3.3 Locations of measured points on and around joint a) Right View and b) Front View .....	62
Figure 3.4 Plate ratio.....	64
Figure 3.5 Real, effective and attached angles of platform.....	64
Figure 3.6 Force direction .....	67
Figure 4.1 Schematics of Software Arrangement.....	72
Figure 4.2 Visual Basic Simulation for initial position .....	74
Figure 4.3 Initial values of platform .....	75

---

Figure 4.4 Lengths of each actuator.....	75
Figure 4.5 Coordinates of Stewart Platform points .....	76
Figure 4.6 Centre of platform coordinates .....	76
Figure 4.7 Rotation angles of centre point.....	77
Figure 4.8 Type of simulation .....	79
Figure 4.9 Speed selection check boxes (modified to work as of radio boxes) .....	80
Figure 4.10 Platform Movement during Hip Joint Walking Simulation .....	81
Figure 4.11 Error box checking if the Stewart Platform is connected.....	82
Figure 5.1 Assembly view of the experimental rig (exploded).....	84
Figure 5.2 Assembly view of the experimental rig .....	94
Figure 5.3 Strain gauge application .....	95
Figure 5.4 Position Control loops schematic (Corp, 2008b).....	103
Figure 5.5 Current loop diagram (Corp, 2008b).....	104
Figure 5.6 Velocity loop diagram (Corp, 2008b) .....	105
Figure 5.7 Position loop diagram (Corp, 2008b).....	106
Figure 5.8 CANopen diagram (Corp, 2008b) .....	108
Figure 5.9 Schematic Diagram of Xenus and POSYS Connections .....	111
Figure 5.10 Xenus Housing Cabinet, SCS Automation & Control.....	116
Figure 5.11 Xenus Housing Setup.....	117
Figure 5.12 Schematic Front View of Rig Showing Joint Interface Location and Arc Size (all dimensions in mm).....	118
Figure 5.13 Connections between Main Regions.....	119
Figure 5.14 Actuator Holders, Bearing Holders, Bearing Holder Caps, Top and Bottom End Attachments.....	120

---

Figure 5.15 Experimental Rig Set up.....	121
Figure 6.1 Schematic of complete system.....	123
Figure 6.2 Step forward function at 3.2A for 20ms.....	126
Figure 6.3 Step forward and reverse function at 3.2A for 10ms .....	127
Figure 6.4 Process Flow Chart .....	128
Figure 6.5 Coordinate system for measured hip contact forces(Bergmann et al., 2001) .....	132
Figure 6.6 Gait analysis data and calculated muscle forces (Bergmann et al., 2001) ..	133
Figure 6.7 Contact force on hip (Bergmann et al., 2001) .....	134
Figure 6.8 Light Weight, Slow Walking Speed .....	137
Figure 6.9 Light Weight, Normal Walking Speed.....	137
Figure 6.10 Light Weight, Fast Walking Speed.....	138
Figure 6.11 Normal Weight, Slow Walking Speed .....	139
Figure 6.12 Normal Weight, Normal Walking Speed .....	139
Figure 6.13 Normal Weight, Fast Walking Speed.....	140
Figure 6.14 Heavy Weight, Slow Walking Speed.....	141
Figure 6.15 Heavy Weight, Normal Walking Speed.....	141
Figure 6.16 Heavy Weight, Fast Walking Speed .....	142
Figure 6.17 Light Weight, Slow Walking Speed .....	144
Figure 6.18 Light Weight, Normal Walking Speed.....	144
Figure 6.19 Light Weight, Fast Walking Speed.....	145
Figure 6.20 Normal Weight, Slow Walking Speed .....	146
Figure 6.21 Normal Weight, Normal Walking Speed .....	146
Figure 6.22 Normal Weight, Fast Walking Speed.....	147

---

Figure 6.23 Heavy Weight, Slow Walking Speed.....	148
Figure 6.24 Heavy Weight, Normal Walking Speed.....	148
Figure 6.25 Heavy Weight, Fast Walking Speed .....	149
Figure 7.1 Light Weight, Normal Walking Speed.....	156
Figure 7.2 Light Weight, Fast Walking Speed.....	157
Figure 7.3 Normal Weight, Slow Walking Speed.....	158
Figure 7.4 Normal Weight, Fast Walking Speed .....	159
Figure 7.5 Heavy Weight, Slow Walking Speed.....	160
Figure 7.6 Light Weight, Slow Walking Speed .....	161
Figure 7.7 Normal Weight, Slow Walking Speed.....	161
Figure 7.8 Heavy Weight, Normal Walking Speed.....	162



---

## Nomenclature and abbreviations

CAN	Controller Area Network
E	Young's Modulus
OSD	Osgood-Schlatter Disease
RSI	Repetitive Stress Injuries
DOF	Degrees-of-Freedom
UPS	Universal Prismatic Spherical
SPS	Spherical Prismatic Spherical
$B_i$	Base Plate Coordinates
$T_i$	Top Plate Coordinates
$\psi$	Euler Angle-Roll
$\theta$	Euler Angle-Pitch
$\phi$	Euler Angle-Yaw
$L_i$	Leg Lengths Vectors
$\mathbb{R}$	Set of Real Numbers
<b>q</b>	Quaternion
$R$	Rotation Matrix
ROM	Range of Motion
BW	Body Weight
x, y, z	Plane Coordinate
<b><math>i, j, k</math></b>	Direction Vectors
$F$	Force
$W$	Weight
R	Electrical Resistance

---

$l$	Length of the Element
$\rho$	Resistivity
$A$	Area of the Element
$V_{EX}$	Excitation Voltage
$V_o$	Output Voltage
$X$	Number of Strain Gauges
PTC	Positive Temperature Coefficient
CME	Copley Motion Explorer
CMO	Copley Motion Objects
DC	Direct Current
PWM	Positive – Width Modulation
PID	Proportional – Integral - Derivative
DAC	Digital – to – Analogue Converter
RAM	Random Access Memory
PCI	Peripheral Component Interconnect
SCS	Servo Components and Systems
IDC	Insulation Displacement Cable

## **Chapter 1. Introduction**

### **1.1 Overview**

Over the past three decades, joint replacement surgery has become an increasingly common procedure. A joint is the part of the body where two or more bones come together, such as the knee, hip or shoulder. Sometimes, the surgeon does not remove the whole joint, but only replaces or fixes the damaged parts. Replacing a joint can relieve pain and help the patient to move as well as feel better.

There are many causes which directly or indirectly affect a joint's functionalities: direct causes are such things as arthritis and injuries related to joint and tissues fracture; indirect causes are attributes such as age, weight and daily activity behaviour. These mainly target cartilage wear and hence improper joint loading. This can cause pain, stiffness and swelling. Diseases and damage inside a joint can limit the blood flow, affecting bone growth and self-repairing.

Total joint replacements are performed in order to provide pain relief and restore joint mobility. The configuration of prosthesis depends on the joint to be replaced and the function to be reproduced; and the materials used in its conception must provide low friction and low wear. Other important criteria to be taken into account are resistance to mechanical failure and resistance to loosening, throughout the life cycle of the prosthesis. These parameters are of great importance, considering the large number of total joint replacements carried out around the world.

Joint replacement is becoming more common. In 2010, 166,328 artificial hip and knee joints were implanted annually in the UK and around 775,000 hip or knee replacements each year in the USA. The lifetime for replacement joints is about ten to fifteen years. Therefore, damaged joints in younger patients may need to be replaced more than once. It is therefore; absolutely necessary that joint replacements should be as reliable as possible in order not to adversely affect the patient.

This large number of total joint replacements creates a business opportunity for companies specializing in the production of artificial human joints. In order to adhere to the considerations previously mentioned, before the devices are cleared for use in surgical procedures, these companies must test these prosthesis, so as to ensure their fitness not only to perform as required but also to last. The tests are performed with the aid of human joint simulators. The purpose of these simulators is to test artificial joint replacement for wear and fracture. Existing joint simulators cater for one joint only whereas the proposed concept is applicable to several joints. This will mean that medical research in this field will no longer require several different simulators.

There are specialised joint simulators for individual human joints, machines used to test an artificial joint under conditions approximating those occurring in the human body. The results of these tests provide an insight into the response of the artificial joints, which the testing party can use to obtain information regarding the limits of performance of the materials and the prosthesis.

Testing of materials, performance and for bio-compatibility is essential for companies engaged in the manufacturing of artificial joints and, as noted before, most of the joint simulators available on the market can simulate the motion of only one specific joint. This can prove costly for companies manufacturing more than one type of artificial joint, not only in monetary terms, but also in terms of the physical space that these machines occupy.

Artificial joint replacement is generally a successful solution for more than 90% of surgical operations. Joint problems which require joint replacement are as follows:

- Infection
- Dislocation
- Wear
- Blood clots
- Loosening
- Injuries to blood vessels and nerves

## **1.2 Motivation**

The purpose of this work is to design and manufacture a device which can be programmed to simulate the motion of several human joints. The device is to be constructed will be a versatile six-degrees-of-freedom robotic system, known as a Stewart Platform, comprising a base plate, platform and six linear actuators. The kinematics and loading will be controlled by a personal computer using multiple axis control cards connected to the actuators. The computer will perform calculations for specific joints during prescribed activities, in order to determine the position, velocity, acceleration and force for each actuator so that the platform can replicate joint movement.

An artificial joint is required for testing the concept and therefore a sample will be required. By measuring the deformation of this joint will give an indication of the forces being applied. This is done by using strain gauges on a universal clamp arrangement that can hold the static part of the joint. This will allow for analysis of the forces acting on the bone.

## **1.3 Objectives**

The objective of this study is to develop a single configurable machine capable of simulating the motion of a number of human joints. This is to be achieved with the use of a six-degrees-of-freedom Stewart Platform where the actuators will drive the platform to replicate the range motion of the desired joint. Inputs to the actuators are to be configurable and transmitted to the actuators using a Visual Basic program. The program outputs two values, for each linear actuator, extension and loading.

## 1.4 Product design specifications

In order to design and develop the six degree of freedom Stewart platform to be used in the biomedical field, the following product design specification needs to be considered:

- The rig should be light in weight and easy to assemble and dissemble.
- The rig should have the ability to move in all six degree of freedom.
- The clamp to hold the fixed bone should be rigid and give accurate reading of the forces acting on the joint.
- The range of motion should be at least 20cm all planes.
- The top plate should be able to rotate at an angle of 30° in order to simulate the motion of a normal human walking.
- The rig should provide a contact force of 1500 Newton.
- The rig should be able to perform two gait cycles in one second.
- The software should be programmable and configurable for different human joint and their activities.
- The software should send commands for the actuators and record feedback data.

## 1.5 Significance of the study

This work has many benefits in basic science and clinical literature. This design of a Stewart Platform mechanism advances the study of human joints. This thesis studies human hip joint kinematics and load analysis. Such analyses are very useful for investigating mobility and natural functionality as well as the variation in motion due to replacement implants. However, it should be noted that the function of this machine is not just restricted to simulating the movement of a single joint. The application of a Stewart Platform to this study is not an easy undertaking. The optimisation and

precision of Stewart Platform has been heavily studied, but rarely for a biomechanical purpose. For this study, it was decided to use the hip joint as a test example. This joint was chosen as it is one of the highest load bearing joints with a large degree of freedom. Also, the hip joint is one of the most common prosthesis and has much commercial interest.

This work was undertaken to study the mobility and load analysis of the artificial hip joint. The simulator can be used in implant design. Testing of materials and performance is essential for companies engaged in the manufacturing of artificial joints and, as noted before, most of the joint simulators available on the market can simulate the motion of only one specific joint.



## **1.6 Thesis outline**

To reach to the stated objective, the study is structured in eight chapters. Appendices with supporting information were included at the end of this thesis. A general overview of the research, motivation, and significance is presented in this chapter. A brief description of each chapter is as follow.

### **Chapter Two: Literature Review**

In this chapter a background of Human Musculoskeletal System and the effects of forces on them are discussed, as well as muscles, ligaments, tendons and joint replacements. This chapter also includes the kinematics and kinetics of the hip. Hip joint kinematic rules are discussed in details using natural body shapes and figures. At the end of this chapter, many published papers on joint simulators are explained.

### **Chapter Three: Theory**

This chapter focuses on the theory of hip joint movement. The chapter mainly deals with the geometric analysis and design of the Stewart Platform, and mathematical modelling of the problem. In the geometric analysis coordinates, links and points associated to the hip structure is presented. It is then followed by inverse problem formulation which is the main mode of analysis.

### **Chapter Four: Software Development**

As the title denotes, this chapter deal with the software aspect of the implementation. Different parts of the written interface in Visual Basic are presented one by one and the operation and function of each part is explained in relation to the theory and hardware.

By the end of the chapter, a reader has a clear idea of the written interface and the input and output variables in the interface.

### **Chapter Five: Design and Manufacturing of the Stewart Platform Simulator**

Theories are put into practice in this chapter. The application of the method can be sought in this chapter by including product design specification, strain gauges and the experiment. All the information needed for implementation is presented such as connections of different component of hardware and assembly of them. The set up for the experiment is also included to extensively make the experiment calibration and settings clear.

### **Chapter Six: Experimental Procedures and Results**

This chapter aims at presenting the procedure and obtained experimental results from the Stewart Platform. The main focus of the study is given to the position and contact force of the hip joint. How forces and position mode are operating can be found in this chapter. Experiments are done and compared to the results of previous work. Different scenarios in the experiments are assumed and their graphs are also included.

### **Chapter Seven: Evaluation of Results**

This chapter aims at analyzing the obtained data as well as discussing the overall design process of the six degree of freedom Stewart Platform. The discussion is based upon the experiments in chapter six with respect to kinematic and loading control. In effect, force, rotation, and displacement are discussed.

**Chapter Eight: Conclusions**

Reviews the work undertaken and make conclusions of the work that was undertaken.

Finally, recommendations for future work are made.

## **Chapter 2. Literature Review**

### **2.1 Human Musculoskeletal System**

#### **2.1.1 Body Frame, Bones**

The skeleton is of great importance in terms of movement; the joints within the skeleton allow several degrees of freedom of motion. Particular bones in the body, due to their length and axes (fulcrum), allow leverage of the body, allowing greater speeds of movement or forces to be attained (Patts 2009).

Different bones, depending on their shape and size, have different functions (Patts 2009). The structure of bone changes with age: younger individuals have softer bones and therefore are less likely to fracture or break their bones. However, with age bones become less supple and more fragile; they are more prone to fracturing, which is why most of those who need joint replacements are older people (Currey, 2002).

The most vital feature of a bone is its strength; this is of great importance in its role in the anatomy. When under compression loads, bones are able to withstand themselves from bending, due to the stiffness of the bone. The stiffness depends on the actual strength, the material and configuration. Bone material is to some degree viscoelastic, i.e. showing both viscous and elastic properties. The angle and load which is acting on the bone alters the strain it is experiencing; for example, when under a longitudinal load, it is under greater strain and thus more likely to fail than when the load is applied circumferentially. However, it should be noted that the bone is stronger when in

compression than in tension. There is no general shape for bones as each differs according to its function however, it may be noted that all bones have a smooth finish, with no abrupt bumps or ridges; this is advantageous in terms of stress concentration as it makes the transition of stress gradual. In Figure 2.1 a graph displays load versus deformation: when the bone is in compression, it can be seen that initially the relationship between the two factors is linear and then the load reduces by a small amount and continues at approximately the same level until the bone specimen breaks, as in elastic-plastic deformation (KidsHealth.org 2011).

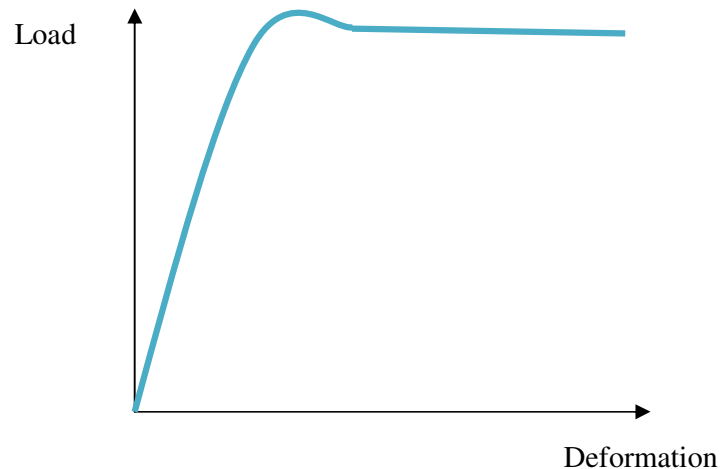


**Figure 2.1 Load versus Deformation of a bone specimen under compression**  
(KidsHealth.org)

### 2.1.2 Muscles, Ligaments and Tendons

The body has 650 muscles altogether, which make up approximately half a human's body mass. There are three different types of muscle:

- Skeletal
- Smooth and
- Cardiac.

Skeletal muscle is attached to the bone by tendons which pull on the bone through the muscle to create movement and therefore supports the skeleton as well as creating the body shape. The muscles are controlled by the brain and nervous system and, after excessive use; they tire and need to rest. Muscles are attached to the bones by tendons. Smooth muscles such as the stomach wall are involuntary; these break down food. Cardiac muscles are found only in the heart and are also involuntary (Hay et al., 1988).

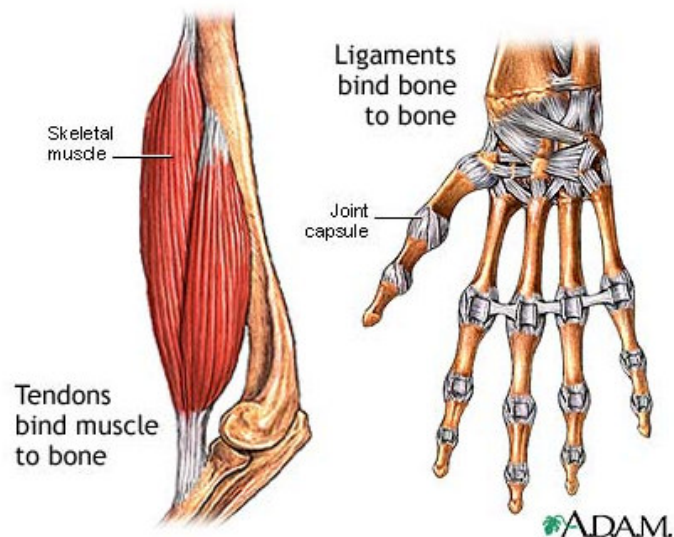


**Figure 2.2 Muscles, Ligaments and Tendons (MedlinePlus 2009)**

Ligaments and tendons are all made of soft collagenous tissue but have different purposes (Figure 2.2). Ligaments are made of connective tissue; they are made up of strong, inelastic, white fibres. They are vital parts of a joint, holding the bones together and they transmit the load from one bone to another. They provide stability for the joints, but they also restrict the movement in all joints. Tendons, for their part, ensure that muscles are attached to the bone and transmit force to the bone and also have a greater tensile strength than ligaments. Tendons provide a layer between bones and muscles which would otherwise be in contact and they also have the important function of storing energy. They are required to be very stiff due to being subjected to loads but should also have low stiffness when flexibility is needed. The strength of a muscle and tendon determines the stability of the joint which they support. Muscles increase in strength when in contraction and reduce when relaxed (Currey, 2002, KidsHealth.org 2011).

### **2.1.3 Joints**

A joint is simply two or more bones working in such a way as to correspond to each other. The bones within a joint are attached by the ligament which stabilizes and reinforces them as well as determining their range of movement.

Different joints in the body have different capacity in terms of movement and restrictions. There are three types of joint classed according to the form of their movement (Patts 2009):

- Fibrous joints
- Cartilaginous joints

- Synovial joints

The fibrous joints are immovable joints, such as the skull; cartilaginous joints, however, can move to some extent. The movement is not as restricted as in a fibrous joint but it is unable to move freely. Synovial joints move freely and have the greatest degree of freedom of all the joints in the body. Synovial joints are connected together by a synovial membrane; this is simply a connective tissue which contains synovial fluid ( Patts 2009). There are six types of synovial joint:

- Ball and Socket: provides the greatest range of motion, for example, hip and shoulder joints.
- Condylod: similar to ball and socket in terms of movement except they cannot rotate, for example, the joints in the fingers.
- Gliding: such joints are restricted and move in only one plane. Can be found in the tarsal and carpal bones.
- Hinge: such joints move like a hinge, for example, elbow and knee joints.
- Pivot: such joints are like the skull which rotates in one plane only.
- Saddle: such joints can move in two planes, for example, thumb joints.

Joints remain attached due to a thick capsule at the articulate surface. Articular cartilage is present in all joints for the same purpose; the thickness varies according to the joint. For the hip joint, which carries much weight and experiences large forces during movement, the cartilage is approximately a quarter of an inch thick. The articular cartilage has a slippery and rubbery consistency, which allows smooth gliding at the joint and also absorbs vibrations. The articular cartilage is attached to the bone through



a capsular ligament; this is a fibrous tissue which is firm enough to provide stability; however, it should still be flexible enough to allow movement (Currey, 2002).

Problems which may occur within a joint vary from one to another and on the patient's diet and lifestyle. Painful symptoms which occur within the joint include inflammation, stiffness and swelling. Problems which occur within bones and joints include:

- Arthritis: Inflammation of the joint.
- Fracture: Bone damage by breaking, snapping or cracking.
- Osgood-Schlatter Disease (OSD): Inflammation of the bone, cartilage or tendon.
- Osteomyelitis: Bone infection due to bacteria.
- Osteoporosis: Weakening of bone tissue, which becomes more prone to damage.
- Repetitive Stress Injuries (RSI): several injuries increase stress in a joint.
- Scoliosis: Spine curvature too extensive.
- Sprain: Twisting of a joint during an activity.

These problems if severe can lead to the need for an artificial joint replacement.

#### **2.1.4 Joint Replacement**

Artificial joints differ from one to another and what is required of them in terms of movement. For instance, hips need to be strong to support the body weight but joints in the finger need to be small and able to bend easily. However, regardless of the joint, all artificial joints need to replicate the original joint as closely as possible so that they move and respond like natural joints. Artificial joints originated around 50 years ago;

since then, improvements in technology have improved them to the point where they are almost identical to a human joint (Currey, 2002).

Artificial joints used to be made up of a combination of metals and plastic, which leads us to their biggest problem. This is that artificial joints do not have a long life; since they suffer wear and tear and eventually wear away and fail altogether. The common polymers used are ultra-high molecular weight polyethylene and ceramic, because these are strong and yet light and, most importantly, they resist corrosion. Another problem is that the same joint in different bodies varies, suggesting that manufacturing is likely to be extremely difficult.

Problems can also occur after the artificial joint has been implanted. An infection can be treated if it is minor, but, if not, recovery surgery is required. In addition, because the artificial joint can never move to exactly the same extent as a healthy joint, the restricted motion causes the blood to flow more slowly and therefore to form blood clots. Wear and loosening are also common, resulting in the spread of parts of the artificial joint or its reaction with other parts of the body. There is also a very slight chance of the prosthetic breaking or of dislocation and nerve damage during the operation(Foundation 2011).

## 2.1.5 Musculoskeletal Structure of the Hip Joint

### 2.1.5.1 Hip Joint, Muscle, Ligaments and Tendons

The hip is the first joint of the lower extremity; it is a ball and socket joint, as shown in Figure 2.3. It displays how the acetabulum has a concave shape, complemented by the convex shape of the femoral head. Both are symmetrical, which allows for a range of motion. The head of the femur is also surrounded by articular cartilage (carrying nutritional fluid) to reduce the stress from the compressive forces and in addition to lubricate the joint, specifically the head of the femur and the acetabulum, where the bones make contact (Kapandji, 1987).

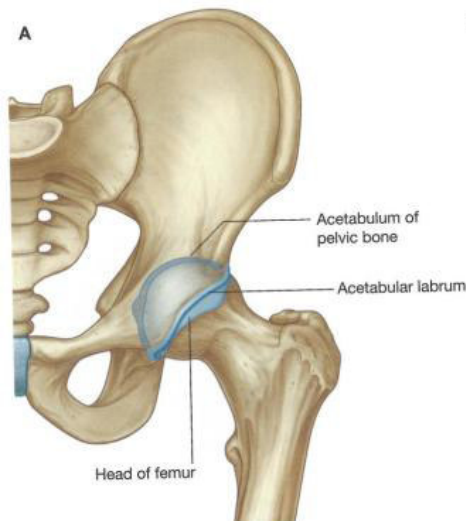


**Figure 2.3 Hip Joint Labelled (Drake, 2010)**

There is also a ligament that is positioned around the edge of the acetabulum, called the labrum; this positioning creates a deeper socket and has the effect of making the joint more stable.

### **2.1.5.2 Prosthesis Hip Replacement**

Artificial hip replacements are the most common joint replacements. Over the years, joint replacement has advanced immensely. The most recent and optimised has been the Exeter hip replacement by Lang and Lee. Due to its smooth finish it does not interfere with the cement, which makes it more secure (Bajekal 2011). Due to the spherical articular surface of the hip joint, it is the easiest to replicate mechanically. However, as with any prosthetic, there are still several problems awaiting solution. These include determining the actual size of the prosthetic required and reducing the abrasion between the joints in contact; the prosthetic also releases debris which can be toxic and there is an issue over the way in which the prosthetic is attached to the bone, where various options can be considered.

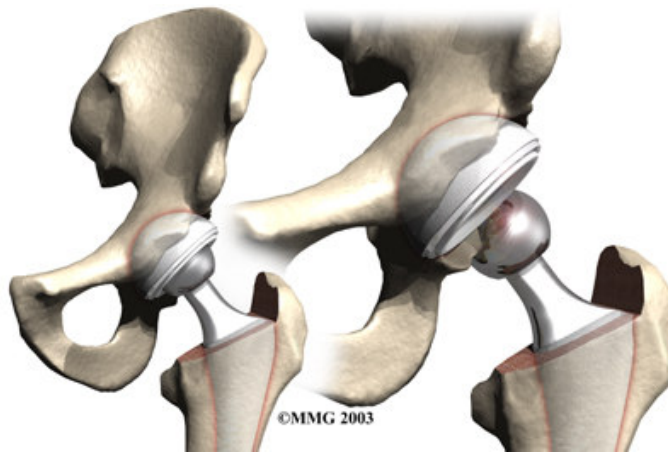


**Figure 2.4 Hip joint replacement (Physiotherapy 2010)**

The problems which tend to occur with post-operative rehabilitation are (Bajekal 2011):

- Infection
- Instability – this can depend on the patient and surgeon, as well as the design and position of the prosthesis.
- Aseptic loosening, when the femoral stem of the artificial joint slackens within the femur bone.
- Implant failure

## **2.2 Joint Biomechanical Analysis**

The free movement of bones is provided by diarthrodial synovial joints. The joints are characterised by three features: a synovial cavity, connective tissue and the cartilage which covers the articulating ends of the bones (Tortora and Grabowski, 2004) acting as a bearing material. One example is in the hip joint, in which articular cartilages cover the acetabular cavity and also the femoral head. This articular cartilage has noticeable lubricating features and a very low coefficient of friction, in addition to a low wear rate (Lipshitz and Glimcher, 1979, Mow and Lai, 1980, Mow, 2005).

It should be noted that this joint suffers degradation and wear from various factors, such as age; nevertheless it generally survives the life of the patient. The problem can be exacerbated by incorrect use, notably, extreme sports, injury, wear and tear trauma and congenital disease (Yang, 2003).

One of the most often investigated diarthrodial joints is the hip joint. This is due to the simplicity of its geometry (ball and socket) and kinematics, apart from its being “one of the largest and most heavily loaded joints” (Dowson, 1981). Most studies of the hip joint have been in vitro or in situ under laboratory conditions (Rushfeldt et al., 1981, Brown and Shaw, 1982, Brown and Shaw, 1983, Ferguson et al., 2003) or in vivo, using instrumented prosthesis (Rydell, 1966, Bergmann et al., 1988, Hodge et al., 1989, Park et al., 1999, Bergmann et al., 2001, Morrell et al., 2005, Hodge et al., 1986, Carlson). Nonetheless, these are mainly intrusive techniques. The use of CT, MRI and ultrasound is increasing, in particular in morphological in vivo studies or for fracture determination

(Jonsson et al., 1992, Nakanishi et al., 2001, Naish et al., 2006, Keller and Nijs, 2009, Barkmann et al., 2010).

Still, tribological and contact mechanics studies are time-consuming and difficult to carry out experimentally and clinically, in particular those including parametric evaluations. In addition, one or both the cartilages always have to be given up in clinical studies involving instrumented prosthesis, because it is impossible to use these models non-invasively. One of the ways to tackle this problem has been to use mathematical models (Paul, 1966, Seireg and Arvikar, 1975, Ipavec et al., 1999, Daniel et al., 2001, Mavcic et al., 2002) which over time have made the results more accurate (Brand et al., 1994, Stansfield et al., 2003).

Another option for studying joints non-invasively is numerical modelling, such as finite/discrete element modelling (Rapperport et al., 1985, Ferguson et al., 2000, Bachtar et al., 2006, Yoshida et al., 2006, Anderson et al., 2008) . Although this type of modelling has often proved beneficial, some cases are geometrically simplified and the effects of biphasic lubrication are not taken into account. Lubrication is known to attenuate the coefficient of friction because of load partitioning (Mow and Lai, 1980). Another disadvantage is that in their physiological loading paradigm and fluid load support in the cartilage these models disregard the relationships in contact mechanics in a complete hip joint.

### 2.2.1 Hip Joint: Kinematics

The body is able to move in three axes (Figure 2.5); the hip specifically has three degrees of freedom and this allows a wide range of motion for the limb. The three axes allows great motion range, as follows (Figure 2.5):

- The transverse axis allows flexion and extension of the hip.
- The sagittal axis controls the adduction and abduction movement.
- The vertical axis allows rotation in both the medial and lateral direction, occurring along the frontal plane.

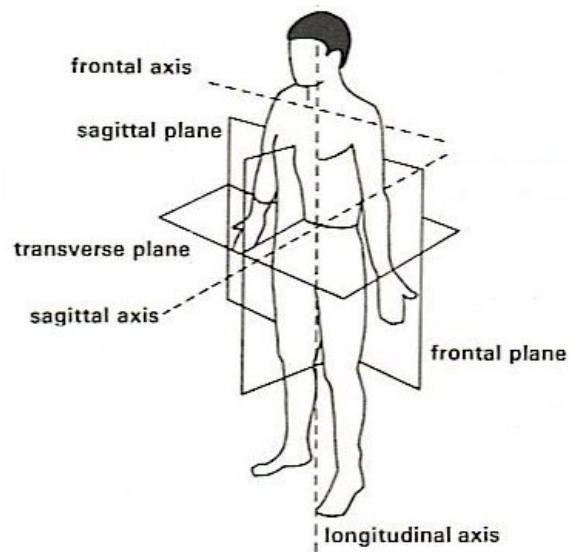


**Figure 2.5 Body showing all three-axes and planes (Kapandji, 1987)**



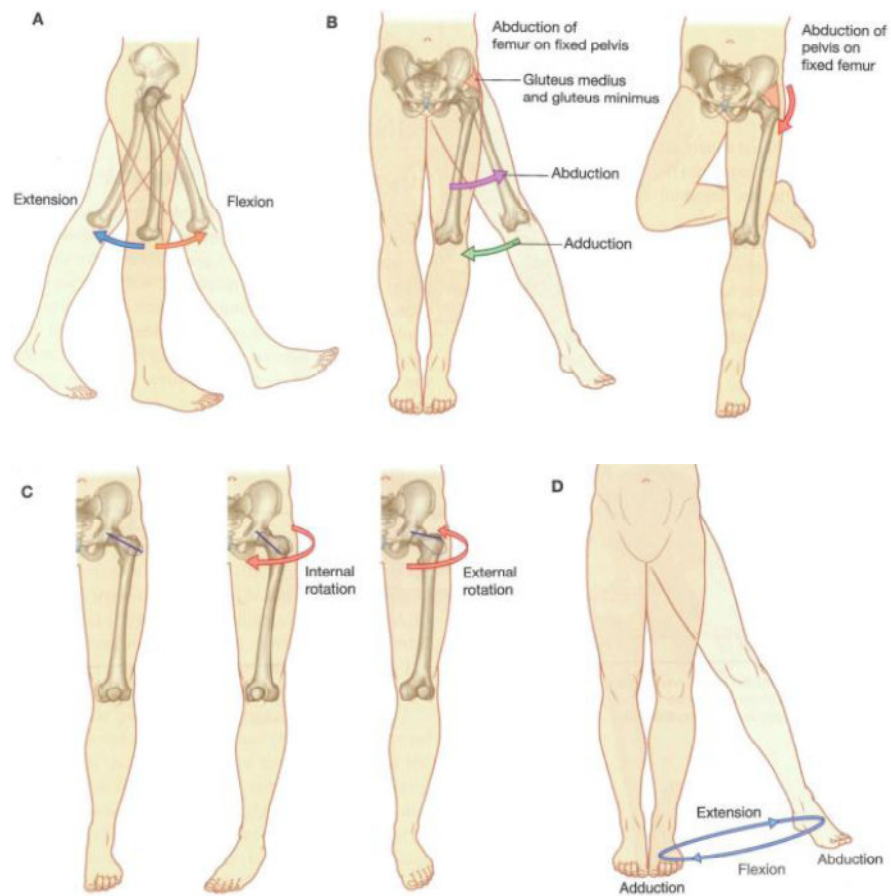


**Figure 2.6 Hip Movements A) Flexion/Extension, B) Adduction/ Abduction, C) Lateral/Medial Rotation, D) Circumduction (Drake, 2010)**

Unlike the shoulder, also a ball and socket joint, the hip joint has a certain degree of interlocking and therefore does not allow for as great a range of motion as the shoulder. It is distinctly more stable than the shoulder and is in fact the most complex joint to dislocate, due its durability and the fact that the parts of the joint fit so well into each other (Kapandji, 1987).

**Flexion:**

The movement of flexion can be described as the movement of the thigh to the trunk.

When the knee is extended the hip can reach a maximum of only 90° but, when the knee is in extension, the thigh can reach 120° and beyond. The degree of movement tends to be greater when the knee is in flexion than in extension; the reason for this is that in the former case, the hamstring relaxes, allowing an increased degree of motion at the hip.

**Extension:**

In general, the movement of extension is less than the degree of flexion. As with flexion, the degree of extension depends on whether or not the knee is extended. When the knee is in extension, the hip can reach 20°, but it reaches only 10° when in flexion. These values are found with an average person, but in practice they vary according to the level of exercise and training engaged in by each individual (Kapandji, 1987).

**Abduction:**

It is called abduction when the lower limbs move outwards, away from the line of symmetry. When one hip moves in abduction, it seems as if the other hip also creates an identical abduction. This is particularly visible after a 30° abduction of one hip, which in fact is due to 15° of abduction in both joints. The maximum abduction is around 90°; once again, as both hips are in fact in abduction, the maximum is only 45°. As mentioned earlier, this degree of abduction is greater for those more used to physical exercise. It should be noted that doing the splits is not a motion in one plane only but is actually a combination of abduction and flexion (Kapandji, 1987).

**Adduction:**

Adduction is the reverse of abduction. It occurs when the lower limbs move towards the line of symmetry, however, one leg is in the path of the other and therefore 'pure adduction' can never be achieved. The greatest degree of adduction is  $30^{\circ}$ . Abduction can occur along with extension, flexion or in both hips.

**Lateral and Medial Rotation:**

The position of reference can be considered where the individual lies face down and bends the knee at a  $90^{\circ}$  angle. When the leg moves to the right of the body medial rotation occurs to a maximum range of  $30^{\circ}$  to  $40^{\circ}$ . Conversely, when the leg is moving toward the centre of the body, it is experiencing lateral rotation, which can reach a maximum of  $60^{\circ}$ .

These combined movements of the hip, when applied simultaneously around the hip, result in a pathway as shown in Figure 2.7. Indicating the maximum range of the hip, this path is called the cone of circumduction, although the shape is not much like a cone. It involves movement in more than one plane (Kapandji, 1987).

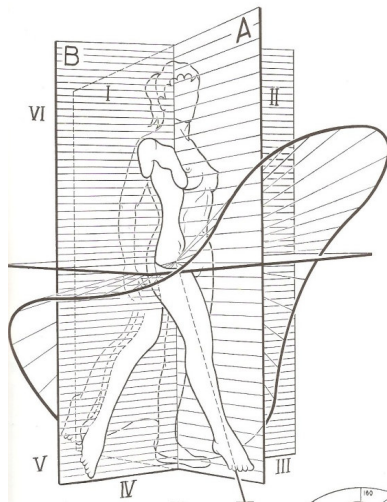


**Figure 2.7 Maximum pathway of motion for the hip (Kapandji, 1987)**

In the study of contact mechanics it is essential to take into account gait analysis or the travelling of the hip joint and its component parts. Walking, sitting, climbing stairs or standing up are among the many everyday activities of normal life. The forces and stresses within the joint depend on the kind of activity engaged in. Thus, spatial movements and the temporal of the femoral head within the acetabular cup need to be comprehended before investigating many functional parameters, such as contact forces and fluid load support. In addition, understanding locomotion or the travelling of joints not only contributes to “proper diagnosis and surgical treatment of joint disease” and designing better prosthesis (An and Chao, 1984), but also contributes to the post-operative rehabilitation of the patients.

The individual segments of the joint can be outlined as hard bodies connected together at the joint and enduring relative angular motion.

Compared to the shoulder joint, it can be inferred that the hip joint gives the body a wider variety of motions. The movements of the hip joint are flexion, extension, abduction, adduction, medial/inner and lateral/outer rotation and circumduction (Drake, 2005). These movements are further elaborated in the following paragraph. The assumption here is that the person concerned is standing.

Flexion is defined as the upward/forward motion of the femur proportional to the upper part of the pelvis, while extension is described as the downward/backward motion. Increasing flexion brings about a sharper angle between the upper part of the pelvis and

the femur. For extension, the opposite is true. The angular movements of the femur about a horizontal anteroposterior axis are called abduction and adduction. Abduction is the movement away from the medial plane, whereas adduction is towards it (Gray 2010). Medial and lateral movement takes place about the vertical/longitudinal axis with spinning motion. Medial rotation is towards the centre of the body whereas lateral rotation is away from it. The circular motion of the femur is called circumduction. This motion of the femur encircles a cone (Gray 2010)

There is a constraint on every range of motion including these. The main reason for the limitations is associated with the different muscles and the construction of different joints and the body as a whole.

Nominal hip joint flexion is approximately  $120^{\circ}$  and extension is around  $20^{\circ}$  (Dowson, 1981, Palastanga, 2006). Nonetheless, including external force for these motions can result in further extension, up to  $130^{\circ}$  and  $30^{\circ}$  respectively (Palastanga, 2006). Abduction and adduction are  $45^{\circ}$  each, since the total of medial and lateral rotation is around  $90^{\circ}$  (Dowson, 1981, Palastanga, 2006).

In Figure 2.8, the typical range of motion curves (Bergmann et al., 2001) is illustrated. The curves are over one cycle of normal walking for an average patient. The positive angles are associated with flexion, abduction and outer/lateral rotation. The cycle starts at the heel strike.

Skin markers are connected to the skin nearer the bony landmarks in order to register the gait. They are roughly flashing LEDs (Crowinshield et al., 1978, Rohrle et al., 1984) or reflective markers (Heller et al., 2001). The movements are registered either by photographic cameras (Crowinshield et al., 1978) or movie cameras (Paul, 1966) which oversee the movement of joints over time. The motion of the markers is captured during the cycle. In modern systems infrared cameras have replaced the older ones (Heller et al., 2001).

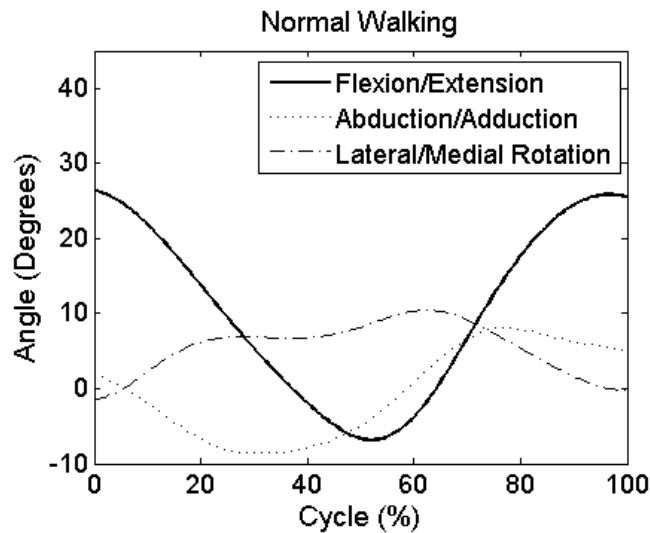


**Figure 2.8 Range of motion during one cycle of normal walking (Bergmann et al., 2001)**

### 2.2.2 Hip Joint: Kinetics

Kinetics in relation to the hip joint is the forces acting on the joint according to the body's motion and activities. For example, the force acting on the hip joint is multiplied by about three when walking and can be multiplied up to six times during more vigorous activity such as running or jumping. By creating a free body force diagram (Figure 2.9), one can calculate the joint reaction force:

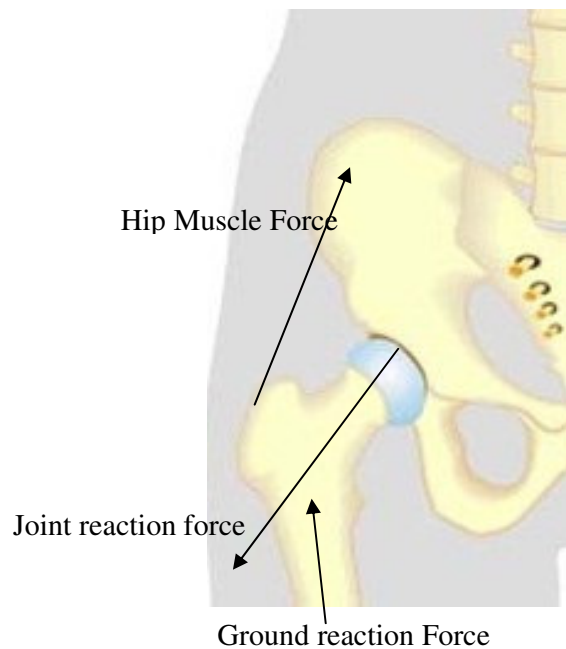


**Figure 2.9 Free body force diagram of hip**

Using equilibrium,  $\sum F = 0$ .

The joint reaction force is a function of the muscle force and the ground reaction force which is due to weight of the body and increased reaction do to the dynamics of body motion. This suggests that the force acting on the hip joint can be reduced by body weight and less strenuous activities (Bajekal 2011).

Forces accompany the motion of the femoral head within the acetabular cup. They depend on the motions listed above, body weight and muscles and they benefit the long term survival of the joint and smooth functioning of the articular cartilage, in particular those within the contacting area.

These forces have substantial importance for investigation. First, they help us to understand diseases such as Osteoarthritis (OA), which are ascribed to mechanical factors. Second, they help us to design state-of-the-art prosthesis which give structural stability to the whole musculoskeletal system and also replace joint function (Paul, 1966).

The first studies of joint kinetics date back to the early twentieth century (Paul, 1966). These joint forces are mostly calculated or measured from gait examination studies (Bergmann et al., 1993, Brand et al., 1994) and include external forces such as those which are exercised by the muscles. Measuring the foot-ground forces was not possible until the development of the foot plate in the 1950s. Subsequently, to predict joint forces cameras were used to capture joint kinematics. Instrumented prosthesis have been used in certain cases to directly calculate these forces (Rydell, 1966, Bergmann et al., 1988, Davy et al., 1988, Brand et al., 1994, Bergmann et al., 2001).

Figure 2.10 illustrates a typical resultant hip joint force versus a time curve in the conditions of normal walking. It has two separate peaks. The first occurs just after the heel strike and the second one occurs before toe off.



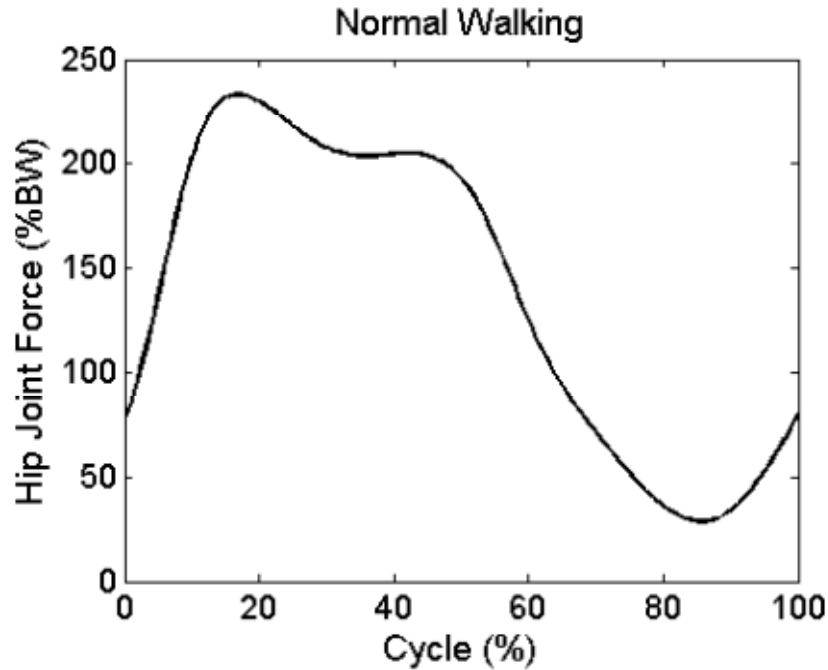


**Figure 2.10 Resultant hip joint force versus a time curve (Bergmann et al., 2001)**

### 2.2.3 Theoretical Studies

Mathematical/analytical gait mechanics have been proposed in order to enhance the hip joint's function (Seireg and Arvikar, 1975, Crowinshield et al., 1978, Johnston et al., 1979, Rohrle et al., 1984, Brand et al., 1994, Duda et al., 1997, Pedersen et al., 1997, Stansfield et al., 2003). The study of the hip joint forces and muscle forces should be given more attention. These forces are mentioned in different studies. The resultant hip joint force through the centre of the femur has in many cases already been responsible for the moments and forces because of the muscles (Rohrle et al., 1984). In other investigations this is ignored, and in consequence hip resultant forces appear too low to be of physiological importance (Crowinshield et al., 1978).

These problems of dynamics require kinematic data as input for making inverse kinematic calculations to predict joint forces, stresses, etc. Certain elements are necessary in order to model the joints precisely. Among these are the parameters, centre of masses and moments of inertia of the bony segments of the joint. The elements can be derived from regression equations (Crowinshield et al., 1978, Park et al., 1999) obtained from the statistical analysis of cadavers (Jensen, 1978, Hatze, 1980) and MRI techniques (Martin et al., 1989, Mungiole and Martin, 1990) are other approaches for deriving these inertial properties. The anthropometric data can be measured directly by video-based systems (Sarfaty and Ladin, 1993) or 3-D laser scanning (Wang et al., 2007) which are non-invasive and subject-specific. Consequently the dimensional data have been derived from radiographs, such as CT or X-ray (Heller et al., 2001, Stansfield et al., 2003). These data, along with skin marker data, are useful when one needs to acquire the situation of the bony landmarks of the lower limbs during gait (Heller et al., 2001). Force plates are used for capturing the external forces (Crowinshield et al., 1978, Heller et al., 2001). Force plates measure foot-ground reaction with a synchronized camera. Afterward these data are used to compute internal joint forces.

The musculoskeletal mathematical model is an indeterminate mathematical problem. In other words, the number of unknowns exceeds the number of equations, making it impossible to obtain a certain solution (Iglic et al., 2002). As such, they have an infinite number of possible solutions and the reduction method (Iglic et al., 1993) and the optimization method (Seireg and Arvikar, 1973, Crowinshield et al., 1978) must be used.

With the reduction method, the number of unknowns in equilibrium equations decreases; hence the problem can be solved. Paul's work is a good example of this method (Paul, 1976). He grouped 22 hip muscles into 6 groups and then crossed out antagonistic muscle activities because he was intended only in the activity between one heel strike and the next. This reduced the number of unknowns to six. For the task of grouping the muscles, electrodes were attached to the skin which engendered electric signals. This approach is called electromyographic; it is based on activated muscles. Consequently, five equations of equilibrium were then solved for level walking, limiting cases of joint forces by taking the value of the muscle with either the longest or the shortest moment arm. The utmost peaks of the hip joint force curve in normal walking were found to be 5.8 and 6.4 times the BW respectively. The corresponding average values were 3.29 and 3.88 times BW respectively. In a further study, a mean hip joint force was predicted for normal walking as 4.9 times BW.

In the work of Iglic and his colleagues, the number of unknowns was reduced by dividing nine muscle segments into three groups. It was assumed that the mean tension in all the muscles in any group was the same (Iglic et al., 1993). The muscle force was proportionate to its relative cross-sectional area and also its average tension. There were six unknowns and six equations; three for the resultant hip joint force components and three for the muscle groups (Iglic et al., 1993, Iglic et al., 2002). The hip joint resultant force was 2.4 times BW for an optimum structure of the pelvis in one- legged stance (Iglic et al., 1993, Dostal and Andrews, 1981).

Optimisation was applied for the first time in 1973 to joint reaction and muscle forces (Seireg and Arvikar, 1973). An objective function is either minimised or maximised on the basis of the problem to be solved. It is formulated as either a linear or non-linear function. The constraints imposed on the system are force/moment equilibrium equations, since the system needs to be in static/dynamic equilibrium (Seireg and Arvikar, 1973) and most of the time these are the only ones required.

Seireg and Arvikar's studies deal with the feasibility of such functions as minimizing muscle forces, muscle work to reach to a particular posture, vertical reaction forces at joints and ligament moments at joints using such activities as standing, leaning and stooping (Seireg and Arvikar, 1973). The maximum joint forces for stooping were 3.3 times BW, using ligament moment minimization, weighted moment minimization criteria and the sum of muscle forces. Normal walking was analysed through the extension of this method by using a minimization of the weighted sum of muscle forces and ligament moments at the three joints of the lower extremity (Seireg and Arvikar, 1975). The maximum resultant hip force in the study was 5.4 times the BW. This model used more realistic description of certain muscles as the lines joining the point of origin and the insertion point. In Paul's model, however, a group of muscles was represented by a line between the centroid of the insertions areas. The limitation of this study was that no supplementary realistic constraints (except for equilibrium equations and determining the values of all the variables as non-negative) were placed on the muscle forces (Seireg and Arvikar, 1973, Seireg and Arvikar, 1975).

Heller and his colleagues analysed a linear optimization model to compare the measured and computed cycle-to-cycle hip contact forces (Heller et al., 2001). The objective function was the minimization of muscle forces with the limitations placed on the peak muscle forces. Normal walking (speed 1.08 m/s) and stair climbing were modelled. In both activities the hip contact forces were between 2 – 3 times BW and the calculated forces were both exaggerated.

Rohrle and his colleagues took the minimization of total muscle forces as the objective function (Rohrle et al., 1984). The walking speed was varied in order to investigate the dependence of the hip joint forces. The variation range was 0.8 – 1.6 m/s. Mean hip joint forces were of 2.9 – 6.9 times the BW for altering gait speed. The relationship between the forces and the gait speed with the hip joint forces was linear, increasing with the speed of walking. The dependence of the forces of hip resultant and contact forces has already been demonstrated (Paul, 1970, Crowinshield et al., 1978). Reports concerned with ground reaction forces show the same results (Andriacchi et al., 1977).

Brand and his colleagues examined the contrast of hip joint forces with those from instrumented prosthesis by an endurance mathematical (Brand et al., 1994). Free level walking speeds of 1.11 – 1.36 m/s were investigated. The mean peak aftermath forces were in the range of 2.5 – 3.5 times the BW, which yields a more satisfactory result than those from instrumented prosthesis (peak predicted forces were only 0.5 times BW higher than the measured values). Nevertheless, the measurements were implemented at various times.

Great improvements have been observed in optimisation techniques since they were first utilized and objective functions and constraints have become more intricate. A two-staged optimisation process was introduced in which the utmost muscle stresses were first minimized and then the sum of muscle and joint forces were minimized (Bean et al., 1988, Stansfield et al., 2003). This method engendered a balanced distribution of forces leading to the conclusion that no particular muscle carried excessive stress.

Stansfield and his colleagues used this two-stage optimization process to collect joint forces (Stansfield et al., 2003). The models used were such activities as walking at speeds of 0.97 – 2.01 m/s, rising from a chair, sitting on a chair and 2-1-2 leg stance. For normal walking (1.43 m/s) the mean peak hip joint contact force was around 3.1 times BW. The forces using instrumented prosthesis during first loading, early and late swing and late stance had values far higher than expected. This was due to not modelling the contribution of the antagonistic muscles to the measured forces.

Frayse and his colleagues joint contact measured force was equal to 4.0 times BW for a walking cycle (Frayse et al., 2009). The joint reaction forces were derived by inverse dynamics and then an optimization scheme was made for 9 healthy subjects to acquire hip contact forces by considering the muscle contractions. Minimizing the sum of squared muscle stresses became the objective function. This had already been introduced by Crowninshield and Brand (Crowninshield and Brand, 1981).

The mathematical models are very useful because they can verify the experimental/clinical outcomes as well as parametric studies can (Johnston et al., 1979,

Rohrle et al., 1984, Iglic et al., 1993), as already seen in the dependence of hip joint forces on walking speed. To study the effects of joints, Johnston and his colleagues came up with a mathematical model of the hip joint replacement and effect of a load on it (Johnston et al., 1979). It was observed that the contact forces were proportional to the femoral shaft-prosthetic neck angle. The placing of the acetabular component was found to be of prime significance in reducing the loads with the optimum position placed in the centre “as medially, inferiorly and anteriorly as was anatomically possible”.

It was shown by Iglic and his colleagues that in the one-legged stance the hip muscle resultant force and the hip joint contact forces depend upon the shape of the pelvis. They used their reduction model for this purpose (Iglic et al., 1993). The increase was observed for both parameters with half the inter-hip distance and also for higher laterally inclined hips.

### 2.2.4 Experimental and Clinical Studies

The first person to use an instrumented prosthesis with strain gauges was Rydell. He planned to make the measurements in vivo contact forces (Rydell, 1966). His investigations showed the typical double peak for walking and an increase in contact forces with increasing walking speed, as estimated in the mathematical paradigms discussed earlier. The contact forces were calculated as high as 2.5 times BW during fast walking at a speed of 1.3 m/sec. The result was the same as the force acting while standing on one leg. Rydell studied two patients and found peak forces of 2.3 and 2.9 times BW in the one-legged stance (Rydell, 1966). The values at first peak were 3.0 and 3.3 times BW for walking speeds of 1.1 m/s and 1.4 m/s. This prosthetic contact had to be kept inside the connective tissue and hence had to be folded up again in order to take measurements, a clear disadvantage of using this prosthesis.

Kotzar and his colleagues studied in two patients the activities ranging from walking, to rising from a chair and ascending stairs, etc. (Kotzar et al., 1991). The maximum peak of 5.5 times BW was obtained at a point of instability when one of the patients was trying to stand on one leg. This study also investigated the relationship of the contact forces to speed.

Bergmann and his colleagues investigated with a focus on the hip joint (Bergmann et al., 1993, Bergmann et al., 1995, Bergmann et al., 1997, Bergmann et al., 2001) using instrumented prosthesis. Their work led to the success of other researchers in the development of the field to the point where it is today. They calculated the forces to be



as low as 0.26 times BW (rising from a chair) and as high as 2.6 times BW (going down stairs).

The speed of gait and its dependence on forces was evident in their studies (Bergmann et al., 1993). An increase was observed in the median peak forces with a rise in walking speed (Bergmann et al., 1993, Bergmann et al., 2001). The analysis of gait data, along with hip joint contact forces and ground reactions forces, have been recorded for such human activities as walking, stair climbing, standing up, etc. Bergmann and his colleagues (Bergmann et al., 2001) found the average peak force of 233% of BW (2.33 times BW) with a speed of 1.08 m/s during normal walking. The joint contact forces were 2.52 times the BW when climbing stairs while for descending stairs they were 2.60 times BW. A high load of 8 times BW in the hip joint was monitored during stumbling by the same group (Bergmann et al., 1993). These experiments cannot be compared with normal hips, since they were carried out on patients with medical conditions. The acetabulum and femoral head are usually replaced so they comprise the natural configuration of the joints. However, the results of the clinical studies were similar to the results which were predicted by the analytical studies. The difference was in the contact forces at the hip, measured using instrumented prosthesis. These forces have usually been found to be lower than those found by analytical investigations (Bergmann et al., 1993, Brand et al., 1994).

### **2.3 Joint simulators**

In the past variety of articular joint simulators platforms have been designed to be applied in medical applications. In this study a review of the available approaches is presented for the case of controlled joint motion simulators. The initial simulation systems did not use the active control approaches; however, these previous works worth mentioning as it would reveals the constraints of the systems and provokes further researches to the recent ones. In addition they create a foundation for the novel systems.

The simulation of joints has been done for various joints. The reason is that it has a widespread use in the field of clinical biomechanics, hence the following lines deals with the history of joint motion simulator and the existing control methodologies.

The systems which were developed in the 1950s were analogous to the recent systems. In 1953, Hicks developed a system which simulated the alteration of a foot under load (Hicks, 1953). The developed system acted as most of the current simulators in which a bone is attached firmly to the actuators. The advantage of the earlier system is that it simulates the application of a body with considerable weight. In other words, the platform could move relative to the load. Systems without a weight attached to them were used to apply loads of not more than 90 kilograms to the tendons. These systems could work only with constant loads, as they were adapted to simple load alteration.

The next generation of simulators appeared in the 1970s (Shaw and Murray, 1973). The aim of having a system with a safety measure between prosthesis development and clinical transplantation led to the production of a knee simulator. Shaw and Murray

came up with a list giving the test results for different motion, prosthesis wear, lifespan and joint stability. It was also noted that the simulator acted approximately not accurately, since it was unable to take into account certain factors, such as the body's tolerance or mechanical acting because of the bone growth. This growth becomes problematic since it occurs around the prosthesis.

The early papers on simulators included down-to-earth methods of joint motion simulator and its constraints. In other words, these papers not only included the strengths of the joint motion simulator but also noted where it was ineffective. Further details were presented regarding knee simulators which were intended to analyse the prosthesis orientation faults. The femur and tibia were inserted via two metal tube sockets, resulting a tool for fixing part of a leg. These sockets are usually more limited than physiologically dynamic joint motion simulator. These physiologic dynamics would be added in the next steps. A good deal of weight was added to the socket which was in conjunction with the femur. The researcher could adjust the distribution of the load by a universal joint between it and the socket. The tibia socket acted as the ankle joint. An active hydraulic cylinder made it possible to bend and extend the knee. Control cycle velocity, rotation limits and some other characteristics of the cycle were governed by valves through a relay logic circuit. This paper was significant because it proposed the first models of a simulator which provides feedback control with switches enabling the system to determine the range of movement and signalling to reverse the direction. This signal was in fact the feedback signal.

A paper by Swanson et al. was released one month after Shawn and Murray's. (Swanson et al., 1973). The system affected an important class of joint motion simulators, examining the wear on products in regular conditions. This debris may have been hazardous to human health. In addition, this system could load in cycles. Swanson et al. gathered all the fragments of the metal which was produced during the examination. They did this by soaking the implanted prosthesis in a temperature-controlled bath. The testing was concerned with the environment of the prosthesis as well as controlling the loading application. The tests were performed in 1 Hz. The frequency was slightly smaller than the ultimate speed. The loads were applied by a 750 watt electric motor. The forces in the joints were monitored and stored to enable the calculation of frictional forces and the moments on the prosthesis to be made.

The accuflexor allowed knee simulations such as walking or using stairs. These actuators were developed to be similar to a slider crank, with the hip acting as the slider and the tibia, the crank and the femur allowing the application of four weights. The first weight was along the slider or hip axis. The second weight was on the upper parts of the leg down to the tibia. The third was a rotation-enabling weight and the fourth was aimed to simulate the sliding of the foot. The combination of load and force control was used to help the system act in any desired trajectory. This system had in fact two objectives: the first was to do a wear test while the second was to yield a clarification of the kinematic of the structure near the joints for use in various prosthesis. The second goal dealt with monitoring the effects of prosthesis in the movements involved in a major type of knee simulator. Today this major simulator has evolved into a better modified system through much redesigning in the last few decades.

Investigations on the designed simulators within the last three decades (Pappas, 1979) illustrate that the progression and development of the systems have been substantial, for example in Hick's system or the system which was actively developed in Purdue with a combination of force and displacement control. Among the four systems, it can be inferred that there are two general types of joint motion simulators: non-physiological wear testers and physiological dynamic simulators.

In the 1980s, Rastegar et al. developed an ankle simulator powered by a hydraulic drill press (Rastegar et al., 1980). The hydraulic press mechanism was used in a lower leg part by applying loads. The loads were calculated by a dynamometer attached to the foot. The system could easily rotate along the ankle axis and be fixed into place by minimum resistance, due to the multiple degrees of freedom in the position of the load and the limited constraint of the ankle. This resulted in a system which was categorized as a non-physiological motion. The data were for the first time collected by a computer for such systems.

Another knee replacement wear tester was presented by Treharne in 1981 (Treharne et al., 1981). Hydraulic systems were controlled by a computer to test different types of prosthesis. The computer provided high loads and quick responses. The feedback of the system was LVDTs (Load cells and linear variable differential transducers). In contrast to cam- driven simulators, the various types of load could be applied to the system. The studied cases were the worst ones. Depending on the condition of human body, the wear simulator was more focused on the physiologic qualities than its dynamic features.

Taking into account those qualifications of the system, a supervised calf serum bath was introduced to simulate the frictions and regulate the heat accordingly.

Another simulator was introduced in 1983 by Ahmed and Bruke (Ahmed, 1983). The main objective of their knee simulator was to assess pressure allotment on the tibial extension. There was no concern with the full extension of bending because the system permitted different kinds of load or the needed joint torque over the angles of the knees. Actuation included merely a hydraulic structure, without any control systems.

A few years later a system with nine actuators was introduced by Gillison (Gillison, 1991). It was a remarkable system because it became an example of a model based control system for the next generation of systems. The displacement feedback minimized the error and load controls opponents to give solidity.

Szklar and Ahmed published a paper in 1987 on the development of a new broad dynamic knee simulator (Szklar and Ahmed, 1987). The dynamic response of the system was investigated to enable a more intense study of body tissues as well as the motion of the knee joints. The system was actuated in the expansion and bending movements only, while it was designed as an unconstrained system. Two cables were included in the system for the flexor and extensor actuators. The frequency of the system was 1.25 Hz, working in harmony by copying the movements of the agonist or in opposition to its co-activation. The feedback had two major features. First, pressure was provided by transducers and, second, it used velocity to signal the system. This

simulator was updated to make foot and floor reactions possible (McLean and Ahmed, 1993). This ability was self-sufficient for the loads.

Joint motion and ligament stretch simulation were carried out in the work of Lewis et al in 1988 (Lewis et al., 1988). Joints tolerated the loads and moments were applied about the tibia. The measuring was done in the system by cables being stretched as the tibia and a firmly fastened femur. Feedback checked the load presence. The force of gravity was discounted by a counterbalance system, making it an exceptional model. The plane was considered to be aligned with the ground surface.

To sum up, data collecting in 1980s took on a standard format because the progress on the knee joint motion simulators was substantial. In addition, loading and displacement models were tested by means of computers. However, there was no standard definition in this decade for the feedback.

The closed loop feedback became more popular in 1990s. A novel system was presented in a paper by Berns et al. (Berns et al., 1990). The system's first experiments were designed to test flexion angles ranging from a full extension to 45°. The determination of angles for a fixed bending state could justify the development of a JSM for testing the elasticity of the knee. The corrected range of knee motions and load applications was feasible with further improvements by Bach and Hull (Bach and Hull, 1995).

The system of Di Angelo et al. (Schopfer et al., 1994) was capable of loading the hip. The test was launched initially from many angles in regard with the femoral extension and used a method to keep the acetabulum fixed. The loading occurred periodically to permit the JSM system to have a stable fixation method and to be tested at the same time. The maximum force was 550 N, which was exercised over the femur resisting to the point of breakdown of the prosthesis.

The structure of current system was developed in 1993 by King et al. (King et al., 1993). The essence of their work was to simulate and test the stability of the elbow under a load. The rotating arms allowed various simulations. The humerus was protected by a jig through the cables attached to the biceps, brachialis and triceps tendons. The advance of the system lay in the ease of adding more muscle and more active control to the elbow simulator. In addition, the system was unique in its integration of active control for subsequent simulators, though this was not included in the first one.

Researchers in Johns Hopkins University (MacWilliams et al., 1999) were the next to investigate a comparison of native and substituted knees in a fully computer controlled situation. The work of McWilliams et al. was presented as considering the control of the load and the actuators, which simulated the hip position, quadriceps muscles, or hamstring muscles. This system was analogous to that of Povlovic et al. except for the position of the ankle, which lacked the horizontal, and a closed loop control system. During the control of the closed loop cycle the foot position could be varied.



Wuelker et al. developed a system in 1995, using more active control than Cain et al. Pneumatic actuators were placed to form a deltoid and rotator cuff simulation (Wuelker et al., 1995). This shoulder simulator took advantage of the relationships between cross sectional areas of the muscles to orient the arm assessing by six ultrasonic sensors.

Introducing feed forward, a combination of feed forward and feedback, became essential for the body of the system with lags and movement speed. This was a novel change made by Stroeve (Stroeve, 1997).

The load of these computer-controlled loading systems was assessed by strain gauges. The step and cycling motions were applied via three degrees of freedom goniometer to measure the angular displacement of the hand. Force feedbacks were applied on muscles to make the trajectory motion more precise. In contrast, the old systems used displacement control. The simulator was capable of simulating small movements such as those of the wrist.

A knee prosthesis wear tester was presented by Walker et al. (Walker et al., 1997). This system was developed to make a run of millions of cycles feasible when necessary. The measurement could entail 30 million cycles. At the same time, awareness of the load rather than displacement became more marked than ever; thus wear testers evolved into more robust models and in different assortments. Ignoring the load specified method could make the problem more convoluted because of the need to produce an independent displacement profile for each.

A servo-hydraulic six-station knee wear simulator was another system presented by Burgess et al. giving the power to test six knees at once (Burgess et al., 1997). This unique quality made the system perfect for long simulations in terms of months.

A foot joint motion simulator was developed in Penn State University by Sharkey and Hamel. The simulation of loading in the state of gait was successfully developed by a closed loop force control, while feedback loops were derived from EMG measurements. The peak of tensions (muscle tension) were precisely compared and specified (such as triceps surae muscle) for the sake of profile-scaling, letting the whole system calculate the remaining tensions (Sharkey and Hamel, 1998).

Another simulator was designed by Li et al. (Li et al., 1999). There are many hints that this system was the first to use 6 DOF robots to make a joint move. The femur was tightly attached to the robot. The tibia was powered by a 6 DOF load cell. Loads were made to hold the leg at various angles while the anterior cruciate ligament (ACL) present were evaluated and registered. The ACL was then removed. By comparing the ACL to the normal case, it became possible to determine the forces.

Computer control systems became the standard for joint motion simulators in the 1990s. Knee simulators were still the most distinguished; nonetheless simulators existed for elbows, wrists shoulders, ankles and hips. In this period a transition from passively loaded static mechanisms was observed.

Joint motion simulators in recent years have exploited closed-loop feedback systems and are completely dependent on the computer. The most significant work on elbow joint motion simulator was published from the University of Western Ontario in the 2000s.

An elbow motion simulator was developed and refined by adding displacement control to the force control (Dunning et al., 2003). The brachialis and biceps were specified for primary movers, using displacement controlled approaches. This allowed the other three of these muscles to function under load control. Linear resistive transducers (LRTs) were integrated to the system to create the displacement feedback to a PID controller managed by LabVIEW.

In 2005 the progress of knee joint motion simulators continued. Maletsky and Hillberry developed a knee joint motion simulator with displacement and managed control more comprehensively (Maletsky and Hillberry, 2005). Before this, most knee simulators had implemented forces at frequencies which were suitable for simulating walking or stair climbing. In Maletsky's work, the objective was to develop a simulator capable of applying forces at frequencies closer to those for more violent activities so that the designed prosthesis could be used with younger patients.

The system offered a lower extremity from the hip downwards. The hip could move upright on a sled and spin around a pin joint attached to the sled. Quadriceps force was provided by a linear actuator attached to the femur. A ball joint was added at the ankle

which resulted three more degrees of freedom. There were three goals in the development of this simulator, which illustrated the broad range of its use: estimation of the ankle bending moment effect on knee loading, measurement of forces on the knee while simulating walking and testing of cross coupling between the knee bending angle and the other axes.

Displacement control of the quadriceps was involved in the control of the system with the rest of the muscles under load control. The design and implementation of the controller was done in LabVIEW. The frequency of operation was approximately 5 Hz.

The use of joint motion simulators goes back over more than 50 years. Simulator developments have been driven by the need to actuate body types in physiological conditions, to clarify the effects of prosthesis. Computer control has greatly helped to tackle the problems of testing parameters and repeatability, thus today it is unlikely that a system without a computer controlled joint motion simulator could generate the most clinically related data.

There are several current two-dimensional hip joint simulators which each use different force track patterns during the gait cycle. Some of these are given in the force track analysis of contemporary hip simulators (Calonius and Saikko, 2003). Evidently, some of these are very simplified models, running in very regular patterns including circular, sinusoidal and linear. During the human gait cycle, such patterns do not occur this way as human movements are much more irregular and can be linear or nonlinear. For an accurate simulation of movement it is necessary to collect data from the subject during a

cycle and take relevant readings at given time intervals during it. If the data acquired in this way are replicated, the simulation of movement achieved will be closer to the actual movement to which the replacement joint will be subjected. Moreover, no joint moves in a truly two-dimensional way, therefore three-dimensional simulations are more life-like.

### **Chapter 3. Theory of Stewart Platform**

This project aims at simulating the movement of the hip joint during walking. Therefore, a mechanical rig and scheme are needed, for which the Stewart Platform has been chosen in this project. This mechanical simulator is considered the most feasible and most effective device to simulate joint motion. Since many projects have been performed with the use of a Stewart Platform, a large wealth of information is readily available to aid in the design and function of the one for this project.

The development of the Stewart Platform can be divided into three phases. The first consists of a literature review of the general Stewart Platform theory, which includes the review of the existing uses for the Stewart Platform, the applications of the study of parallel-link chains and the kinematics and control schemes. In the second phase, the platform was modified to achieve the desired specifications for its intended use. The design and construction of the Stewart Platform comes in the third phase. This phase involved the design of the base and platform plates and the design of the joints and holders for the placing of the electromagnetic actuators.

The Stewart Platform is a member of the family parallel manipulators. These are closed loop mechanisms in which the two bodies (base and platform) are connected by independent kinematic chains actuated in parallel. This configuration allows the manipulator to have “greater rigidity and superior positioning capability” (Dasgupta and Mruthyunjaya, 2000). Other advantages of this type of mechanism include fast dynamic

response and a large load-to-weight ratio. They also have their disadvantages. Fong (Fong, 1990) mentions the restriction of the workspace due to the parallel links; the manoeuvrability and range of motion is much smaller than with open kinematic chains and, given the equivalent amount of hardware and approximately close to singular points, manipulator loading may result in excessive tensile/compressive actuator stresses.

The structure known as Stewart Platform as its origins in the design by D. Stewart, of a 6 degrees-of-freedom (DOF) which simulated flights conditions by generating general motion in space. His mechanism consisted of “a triangular platform supported by ball joints over three legs of adjustable lengths and angular altitudes connected to the ground through two-axis joints” (Dasgupta and Mruthyunjaya, 2000).

The platform became a fully parallel-actuated mechanism with the use of six linear actuators in parallel, as suggested by V. E. Gough. These actuators are connected to the base by universal joints and by spherical joints to the platform. This is the Universal Prismatic Spherical (UPS) configuration. Alternatively the actuators can be connected to both the base and platform by spherical joints (SPS). 6-UPS and 6-SPS manipulating structures are identical to each other with respect to the input output relationship and they are also both actuated at six prismatic joints of the legs. The difference between them is that the 6-SPS has six passive DOFs about its axis corresponding to the rotation of each leg (Dasgupta and Mruthyunjaya, 2000).

### 3.1 Geometric Analysis of Stewart Platform

The general Stewart Platform consists of two bodies connected by six links. The system is “topologically symmetrical” (Fong, 1990) and one of the bodies (normally the lower one) is called the base and the other is then called the platform, with one end of each link located in each of the bodies.

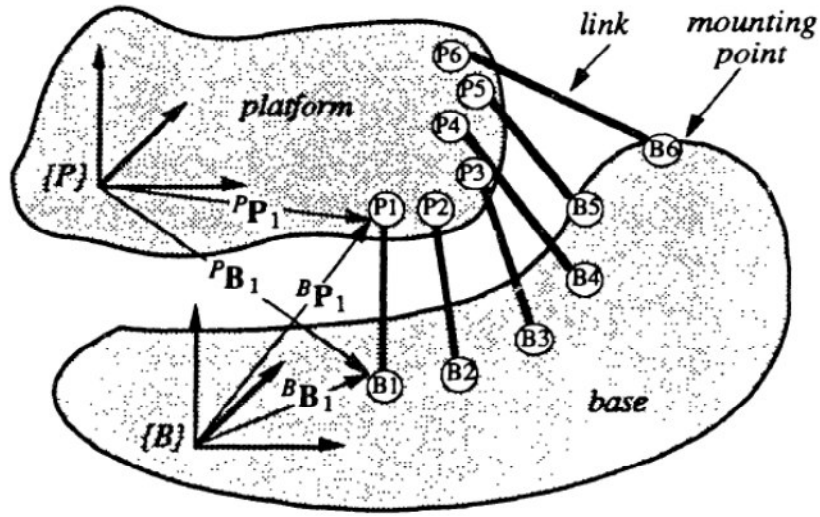


Figure 3.1 General Stewart Platform. (Fong, 1990)

A coordinate frame is attributed to the base (B) and to the platform (P). Vectors to these coordinate frames describe the mounting points in each body, as shown above. The design of the Stewart Platform for this project was based on a paper by Azevedo et al. (Azevedo et al., 2008) in which the authors consider the inverse and the forward kinematic for the platform and provide methods to deal with architectural singularities for any given Stewart Platforms. What follows is a description of their study.



If the base plate and the platform plate are identical regular hexagons placed on top of each other, extra degree of freedom will cause the system to slide and collapse which is independent from the lengths of the six legs. While here the architecture is singular, therefore, configurations may be obtained which do not allow for the determination of the position of the platform by fixing the lengths of the legs.

This problem can be avoided by modifying the hexagonal plates to what is shown in Figure 3.2, where the platform is a rescaled and rotated copy of the base.

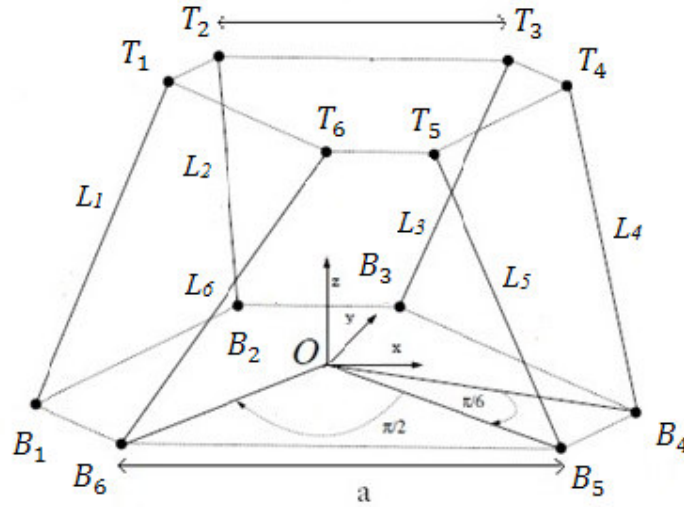


**Figure 3.2 General Stewart Platform (Azevedo et al., 2008)**

The platform in Figure 3.2 shows that the coordinate systems  $O$  and  $O'$  are fixed to the base and the mobile platforms. Vectors  $L_i, i = 1, 2, \dots, 6$  describe the platform geometry and are defined by  $L_i = T_i - B_i, i = 1, 2, \dots, 6$ , where  $B_i$  and  $T_i$  are the base and top coordinates, respectively. Nevertheless, this configuration may still have singularities

which must be taken into account when designing a Stewart Platform. If the singularities are not outside the working area, they will affect the behaviour of the platform. If the singularity trajectories were not detected and sliding along these trajectories occurs, they could cause the platform to collapse. The order of magnitude of the errors in the determination of the lengths of the six legs and in the joints may be considered negligible.

With this assumption, the mechanical problems caused by the lack of total precision in the components can be ignored and it is possible to formulate a working hypothesis which states that “in order for a Stewart Platform to become uncontrollable, there has to exist a continuum of positions of the top platform corresponding to the same (fixed) values of the leg lengths” (Azevedo et al., 2008).

### **3.1.1 The Inverse Problem: lengths as a function of position**

This Stewart Platform has six degrees of freedom and the centre of the top platform is given by the coordinates  $x, y, z$ . The Euler angles *pitch*, *roll* and *yaw* define the inclination of the top platform relative to the base. The reference point is taken at the centre of the circle which passes at all six points of the base. This circle is given a radius of 1 and thus the coordinates of the six points in the base where the legs are supported are given by:

$$B_1 = \left( \cos \frac{\pi}{12}, \sin \frac{\pi}{12}, 0 \right) \quad [3.1]$$

$$B_2 = \left( \cos \frac{7\pi}{12}, \sin \frac{7\pi}{12}, 0 \right) \quad [3.2]$$

$$B_3 = \left( \cos \frac{9\pi}{12}, \sin \frac{9\pi}{12}, 0 \right) \quad [3.3]$$

$$B_4 = \left( \cos \frac{15\pi}{12}, \sin \frac{15\pi}{12}, 0 \right) \quad [3.4]$$

$$B_5 = \left( \cos \frac{17\pi}{12}, \sin \frac{17\pi}{12}, 0 \right) \quad [3.5]$$

$$B_6 = \left( \cos \frac{23\pi}{12}, \sin \frac{23\pi}{12}, 0 \right) \quad [3.6]$$

The top platform and the base are related by a yaw rotation of  $\pi$  and a  $\frac{2}{3}$  rescaling factor.

The points on the base plate would be translated to the top plate by a transformation matrix called  $R$ . The following angles  $\psi$ ,  $\theta$  and  $\phi$  are related to  $X$ ,  $Y$ , and  $Z$  respectively. Therefore the matrix  $R$  can be used to find the corresponding points in the top platform. In matrix  $R$ ,  $x, y, z$  represent the coordinates of the centre of the top platform and  $\psi$ (roll),  $\theta$ (pitch) and  $\phi$ (yaw) are the Euler angles which are used to rotate the position of the center of platform. The following matrix represents the  $R$ :

$$R = \begin{bmatrix} \frac{-2\cos(\psi)\cos(\theta)}{3} & \frac{-2(-(\cos(\phi)\sin(\psi) + \cos(\psi)\sin(\theta)\sin(\phi)))}{3} & \frac{-2(\cos(\psi)\cos(\phi)\sin(\theta) + \sin(\psi)\sin(\phi))}{3} \\ \frac{-2\cos(\theta)\sin(\psi)}{3} & \frac{-2(\cos(\psi)\cos(\phi) + \sin(\psi)\sin(\theta)\sin(\phi))}{3} & \frac{-2(\cos(\phi)\sin(\psi)\sin(\theta) - \cos(\psi)\sin(\phi))}{3} \\ \frac{-2\sin(\theta)}{3} & \frac{2\cos(\theta)\sin(\phi)}{3} & \frac{2\cos(\theta)\cos(\phi)}{3} \end{bmatrix} \begin{bmatrix} x \\ y \\ z \\ 1 \end{bmatrix} \quad [3.7]$$

By multiplying the above matrix in the matrix of the position of the aimed point, the corresponding point in the top platform would be calculated. It should be mentioned that, because the top platform have been rotated by  $\pi$ , thus to find the for example point  $B_4$  in the top plate, the coordinates of  $B_1$  must be multiplied in the matrix  $R$  as  $B_1$  and  $B_4$  are different in  $\pi$ .

In order to find the length of the actuator of the rig, the position of point in top plate must be subtracted of the position of point in the base plate.

The leg lengths are calculated with the norms of the vectors as follows:

$$\begin{aligned} \mathbf{L}_1 &= R(\mathbf{B}_4) - \mathbf{B}_1, \mathbf{L}_2 = R(\mathbf{B}_5) - \mathbf{B}_2, \mathbf{L}_3 = R(\mathbf{B}_6) - \mathbf{B}_3, \mathbf{L}_4 = R(\mathbf{B}_1) - \mathbf{B}_4, \mathbf{L}_5 = \\ &R(\mathbf{B}_2) - \mathbf{B}_5, \mathbf{L}_6 = R(\mathbf{B}_3) - \mathbf{B}_6. \end{aligned}$$

With  $L_i, i = 1, \dots, 6$ , the norms, the following formulae is obtained:

$$\begin{aligned}
& |L_1(x, y, z, \psi, \theta, \phi)|^2 \\
&= \left( \frac{-(1 + \sqrt{3})}{2\sqrt{2}} + x + \frac{\sqrt{2} \cos(\psi) \cos(\theta)}{3} \right. \\
&\quad \left. + \frac{\sqrt{2}(-(\cos(\phi) \sin(\psi) + \cos(\psi) \sin(\theta) \sin(\phi)))}{3} \right)^2 \\
&\quad + \left( \frac{-(-1 + \sqrt{3})}{2\sqrt{2}} + y + \frac{\sqrt{2} \cos(\theta) \sin(\psi)}{3} \right. \\
&\quad \left. + \frac{\sqrt{2}(-(\cos(\psi) \cos(\phi) + \sin(\psi) \sin(\theta) \sin(\phi)))}{3} \right)^2 \\
&\quad + \left( z + \frac{\sqrt{2} \sin(\theta)}{3} - \frac{\sqrt{2} \cos(\theta) \sin(\phi)}{3} \right)^2 \tag{3.8}
\end{aligned}$$

$$\begin{aligned}
& |L_2(x, y, z, \psi, \theta, \phi)|^2 \\
&= \left( \frac{-(1 + \sqrt{3})}{2\sqrt{2}} + x + \frac{(-1 + \sqrt{3}) \cos(\psi) \cos(\theta)}{3\sqrt{2}} \right. \\
&\quad \left. + \frac{(1 + \sqrt{3})(-(\cos(\phi) \sin(\psi) + \cos(\psi) \sin(\theta) \sin(\phi)))}{3\sqrt{2}} \right)^2 \\
&\quad + \left( \frac{-(1 + \sqrt{3})}{2\sqrt{2}} + y + \frac{(-1 + \sqrt{3}) \cos(\theta) \sin(\psi)}{3\sqrt{2}} \right. \\
&\quad \left. + \frac{(1 + \sqrt{3})(\cos(\psi) \cos(\phi) + \sin(\psi) \sin(\theta) \sin(\phi))}{3\sqrt{2}} \right)^2 \\
&\quad + \left( z + \frac{(-1 + \sqrt{3}) \sin(\theta)}{3\sqrt{2}} - \frac{(1 + \sqrt{3}) \cos(\theta) \sin(\phi)}{3\sqrt{2}} \right)^2 \tag{3.9}
\end{aligned}$$

$$\begin{aligned}
& |L_3(x, y, z, \psi, \theta, \phi)|^2 \\
&= \left( \frac{1}{\sqrt{2}} + x - \frac{(1 + \sqrt{3}) \cos(\psi) \cos(\theta)}{3\sqrt{2}} \right. \\
&\quad \left. + \frac{(-1 + \sqrt{3})(-\cos(\phi) \sin(\psi) + \cos(\psi) \sin(\theta) \sin(\phi))}{3\sqrt{2}} \right)^2 \\
&\quad + \left( -\left(\frac{1}{\sqrt{2}}\right) + y - \frac{(1 + \sqrt{3}) \cos(\theta) \sin(\psi)}{3\sqrt{2}} \right. \\
&\quad \left. + \frac{(-1 + \sqrt{3})(\cos(\psi) \cos(\phi) + \sin(\psi) \sin(\theta) \sin(\phi))}{3\sqrt{2}} \right)^2 \\
&\quad + \left( z - \frac{(1 + \sqrt{3}) \sin(\theta)}{3\sqrt{2}} - \frac{(-1 + \sqrt{3}) \cos(\theta) \sin(\phi)}{3\sqrt{2}} \right)^2 \quad [3.10]
\end{aligned}$$

$$\begin{aligned}
& |L(x, y, z, \psi, \theta, \phi)|^2 \\
&= \left( \frac{1}{\sqrt{2}} + x - \frac{(1 + \sqrt{3}) \cos(\psi) \cos(\theta)}{3\sqrt{2}} \right. \\
&\quad \left. - \frac{(-1 + \sqrt{3})(-\cos(\phi) \sin(\psi) + \cos(\psi) \sin(\theta) \sin(\phi))}{3\sqrt{2}} \right)^2 \\
&\quad + \left( -\left(\frac{1}{\sqrt{2}}\right) + y - \frac{(1 + \sqrt{3}) \cos(\theta) \sin(\psi)}{3\sqrt{2}} \right. \\
&\quad \left. - \frac{(-1 + \sqrt{3})(\cos(\psi) \cos(\phi) + \sin(\psi) \sin(\theta) \sin(\phi))}{3\sqrt{2}} \right)^2 \\
&\quad + \left( z - \frac{(1 + \sqrt{3}) \sin(\theta)}{3\sqrt{2}} - \frac{(-1 + \sqrt{3}) \cos(\theta) \sin(\phi)}{3\sqrt{2}} \right)^2 \quad [3.11]
\end{aligned}$$

$$\begin{aligned}
& |L_5(x, y, z, \psi, \theta, \phi)|^2 \\
&= \left( \frac{-1 + \sqrt{3}}{2\sqrt{2}} + x + \frac{(-1 + \sqrt{3}) \cos(\psi) \cos(\theta)}{3\sqrt{2}} \right. \\
&\quad \left. - \frac{(1 + \sqrt{3})(-\cos(\phi) \sin(\psi) + \cos(\psi) \sin(\theta) \sin(\phi))}{3\sqrt{2}} \right)^2 \\
&\quad + \left( \frac{1 + \sqrt{3}}{2\sqrt{2}} + y + \frac{(-1 + \sqrt{3}) \cos(\theta) \sin(\psi)}{3\sqrt{2}} \right. \\
&\quad \left. - \frac{(1 + \sqrt{3})(\cos(\psi) \cos(\phi) + \sin(\psi) \sin(\theta) \sin(\phi))}{3\sqrt{2}} \right)^2 \\
&\quad + \left( z + \frac{(-1 + \sqrt{3}) \sin(\theta)}{3\sqrt{2}} + \frac{(1 + \sqrt{3}) \cos(\theta) \sin(\phi)}{3\sqrt{2}} \right)^2 \tag{3.12}
\end{aligned}$$

$$\begin{aligned}
& |L_6(x, y, z, \psi, \theta, \phi)|^2 \\
&= \left( \frac{-(1 + \sqrt{3})}{2\sqrt{2}} + x + \frac{\sqrt{2} \cos(\psi) \cos(\theta)}{3} \right. \\
&\quad \left. - \frac{\sqrt{2}(-\cos(\phi) \sin(\psi) + \cos(\psi) \sin(\theta) \sin(\phi))}{3} \right)^2 \\
&\quad + \left( \frac{-1 + \sqrt{3}}{2\sqrt{2}} + y + \frac{\sqrt{2} \cos(\theta) \sin(\psi)}{3} \right. \\
&\quad \left. - \frac{\sqrt{2}(\cos(\psi) \cos(\phi) + \sin(\psi) \sin(\theta) \sin(\phi))}{3} \right)^2 \\
&\quad + \left( z + \frac{\sqrt{2} \sin(\theta)}{3} - \frac{\sqrt{2} \cos(\theta) \sin(\phi)}{3} \right)^2 \tag{3.13}
\end{aligned}$$

### 3.2 Calculate motion geometry by markers

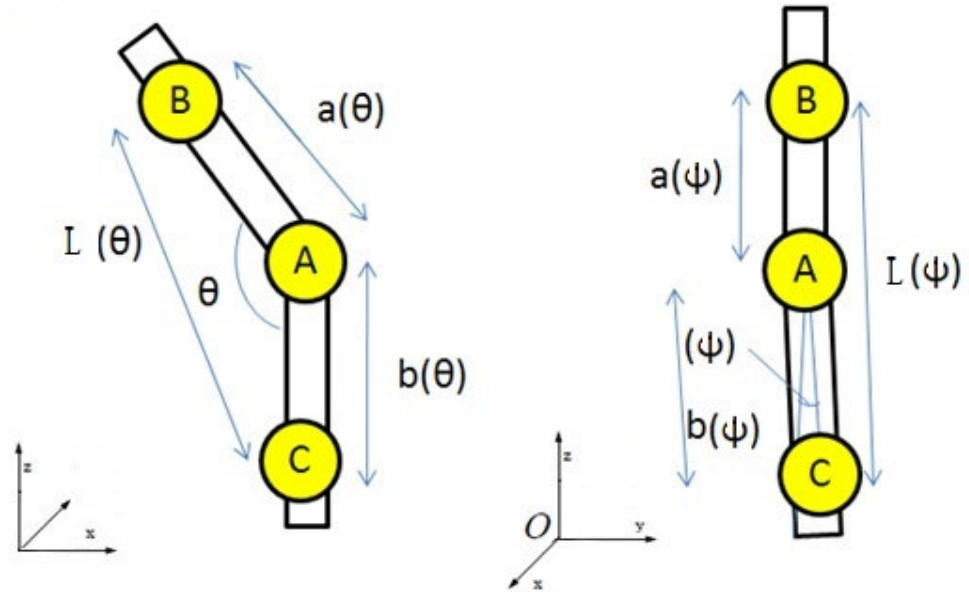


**Figure 3.3** Locations of measured points on and around joint a) Right View and b) Front View

To obtain data on a joint it is necessary to monitor the coordinates for the central location of the joint given by A in Figure 3.3, an arbitrary location on one connecting bone and another arbitrary point on the other connecting bone given by points B and C. The three spatial coordinates of each of these should be measured at every time interval



during the performance of the activity. This data can be used to determine the angles theta  $\theta$  and psi  $\psi$ .

This is done by calculating the lengths a, b and L for  $\theta$  and  $\psi$  using

$$a(\theta) = \sqrt{(xA - xB)^2 + (zA - zB)^2} \quad [3.14]$$

$$b(\theta) = \sqrt{(xC - xB)^2 + (zC - zB)^2} \quad [3.15]$$

$$L(\theta) = a(\theta)^2 + b(\theta)^2 - 2a(\theta)b(\theta)\cos(\theta) \quad [3.16]$$

$$a(\psi) = \sqrt{(yA - yB)^2 + (zA - zB)^2} \quad [3.17]$$

$$b(\psi) = \sqrt{(yC - yB)^2 + (zC - zB)^2} \quad [3.18]$$

$$L(\psi) = a(\psi)^2 + b(\psi)^2 - 2a(\psi)b(\psi)\cos(\psi) \quad [3.19]$$

Then applying the Cosine Rule to relevant angles would lead to:

$$\theta = \cos^{-1}\left(\frac{a(\theta)^2 + b(\theta)^2 - L(\theta)^2}{2a(\theta)b(\theta)}\right) \quad [3.20]$$

$$\phi = \cos^{-1}\left(\frac{a(\psi)^2 + b(\psi)^2 - L(\psi)^2}{2a(\psi)b(\psi)}\right) \quad [3.21]$$

The platform is arranged such that lengths 2→3, 4→5 and 6→1 are 0.16326530 times that of lengths 1→2, 3→4 and 5→6.

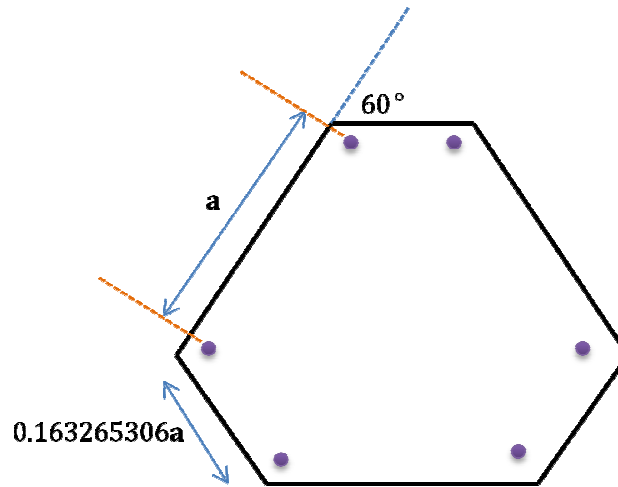


Figure 3.4 Plate ratio

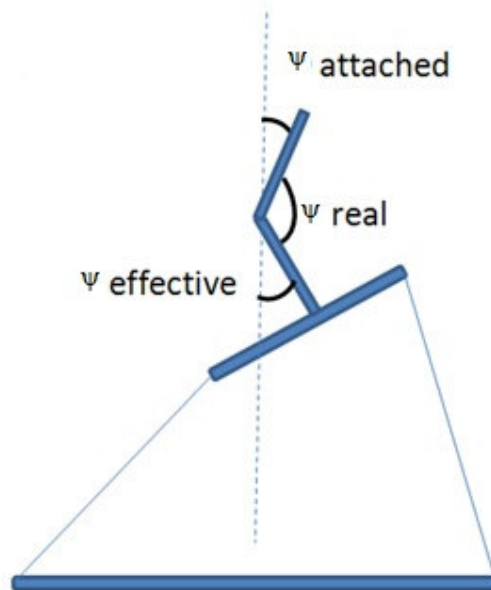


Figure 3.5 Real, effective and attached angles of platform

As expected from looking at the diagram, for any instance the sum of these angles is  $\pi$  radians. The corresponding  $\psi$  angle and three spatial coordinates of the top plate to achieve this motion are then calculated in the programming code.

In this project, the data used for walking and running are taken from (Hamill and Knutzen, 2009, Cavanagh, 1990) in two dimensions; the third dimension is calculated by using of a Sine wave approximation tailored to the nature of the joint. The set of data used is given in the Appendix 2. The attachment angle used is that of the hip joint for walking, as the focus point in this project.

The code calculate the angle  $\varphi$  necessary for the top of the moving bone to remain in the same location and the spatial coordinates of the centre point of the platform relative to the centre of the base plate. If the modulus of  $\psi$  was greater than that of  $\theta$  then the value of the phi would be  $\varphi = \frac{\tan\theta}{\tan\psi}$ , in contrast if the value of  $\psi$  was smaller,  $\varphi = \frac{\tan\psi}{\tan\theta}$ .

The coordinates of the centre point are calculated these three angles by working out their x, y and z displacements from the contact point of the bones according to the length of the moving bone using:

$$x(13) = x(14) + \frac{l(2)}{\sqrt{1 + 1/\tan^2\varphi + 1/\tan^2\theta}} \quad [3.22]$$

$$y(13) = y(14) - \frac{l(2)}{\sqrt{1 + \frac{1}{\tan^2 \psi} + \frac{1}{\tan^2 \phi}}} \quad [3.23]$$

$$z(13) = z(14) - \frac{l(2)}{\sqrt{1 + \tan^2 \theta + \tan^2 \psi}} \quad [3.24]$$

The positive and negative signs are adjusted according to the signs of  $\theta$  and  $\psi$ . These formulas will be used for calculation of the coordinate of the plate by use of coordinate of the centre of the smaller sphere which plays the role of head of femur which is called HF in this study.

These measurements to be processed in this way can be taken using three dimensional instrumentation including Segmental Kinesiological Analysis, Goniometers, Electromagnetic and Acoustic Sensors, Photogrammetric Reconstruction, Accelerometers and Dynamic Force Estimates among other methods. This can be done with fixed or moving cameras depending on user preference and activity, which is available in the book called “Three-Dimensional Analysis of Human Movement” (Dumbleton, 1981). In this project due to complications encountered during the motion capture work, it was decided to use published kinematics and kinetics data. However the above section is included for those intending to follow this work.

As it has been explained before, by use of matrix R position of the top plate can be identified according to the coordinates of the centre of the plate and Euler angles. Since the position of the centre of the top plate is not identified, more information is required

to calculate the coordinate of the centre of plate. The location of this point is important in order to calculate of the actuators length. Because transformation matrix by use of Euler angles and coordinate of the centre of the top plate can calculate the length of the actuators.

The following figure shows the simplified structure of relationship between actuators, top plate, arm, and two spheres.

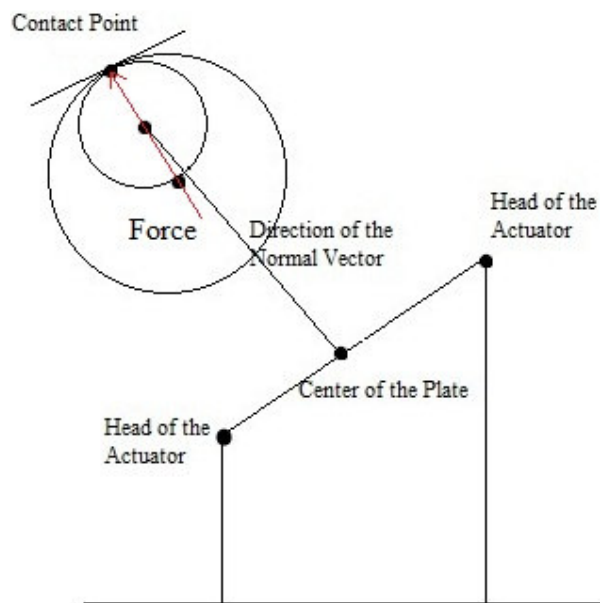


**Figure 3.6 Force direction**

As shown on the above figure, the contact force has to go through the centre of the both circles; the bigger circle is the socket and the smaller one representing the ball representation of the hip joint. Since the bigger sphere is assumed to be fixed, if the

direction of the force was identified the coordinate of the centre of the ball would be calculated.

In Figure 3.6 the small sphere (ball) is the representation of the head of the femur (**CF**) with the radius of  $r$  and the bigger sphere is for the hip joint with centre of the socket (**CJ**) with radius of  $R$ .

By use of three strain gauges inserted on the metal plate attached to the hip, the force components can be calculated as it will be explained later. Therefore, as explained before this vector has to go through the centre of the both circle, the vector  $\vec{m}$  is defined as the normal vector of the force which shows the direction of the force. Consequently, the coordinate of the normal vector of the contact force would be calculated:

$$\vec{m} = (\vec{f}_x + \vec{f}_y + \vec{f}_z) / \sqrt{(f_x^2 + f_y^2 + f_z^2)} \quad [3.25]$$

Coordinate of the centre of bigger circle:

$$\mathbf{CJ}(x_{CJ}, y_{CJ}, z_{CJ})$$

The coordinate of the contact force point would be:

$$\mathbf{CF}(x_{CF}, y_{CF}, z_{CF}) = \mathbf{CJ}(x_{CJ}, y_{CJ}, z_{CJ}) - (R - r)\mathbf{m} \quad [3.26]$$

### 3.3 Force Feedback Motion

Once the femur head was driven to the contact point, contact forces needs to be generated. Forces  $f_x$ ,  $f_y$ ,  $f_z$  are known from literature. The problem is to calculate the six actuator forces in order to generate the required force vector. For this:

The force equation given

$$\sum f_{ac_i} = f \quad [3.27]$$

$f_{ac_i}$  is the force magnitude for the  $i^{\text{th}}$  actuator.

$$\text{Defining } \mathbf{l}_i = \frac{\mathbf{L}_i}{|\mathbf{L}_i|} \quad [3.28]$$

$$\text{Where } \mathbf{f}_{ac_i} = f_{ac_i} \mathbf{l}_i \quad [3.29]$$

$$\mathbf{r}_i \times \mathbf{f}_{ac_i} = 0 \quad [3.30]$$

Where

$$\mathbf{r}_i = \mathbf{CF} - \mathbf{T}_i \quad [3.31]$$

In this case the top plate is in equilibrium about centred point. So now we have six equations with six unknowns we can solve the problem and find the force required for each actuator.

The overall purpose of the mathematical algorithms is to find the coordinates of the centre of the top plate. The equations 3.5 to 3.8 gives the lengths of the actuators according to the Euler angles and position of the centre of the top plate (CP). Now the

relationship between the coordinates of centre of the small sphere (Head of femur) and centre of the top plate would be:

$$x(CP) = x(CF) + \frac{L}{\sqrt{1 + \frac{1}{\tan^2 \varphi} + \frac{1}{\tan^2 \theta}}} \quad [3.32]$$

$$y(CP) = y(CF) - \frac{L}{\sqrt{1 + \frac{1}{\tan^2 \psi} + \frac{1}{\tan^2 \varphi}}} \quad [3.33]$$

$$z(CP) = z(CF) - \frac{L}{\sqrt{1 + \tan^2 \theta + \tan^2 \psi}} \quad [3.34]$$

The coordinate of the actuators would be depended on the components of centre of the platform, which are directly related to the coordinate of the force contact point and the direction of the force. In other words, the above equations are the base of the mathematical equations between the Euler angles which are the input data and the contact force which is identified by the feedback from the strain gauges. Theses information according to the explained algorithm would go under process in the control system which is provided with the computer programming to modify the location of the actuators in order to find the optimized location of the force and produce the desired amount of force.

One of the limiting factors of the Stewart Platform is the range of motion of the angles because of its configuration. In this project this problem is exacerbated. The movement of the platform is determined in such a way that the top end of the bone attached to the platform remains in the same place. This means that, for the rotation of a joint, the platform must rotate and translate simultaneously, which makes for a higher difference



between the maximum and minimum extended lengths of the actuators. The platform geometry has been designed such that it will allow 0.575 radians of rotation in positive and negative directions. This will accommodate some of human joint movement.

For the purposes of this project, the platform simulates the hip during walking. There are six independently controlled linear actuators controlled from one computer. Each actuator interacts with an amplifier which interprets the signal from the computer and translates it into instruction for the actuator. It also collects the feedback signal from the actuator and interprets it to the computer. It interacts with the computer using a serial RS232 connection to the amplifier.

The amplifier and actuator combination simulates the motion by using position control to bring the platform to the required position and then switching to force feedback control to apply the load.

Since this study aims to simulate hip joint motion during walking, in the current chapter, it has sought to present the background theory regarding what was used to create the platform used for measurement. Equations 3.8 to 3.13 helps to calculate the necessary parameters and factors which could be used to demonstrate the position of points for simulating the hip joint action in walking. By inputting these desired data, the program could simulate the movement of the joint.

## Chapter 4. Software Development

### 4.1 Introduction

In this chapter, the use of a bespoke Visual Basics program will be discussed. This program serves three purposes; to generate the required data from user inputs based on speed and weight, to act as an interface between the computer and the physical rig with the use of Copley Motion Objects; which allows control of the actuators and finally to record the data at regular intervals during the duration of the experiment from both the actuators and the connected strain gauge. A software design specification is drawn and the initial prototype is observed.

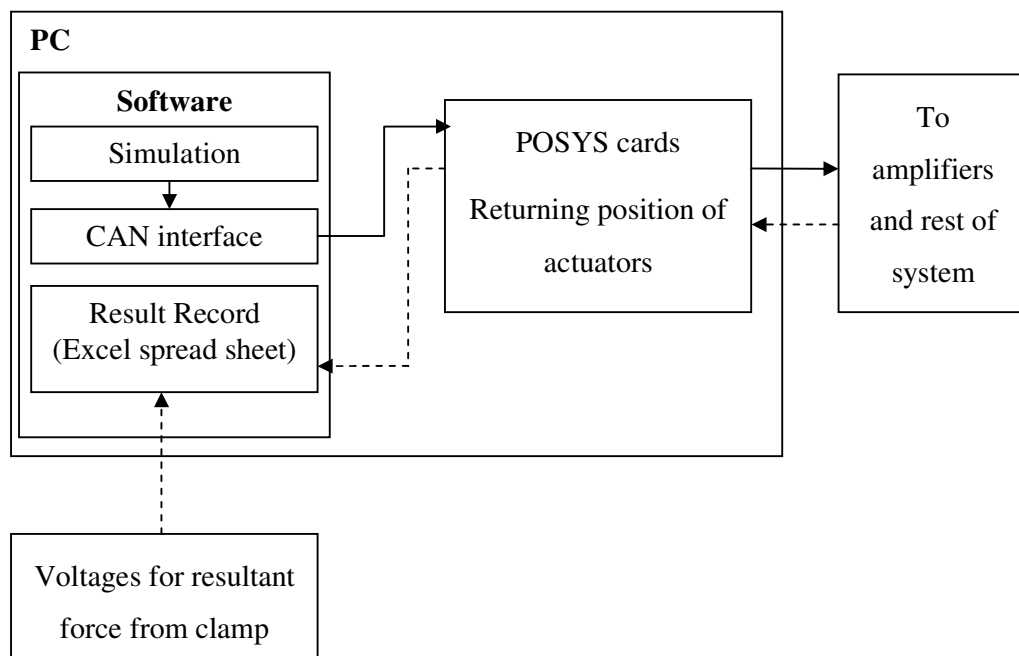


**Figure 4.1 Schematics of Software Arrangement**

## **4.2 Software Design Specification**

This is a formal layout of what the program created in this thesis set out to do.

- Recreate a mathematical model of the movement of a two segment human linkage (both kinematic and kinetic) based on applying user inputs of weight and activity to a data base model, producing forces and movement angles in three dimensions.
- Translate the calculated model into a trajectory of a single point (centre of the platform). Read Euler angles from excel file.
- Command the Stewart Platform to follow this trajectory by calculating the required extension of each leg periodically
- Create the required contact force once in each step orientation.
- Log the displacement of each actuator and translate it to the overall displacement of the single point created by the force.
- Log the reading from three strain gauges.

It was decided that the best approach to creating this command and record software would be to implement a Control Area Network (CAN) system provided by the designers and manufactures of the actuators and the amplifiers. Copley Motion Objects programming library could seamlessly integrate into the simulation software as it is compatible with Visual Basics.

### 4.3 Simulation Data Generator and Stewart Platform Driver

The 3D program developed was capable of simulating human movements in six degree of freedom. The program is capable of simulating different (any) joint movement. The time is denoted according to millisecond and there is a stop button where you can stop the simulation at any time. Also the interface shows the coordinates of the base and top plate.

Below, is the front end of the program, the graphical user interface (GUI). The interface window has been divided into 8 different regions as shown and numbered in Figure 4.2. In this chapter we will go through these regions and show what they represent.

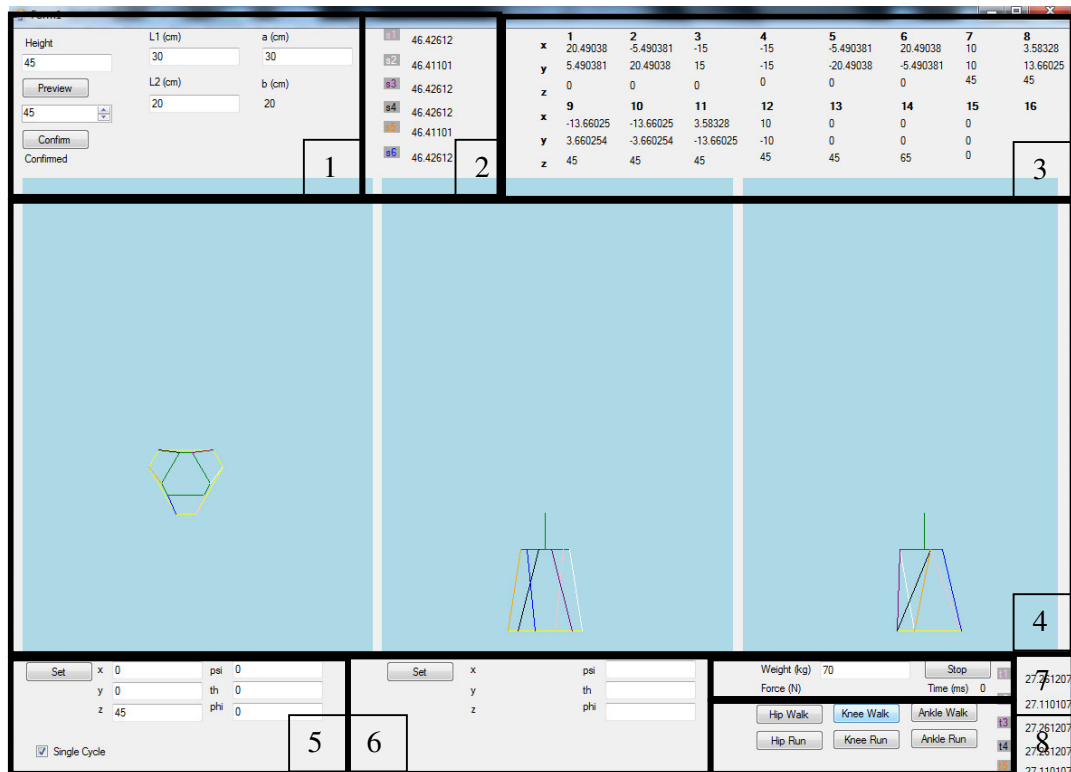


Figure 4.2 Visual Basic Simulation for initial position

Height	L1 (cm)	a (cm)
<input type="text" value="45"/>	<input type="text" value="30"/>	<input type="text" value="30"/>
<input type="button" value="Preview"/>	L2 (cm)	b (cm)
<input type="text" value="45"/>	<input type="text" value="20"/>	<input type="text" value="20"/>
<input type="button" value="Confirm"/>		

**Figure 4.3 Initial values of platform**

In region 1 Figure 4.2, initial values were entered in order for the simulation to adjust the platform for the required bone attachment lengths. As in Figure 4.3 it can be seen that these values should only be changed if you are using different joint attachment or actuator length.

s1	46.42612
s2	46.41101
s3	46.42612
s4	46.42612
s5	46.41101
s6	46.42612

**Figure 4.4 Lengths of each actuator**

In region 2 in Figure 4.22 is shown in Figure 4.4, the length of each actuator is shown. The actuators lengths are labelled in the same colours correspond to the graphical

representations given in region 4 which show above, front and left views of the arrangement.

	<b>1</b>	<b>2</b>	<b>3</b>	<b>4</b>	<b>5</b>	<b>6</b>	<b>7</b>	<b>8</b>
<b>x</b>	20.49038	-5.490381	-15	-15	-5.490381	20.49038	10	3.58328
<b>y</b>	5.490381	20.49038	15	-15	-20.49038	-5.490381	10	13.66025
<b>z</b>	0	0	0	0	0	0	45	45
	<b>9</b>	<b>10</b>	<b>11</b>	<b>12</b>	<b>13</b>	<b>14</b>	<b>15</b>	<b>16</b>
<b>x</b>	-13.66025	-13.66025	3.58328	10	0	0	0	
<b>y</b>	3.660254	-3.660254	-13.66025	-10	0	0	0	
<b>z</b>	45	45	45	45	45	65	0	

**Figure 4.5 Coordinates of Stewart Platform points**

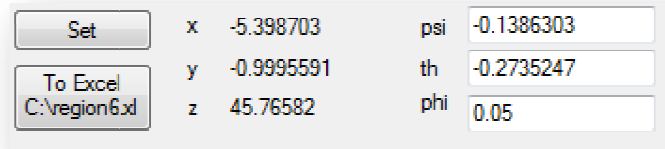
The corners coordinates of the top and base of the platform are given in region 3 Figure 4.2 along with point 13 which is the centre of the platform, point 14 at the top of the fixed bone and point 15 which is the centre of the base plate used as a reference for the other point. Region 3 Figure 4.2 has been shown in Figure 4.5.

x	<input type="text" value="0"/>	psi	<input type="text" value="0"/>
y	<input type="text" value="0"/>	th	<input type="text" value="0"/>
z	<input type="text" value="45"/>	phi	<input type="text" value="0"/>

☐ Single Cycle

**Figure 4.6 Centre of platform coordinates**

Region 5 Figure 4.2 can be used to program in the coordinates and rotations of the centre point of the platform and calculate how the platform would reconfigure to this as shown in Figure 4.6.



Set	x	-5.398703	psi	-0.1386303
To Excel	y	-0.9995591	th	-0.2735247
C:\region6.xls	z	45.76582	phi	0.05

**Figure 4.7 Rotation angles of centre point**

Region 6 in Figure 4.2 can be used to specify the rotations theta and phi of the centre point of the platform so that the angle psi and coordinates x, y and z can be calculated so that the top point of the moving bone stays in the same location.

A sample from the Visual Basic code with comments is given in the Appendix 6. The pseudo-code is shown below.

The code uses the inserted a, l(1), l(2) and height functions in order to calculate initial positions:

*Insert a, h, l(1) and l(2) lengths and calculate b*

*Calculate base coordinates using a*

*Insert initial angles as 0*

*Calculate displacement vectors of actuator*

*Calculate joint interface location using h and l(2)*

*Calculate coordinates of unmoved moving plate using addition of vector components*

*Calculate and output the extended length of actuators using modulus of components*

*Plot graphic of animation*

This can be adjusted until desired settings are reached and then confirmed.

The program can be programmed to move the platform in an unrestricted fashion by specifying the values of all of the platforms six degrees of freedom for the centre point of the moving platform:

*Recall base coordinates*

*Insert 3 spatial coordinates and 3 rotations for centre point of platform*

*Calculate required extension components of actuators to achieve platform position*

*Calculate coordinates of unmoved moving plate using addition of vector components*

*Calculate and output the extended length of actuators using modulus of components*

*Plot graphic of animation*

By specifying two of the rotations the code can calculate the corresponding third angle and three spatial coordinates of the centre point of the platform required to maintain the joint interface as relates to the intended use of the platform:

*Recall base coordinates*

*Insert two specified angles*

*Calculate required third angle and spatial coordinates*

*Calculate required extension components of actuators to achieve platform position*

*Calculate coordinates of unmoved moving plate using addition of vector components*

*Calculate and output the extended length of actuators using modulus of components*



*Plot graphic of animation*

This concept is used for the simulation of joint movement using the same calculation but specifying the values of the two angles calculated for the joint activities. The number of increments an activity is divided into will affect the precision of results:

*Start timer for joint activity*

*Recall base coordinates*

*For each time instant insert predefined two angles for joint activity*

*Calculate required third angle and spatial coordinates*

*Calculate required extension components of actuators to achieve platform position*

*Calculate coordinates of unmoved moving plate using addition of vector components*

*Calculate and output the extended length of actuators using modulus of components*

*Plot graphic of animation*

Weight (kg)	70	Stop
Force (N)	1510.74	Time (ms) 567
Hip Walk	Knee Walk	Ankle Walk
Hip Run	Knee Run	Ankle Run

**Figure 4.8 Type of simulation**

As seen in Figure 4.8, there is a button to stop the joint simulation at any time. Also the figure shows the different types of simulations that the Visual Basic program can do according to the user preference, this is to be used in further projects of simulating other joints. The options are presented for hip, knee, and ankle in two modes, walk mode and run mode. For the purpose of this project, only varying walking speeds have been used.

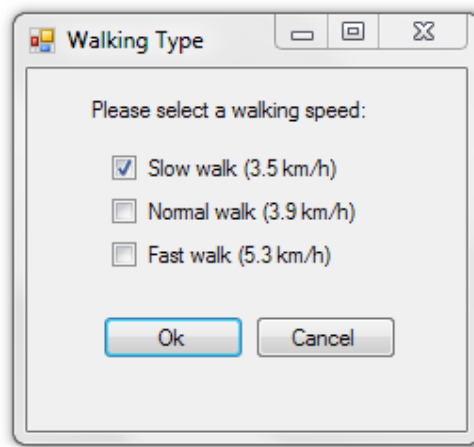


**Figure 4.9 Speed selection check boxes (modified to work as of radio boxes)**

In this particular version of the software, when hip walk is selected, a window box is shown offering the various speeds available, as shown in Figure 4.9 above. This selection changes the body weight percentage applied at different points of the gait cycle.

The kinematics Visual Basic program was linked directly with the POSYS by using Copley Motion Object. The Visual Basic program provides the kinematic calculations

and then real time simulations for the platform for the activities. Figure 4.10 show the platform movement during hip joint walking simulation.

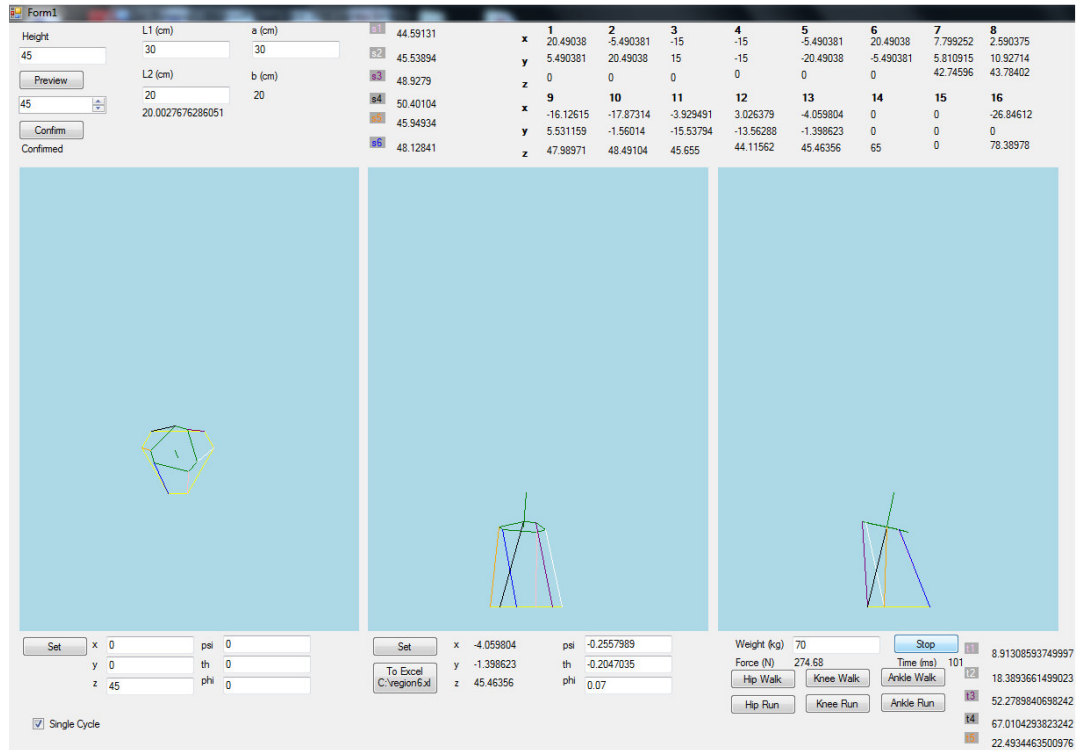


**Figure 4.10 Platform Movement during Hip Joint Walking Simulation**

The procedure for the experiment can be seen in greater detail in the following chapter.

## 4.4 Experiment Runtime and Data Logging

The program will automatically assume that the Stewart Platform is connected and will try to drive it as soon as the simulation is run. If it cannot detect the CAN, the user will be prompted with Figure 4.11

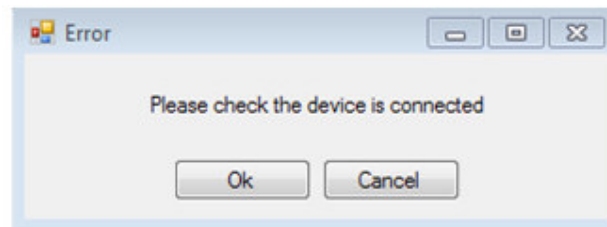


**Figure 4.11 Error box checking if the Stewart Platform is connected**

Once this is confirmed, the experiment execution is run by sending the commands from the simulation to the CAN interface. The following pseudo-code describes the operation.

(Per step)

*Get actuator extensions from simulation*

*Send actuator command extensions to POSYS in position mode*

*Wait for actual extensions to equal command extension //platform moves into orientation*

*Switch to current mode*

*Command relative current for command force*

*Log strain gauge data from USB connected PICO to excel file*

*Switch back to position mode*

*Log actual actuator extensions after force applied*

*(Repeated for each step)*

## Chapter 5. Design and Manufacturing of the Stewart Platform Simulator

### 5.1 Introduction

This chapter will focus on the design and manufacture of one of the main element in the universal human joint simulator system; the Stewart Platform. This device was designed and assembled within the duration of this project, at the dynamics laboratory and workshop at Brunel University as seen in Figure 5.1.

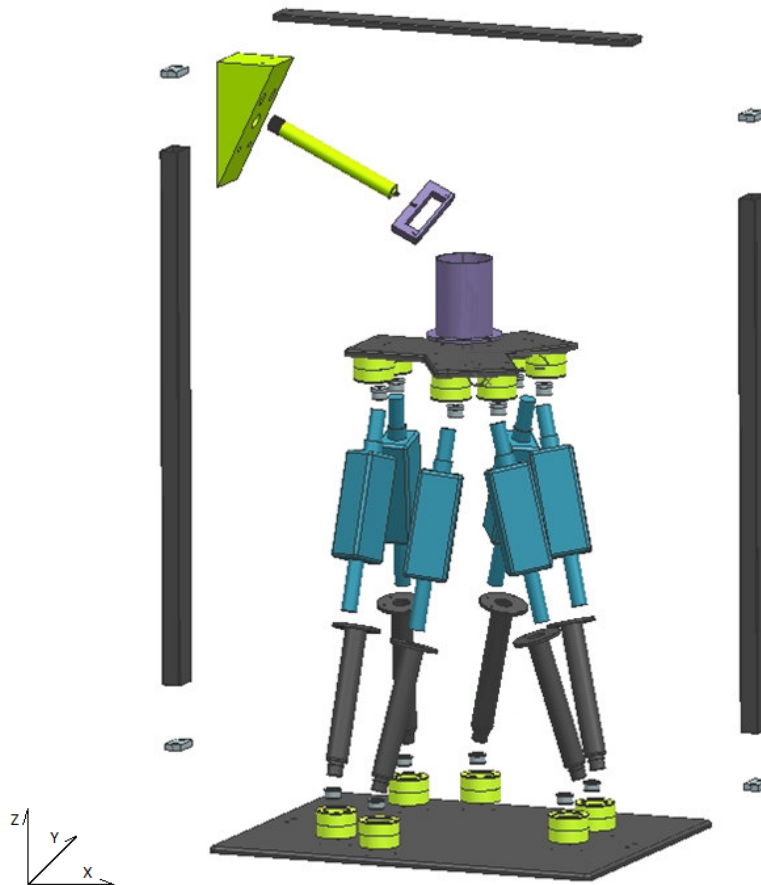


Figure 5.1 Assembly view of the experimental rig (exploded)

In terms of designing the platform, the link lengths determine how well the Stewart Platform can move. When the links are fairly short, the platform is stiff and has high positioning accuracy. However, when the links become longer, they need a larger workspace; biomechanical purposes require a great deal of freedom. As a suggestion, a small top plate is the better option. This chapter will include the final design and the assembly of the Stewart Platform. In addition to this, an arch was designed, to attach a stationary bone above the Stewart Platform and a bone fixed to the top plate so that it could move around the stationary point accordingly. The stationary bone was not positioned directly above; because joints move more in flexion than extension, the static bone was placed at an angle, so human activity could be modelled more accurately and thus reach a wider range of angles (Ulucay, 2006).

The maximum attainable force of the platform can be calculated by the maximum thrust of an actuator multiplied by the number of actuators, minus the weight of the moving plate and the components of force lost due to directionality (nominal  $35^\circ$  taken)

$$F_{total} = 6F_{act}\cos\theta - W_{plate} \quad [5.1]$$

$$F_{total} = 6(312)(\cos(35)) - (9.81 \times 2.7025) = 1506.94N$$

The total achievable angle is  $\pm 0.575$  radians or  $32.945^\circ$  in each direction. Due to the fixed bone attached to the incline mounting, a slight constraint occurs in the range of motion, as the fix bone is unable to move as it would naturally.

## **5.2 Product Design specification**

### **Mechanical Requirements**

- The bone to be moved has to be securely attached to the top plate of the Stewart Platform and allow for other bones to be easily fitted.
- Likewise, a static bone had to be positioned above the moving bone (and fitted) and thus a detachable device to hold this bone also had to be designed so different forms of attachment could be positioned for various types of bone.
- In order for the simulator to replicate the movement of the hip joint during walking the Stewart Platform must be able to move 20cm in the flexion plane to allow for full range of motion. However due to the symmetrical nature of the Stewart Platform, this required would have to apply to the extension plane as well.
- To allow for hip joint simulation of all usual activities, the Stewart Platform would need to have a range of motion of  $\pm 30^\circ$  in the pitch plane, however due to the symmetrical nature of the Stewart Platform; this requirement would have to apply to the rotation and yaw planes as well.
- The Stewart Platform has to be able to recreate forces created within the hip joint at varying activities. However, as the cost of higher powered actuators exceeded the budget for this project; a scaling factor of two thirds was used to match the available affordable linear motors. For this reason, the



maximum force required is 1506N (based on two thirds of the maximum force produced in Bergmann's hip joint force study).

### **Control Requirements**

- The actuators must provide position feedback when queried.
- The control program should incorporate the input of body weight, activity, sample bone length used and the joint in question, in order to calculate kinematics and loading.
- This should be achievable in a user-friendly manner.
- Actuator tuning and verification.
- This control program required the use of Copley Motion Objects and be easily adjusted in Visual Basic.

### **Health and Safety**

- The platform had to be easy and safe for the subjects to use in terms of its design and set up.
- An emergency stop button would have to be installed close to the operator, away from the machine.

### 5.2.1 Base Plate

All the concept designs for the platform and the base plate were created using the following equations, which give the six co-ordinates for each leg base points ( $B_i$ ),  $i$  being the actuator number. Where the radius of the circle is one, this has been an alteration for the top plate and the base plate. Vectors  $B_1$  to  $B_6$  apply to the base plate and vectors  $T_1$  to  $T_6$  to the top plate, these are calculated in the theory section. The design of the base plate is displayed in Appendix 3, showing the necessary co-ordinates for the platform and the pillars of the arch, so the base required for the pillars has the base of the platform integrated into the design. The three holes positioned in an equilateral triangle are for the bearing attachments displayed later in the chapter, for the purpose of rigidity. A fillet made of aluminium was added on all the upper face edges and the corners, regions which would be accessible to the user, in order to avoid sharp edges and provide a better overall appearance.

### 5.2.2 Top Plate

The top plate of the Stewart Platform was made of aluminium because it is light in weight and rigid. Appendix 3 shows the holes required for the bearing attachment, which were the same as those on the base plate, because the bearing attachment design used was the same for both plates. For safety reasons and overall better appearance, all the edges were smoothed and rounded off on the upper surfaces only, because the bearings were to fit underneath.

### **5.2.3 Top of the Arch**

The top of the arch was a simple bar with four holes at each end to attach them. The design has smoothed edges, for health and safety purposes and also to improve the overall appearance of the component. The pillars and the top of the arch had to be stable and secure to ensure that they did not move when the platform did, because this would have made the rig unstable. Both the pillars and top of the arch were made of steel in view of the loading that they would experience.

### **5.2.4 Stationary Bone Attachment**

This stationary bone attachment was fixed into one of the top corners by four screws, two in the top bar and two in one pillar. The pole for the pelvis holder screwed into the central hole. This hole is a normal part of the surface, which was inclined at an angle such that the joint interface of the pelvis was held in the central location at the correct height.

### **5.2.5 Fixing Pole**

This fixing pole connected the corner piece to the pelvis holder. The end connected to the pelvis holder had an 8mm thread 10mm in length to let it screw into the holder. The end connected to the corner piece was threaded on its main diameter of 25mm for this purpose. The length of this part corresponded to the length of the corner piece, in order to hold the joint interface of the pelvis in the centre at the correct height. The cylindrical

nature and large diameter of the pole was chosen to ensure minimum bending would occur along the holder.

### **5.2.6 Pelvic Clamp**

Due to the complexity of the pelvic bone, an attachment was designed specifically for the pelvic bone. The main function of this object was to hold the pelvic bone in the position it would have in the human body. The pelvic holder is in essence a clamp. It is a two-part component so that the pelvic bone can be easily inserted and removed. To fix the bone, the two parts in the device were screwed together. Once screwed in, they would allow the pelvic bone no degrees of freedom. Also, to take account of future uses for the platform, the pelvic holder was detachable from the test rig.

### **5.2.7 Actuator Holder**

The actuators to be used in the Stewart Platform were the ServoTube STA2504s from Copley Controls. The rod within the actuator moves up and down with a length range of approximately 300mm. The actuators require a holder and hence have a form of attachment to the bearing, extending the range of motion of the Stewart Platform.

The actuator holder had a flat circular surface with corresponding holes to the actuator so they could be connected. The pole was hollow and when the actuator was at minimum length the rod was completely within the hollow pole, but when it was at maximum length, the hollow pole was empty. There was also an additional shaft to be

positioned in the bearing; this remained fixed in the bearing, with an additional piece on the other side of it. The point of contact between the holder and actuator was designed to have a circular end. The material to be used was mainly aluminium, but a steel shaft was inserted for the sake of durability.

### **5.2.8 Rod Attachment**

At the top of the thrust rod, this part was screwed on the rod in order to keep it inside the bearing. The top of this part had a diameter of 27mm, 1mm over the edge on each side so that it was larger than the bearing hole but not by so much as to inhibit movement. The thickness of the top part was 2mm, making it thick enough to stop deflection but not too thick to inhibit motion. The bottom of this part had to go inside of the bearing and therefore had a diameter 0.2mm less than the bearing. There were six of these, one for each thrust rod.

At the bottom of the cylinder holder, this part was attached using an M8 screw with a bolt, so as to hold the attachment in place within the bearing. The top part of the top attachment was 2mm wider in diameter than the bearing, in order to have a border of 1mm all around it. This was enough to keep it in place without its getting in the way. Like the top attachment, it was 2mm thick. This part had a hole in it to fit the screw but shorter and was hollowed out so that the screw could not protrude. The entire bottom part of this part was inside the bearing along with part of the cylinder holder. There were six of these, one for each cylinder holder.

### **5.2.9 Bearing Attachment**

This part was designed to encase the bearing so that it held each bearing firmly and attached it to its position on the top or bottom plate. It also had to allow the top of the thrust rod and base of the cylinder holder to emerge from it and attach them in place. The bearing casing sat on the perimeter of the smaller hole with the bearing protruding and the attachment device free to move inside the hole. The top of the bearing casing was held in place by the bearing casing lid which was screwed into the three holes at the top. The thrust rod or cylinder holder came out of the other end of the bearing. This part of the design had a diameter slightly above that of the bearing casing so that it would fit securely. The height of the bearing casing fixture was slightly below that of the bearing casing so that the lid part held in the bearing firmly when screwed on tight, to prevent the bearing from rattling. These parts were attached to the plates using the three screws on the bottom. Appendix 3 shows the bearing holding cap which was placed on the top of the bearing attachment through its holes when the bearing was inside in order to keep it there during operation. Its inner diameter was slightly below that of the bearing casing but higher than that of the bearing so that it did not contact it at all. The thickness was kept low in order to prevent it from interfering with the operation.

### **5.2.10 Femur Attachment**

The design shown in Appendix 3 has as its main characteristic simplicity of manufacture and the ability to hold securely a femur bone and the stem component of an artificial hip-joint. These two objects are of different dimensions and shape; therefore it

was decided that the most appropriate design for the task of testing both of them using a single holder would be a hollow cylinder with a big enough diameter to allow the femur (the larger object) to be comfortably inserted into it. The femur bone and the stem would then be held in place by four screws inserted transversely through the cylinder. This method of holding accommodates the variation of dimension and shape between the femur bone and the stem. This “bone holder” was designed as to have the lowest weight possible and to have a base which fitted into the available space on the top plate of the platform, to which it was screwed. Since the platform might be used in the future to simulate the motion of other human joints, the holder was made to easily remove from the platform.

#### **5.2.11 Assembly and exploded view of the test rig**

The assembly view of the previously mentioned parts can be seen in Figure 5.2. For the purpose of visualisation, actuators have been included so as to give some idea of the experimental set up. This shows two pillars connected to both the base and the arch, giving a stable arrangement. The stationary bone attachment assembled shows how the three components – the stationary bone attachment, fixing pole and pelvic clamp – fit together, giving an indication of where the pelvic bone rested in the closed loop component. Note that the pelvic bone attachment is positioned closely to the femur holder, so they make contact with one another; when the plate moves, they should remain in contact. The femur holder is fixed firmly on the platform and underneath are

six bearing attachments, which are fixed to the rod of the actuators using the top rod attachment.

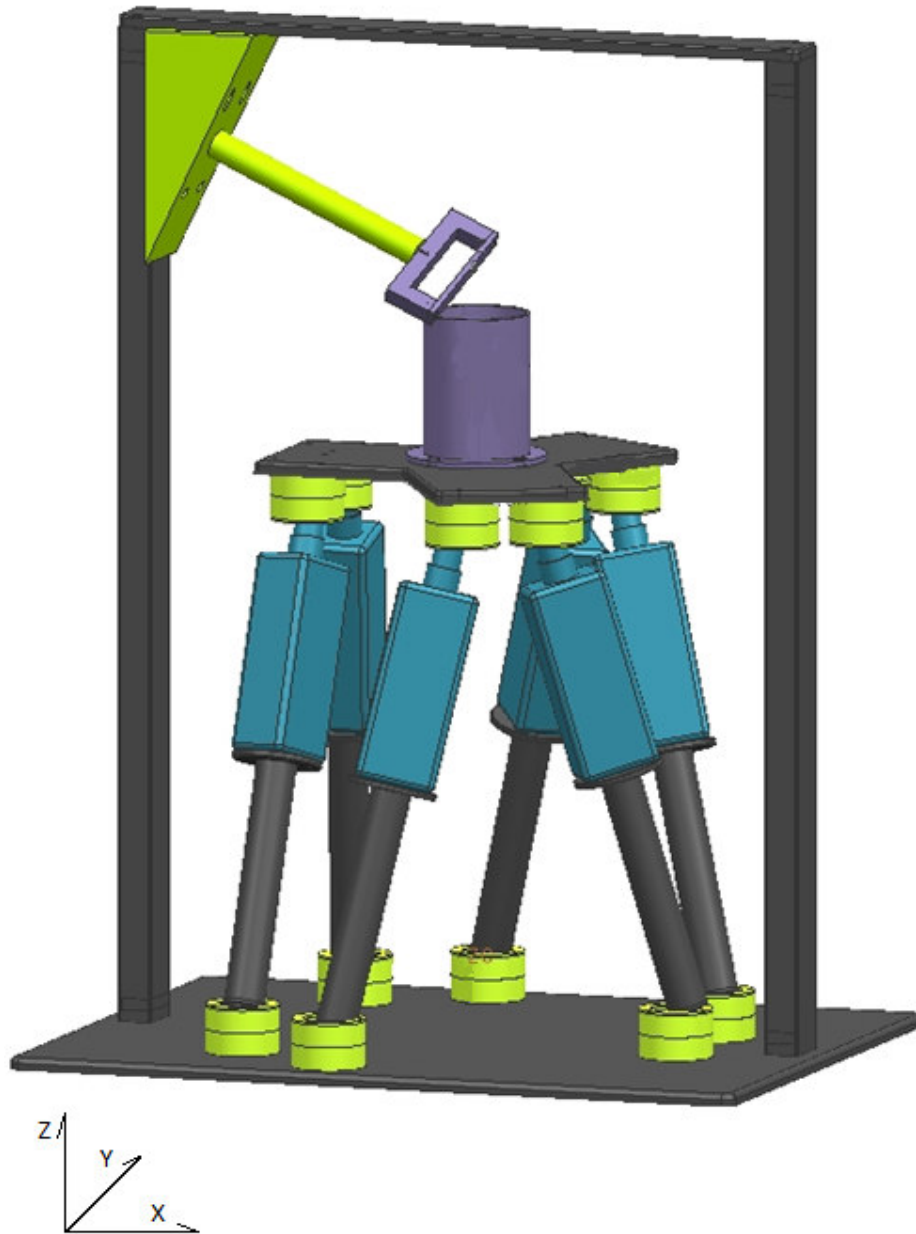


**Figure 5.2 Assembly view of the experimental rig**



### 5.3 Strain Gauges

For the purpose of this project, the strain gauges were used to measure bending in the device holding the bones. Appendix 5 shows introduction and type of strain gauge used in this project. It was not necessary to determine torsion or shear strain and thus a Half Bridge was sufficient and was cheaper than a Full Bridge, although more accurate than a Quarter Bridge and was temperature compensated.

These strain gauges were arranged on a holding clamp, which holds the static part of any joint. A plan of this clamp can be seen in Figure 5.3.

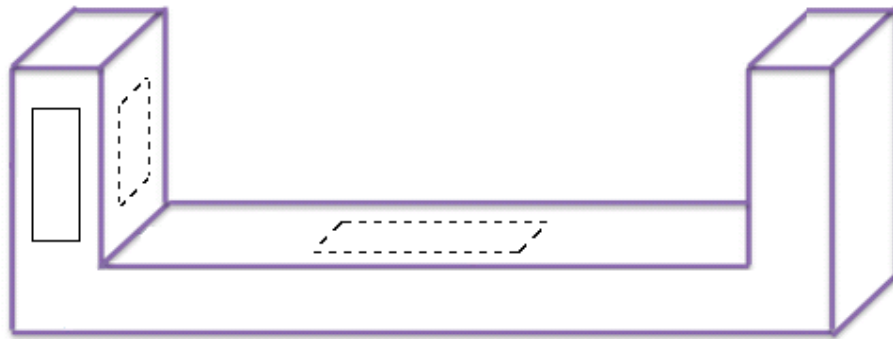


**Figure 5.3 Strain gauge application**

Because the electrical output of the strain gauges is small, approximately less than 10mV/V, a method of amplification was needed to enhance the signal and therefore increase the resolution in measuring by improving the signal to noise ratio.

### **5.3.1 Calibration of strain gauge**

One of the stages of this study was to measure the applied force on the bone. The chosen method for this step was measuring the force by use of strain gauges. As it has been explained before, strain gauges can measure the displacement of the material locally within the length of the gauge which is created by the force and display the voltage corresponding the change of resistance associated with the change of the length. The experimented results would be used to calculate the applied force. However, in this section to find a mathematical equation of the physical conceptions, it has been tried to identify the strain gauge balance calibration matrix for the relationship between force and voltage. Based on the results from the investigation, an optimum calibration model is recommended for use in the force recording system.

The aim of the balance calibration is to gain the calibration coefficients which enable the voltage output to be converted into the corresponding force readings. The relationship between the force and the voltage provides the mechanism with a feedback system which measures the force according to the corresponding voltage and then later can be compared with findings from other experiments (Bergmann et al., 2001).

There are many ways to describe the relationship between the forces and voltage output for a particular balance. As the order of the calibration model increases, the complexity of the mathematical expressions would be increased. Due to the imperfection of balance design and the combined loading condition, a linear calibration model was used to account for the interaction effect between different components of the balance.

The goal of this investigation was to find the relationship between the force components and the corresponding voltage. Therefore, the following equation has been created:

$$F_x = K_{x1}V_1 + K_{x2}V_2 + K_{x3}V_3 \quad [5.2]$$

$$F_y = K_{y1}V_1 + K_{y2}V_2 + K_{y3}V_3 \quad [5.3]$$

$$F_z = K_{z1}V_1 + K_{z2}V_2 + K_{z3}V_3 \quad [5.4]$$

It is expected that force acting in x direction will induce three voltages coming from three strain gauges (three are assembled in 3 orthogonal directions although they do not need to be completely orthogonal for the calculations). It has been assumed that the relationship between the force and the voltage is linear. Since each equation has three unknown parameters, there are nine parameters which need to be identified. Consequently, nine equations are needed to solve the above equations and identify the unknown parameters.

In experimentation, by applying the determined force three times in the desired direction for each of the force components, three equations will be obtained. Solving these equations will give unknown coefficients. However increasing the sampling points will make the calculation of coefficients more accurate. For larger number of points the least square method is applied to minimise error.

In order to find the coefficients, many different forces have been applied on the object at each time in one direction and the produced voltage by the strain gauge has been measured, for  $x$  force calibration, taking three force sampling, gives

[5.5]

$$\begin{bmatrix} f_{x1} \\ f_{x2} \\ f_{x3} \end{bmatrix} = \begin{bmatrix} V_{11} & V_{21} & V_{31} \\ V_{12} & V_{22} & V_{32} \\ V_{13} & V_{23} & V_{33} \end{bmatrix} \begin{bmatrix} K_{x1} \\ K_{x2} \\ K_{x3} \end{bmatrix}$$

Each  $K$  can be found by:

$$[K_x] = [V]^{-1}[f_x] \quad [5.6]$$

For larger number of sampling points, the least squared method is used, by defining the error  $e$  as,

$$e = (K_{x1}V_1 + K_{x2}V_2 + K_{x3}V_3 - F_x)^2 \quad [5.7]$$

Minimising the error,

$$\frac{\partial e}{\partial K_{x1}} = \sum 2((K_{x1}V_1 + K_{x2}V_2 + K_{x3}V_3 - F_x))V_1 = 0 \quad [5.8]$$

$$\frac{\partial e}{\partial K_{x2}} = \sum 2((K_{x1}V_1 + K_{x2}V_2 + K_{x3}V_3 - F_x))V_2 = 0 \quad [5.9]$$

$$\frac{\partial e}{\partial K_{x3}} = \sum 2((K_{x1}V_1 + K_{x2}V_2 + K_{x3}V_3 - F_x))V_3 = 0 \quad [5.10]$$

$$\sum_{i=1}^n \begin{bmatrix} f_{x1} V_{1i} \\ f_{x2} V_{2i} \\ f_{x3} V_{3i} \end{bmatrix} = \sum_{i=1}^n \begin{bmatrix} V_{1i} V_1 & V_{2i} V_1 & V_{3i} V_1 \\ V_{1i} V_2 & V_{2i} V_2 & V_{3i} V_2 \\ V_{1i} V_3 & V_{2i} V_3 & V_{3i} V_3 \end{bmatrix} \begin{bmatrix} K_{x1} \\ K_{x2} \\ K_{x3} \end{bmatrix} \quad [5.11]$$

Now Equation 5.11 can be solved for three  $K_x$  values.

Similarly equations 5.7 to 5.11 needs to be formulated for forces in y and z direction then the applied force and the measured voltage have been put in the equation to solve the nine equations with nine unknown parameters which the below coefficients have been calculated:

$$K_{x1} = 34.61, \quad K_{x2} = 119.9, \quad K_{x3} = 231.42$$

$$K_{y1} = 274.12, \quad K_{y2} = 58.2, \quad K_{y3} = 163.52$$

$$K_{z1} = 173.7, \quad K_{z2} = 239.5, \quad K_{z3} = 41.7$$

These coefficients were calculated by applying 19 increasing forces along the three axes starting with 0 force to 1800N, increasing 100N at each sampling point.

## 5.4 Experimental Set Up

### 5.4.1 Equipment

This chapter examines the components used in the construction of the Stewart Platform and refers to information from the parts' manufacturer. (Corp, 2008a, Corp, 2008b, GmbH, 2008).

#### Copley Controls Servo Tube Actuator

Six ServoTube actuators as seen in Appendix4 are used for driving the Stewart Platform, as they provide great precision and control. Each ServoTube delivers a static force of 51 Newtons and have a peak force of 312N. It requires no external encoder and its magnetic design allows for accuracy of 12 micron. The ServoTube control is achieved with tuning software which incorporates the Xenun amplifier. The position sensor outputs analogue, differential sine and cosine signals, providing position feedback. Altogether, the six actuators would have a net force on the Stewart Platform of 1506.94 Newtons.

**Table 1 Mechanical Specifications (Corp, 2008a)**

Forcer Type	Value	Units
Maximum stroke	309	mm
Forcer mass (excluding thrust rod and cable)	1.25	kg
Thrust rod mass/metre	3.5	kg/m

## **Copley Controls Xenus XTL**

### **Amplifier:**

The S version of the Xenus as seen in Appendix 4 controls the Servotube actuators supports its analogue sin/cos encoders. The Xenus amplifier can operate as a node on a CANopen network. In this mode of operation, the amplifier takes instructions from a master application over a CAN network and performs torque, velocity and position profiling, interpolated motion and homing operations. Multiple drives can be synchronized for coordinate motion. For this experiment, the interpolating positioning mode was used in a CAN network set up with the POSYS cards.

### **CME2:**

Copley Controls CME 2 Software communicates with Xenus through RJ45 cable from the POSYS cards. CME 2 provides all the operations required to configure the amplifier. Using a single RJ45 connection to one amplifier the other amplifiers can be linked together by CAN bus connections in a CAN network. The motor amplifier data can save .ccm and .ccx files, which is individual for each actuator depending on tuning and the model. The amplifier files include all the amplifier settings and the motor data, thus making it possible to set up one amplifier by copying the configurations from another.

**CMO:**

Copley Motion Objects (CMO) is affectively a programming library made readily available to allow system programming to be easily performed. CMO also provides COM objects which can be used by Visual Basic to communicate with and control an amplifier over the CAN network.

**Amplifier power:**

Within Xenus there are three isolated power distribution sections: +24Vdc, logic/signal and high power. An internal DC/DC converter operates from the +24Vdc logic supply input and creates the required logic signal operating voltages: the voltage required for the high voltage control and a +5Vdc supply for powering the motor encoder and Hall circuits. The amplifier derives the internal operating voltages from a separate source, which allows it to stay online in the event of the mains having to be disconnected in case of an emergency stop. The CAN bus and network connection can then remain active so that the amplifier can be monitored by the control system when the mains power is removed.

The mains power drives the high voltage section. It is rectified and capacitor-filtered to produce the DC link power which drives the pulse width modulation inverter, where it is converted into the voltages driving a three-phase brushless motor.



### Commutation Modes:

The amplifier supports brushless sinusoidal commutation. When in this mode of commutation, an encoder is required for all modes of operation.

### Operating Modes and Control Loops:

The amplifiers use current, velocity and position nested control loops to control a motor in the associated operating modes. In position mode, it uses all three loops. Figure 5.4 shows that the position loop drives the nested velocity loop, which in turn drives the nested current loop. The velocity loop drives the current loop in the velocity mode. In the current mode the current loop is driven directly by external or internal current commands.

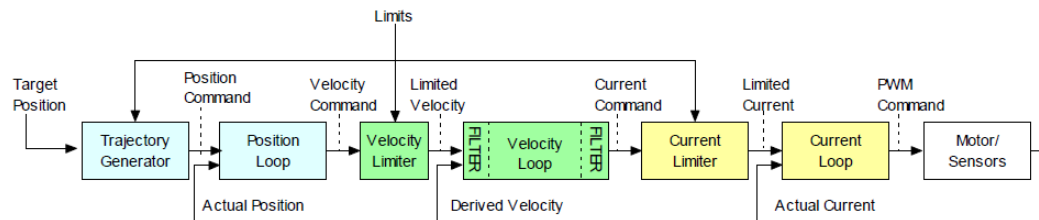
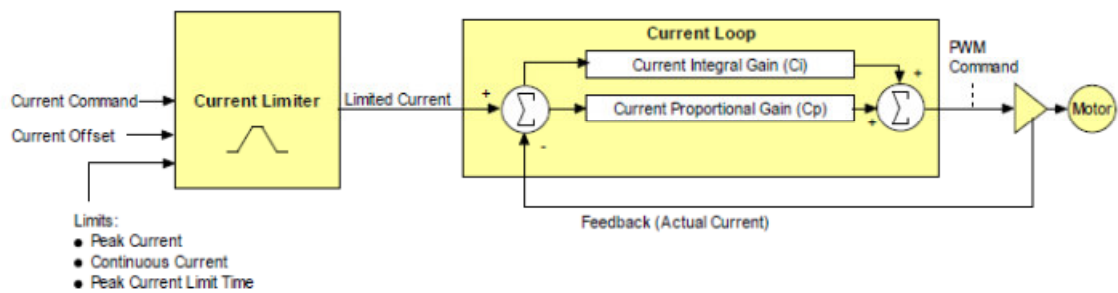


**Figure 5.4 Position Control loops schematic (Corp, 2008b)**

The attributes of these loops include command input, where a value is provided for every loop that it then tries to control. Limits can be set on each loop in order to protect the motor and the mechanical system. The servo control loops receive feedback from the device that they are controlling. Loop attributes denoted as gains are constant values used in the mathematical equation of the servo loop. These values can be tuned during

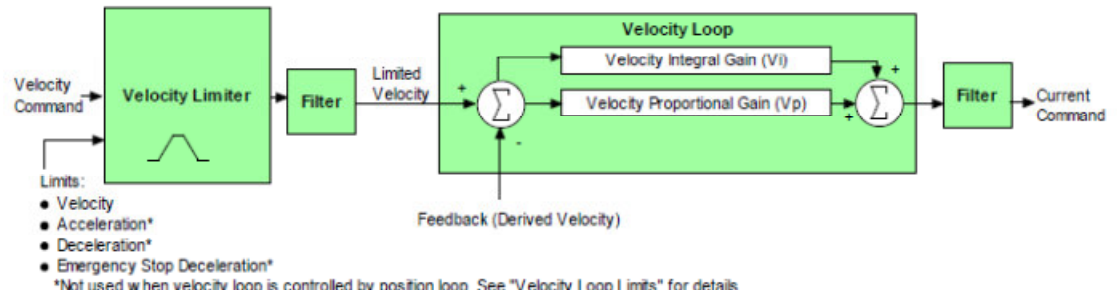
the setting up of the amplifier so as to improve the loop performance. The output control signal generated by the loop can be used as the command signal to another control loop or the input to a power amplifier.

### Current Mode and Current Loop



**Figure 5.5 Current loop diagram (Corp, 2008b)**

The current loop inputs are: the amplifier's analogue or pulse width modulation inputs; a network command, CANopen, or RJ45 Serial; a Copley Virtual Motion control program; and the amplifier's internal function generator. The current command is generated by the velocity loop in velocity or position modes. The current command can be limited according to the peak current limit, the continuous current limit, the rate of change in current command and the maximum amount of time that the peak current can be applied to the motor before it must be reduced to the continuous limit or generate a fault. The current loop output is a command which sets the duty cycle of the pulse width modulation output stage of the amplifier. CME 2 software can automatically determine the current loop gain values for the motor.

**Velocity Mode and Velocity Loop**

**Figure 5.6 Velocity loop diagram (Corp, 2008b)**

In the velocity mode (Figure 5.6) the inputs can come from the same sources as in the current mode. The velocity loop command can be limited, in order to protect the motor and the mechanical system, by setting the maximum acceleration velocity command input to the velocity loop. Acceleration and deceleration limits can be set in order to limit the respective maximum rate of their commanded velocity input to the velocity loop. The velocity loop output is a current command used as the input to the current loop.

### Position Mode and Position Loop

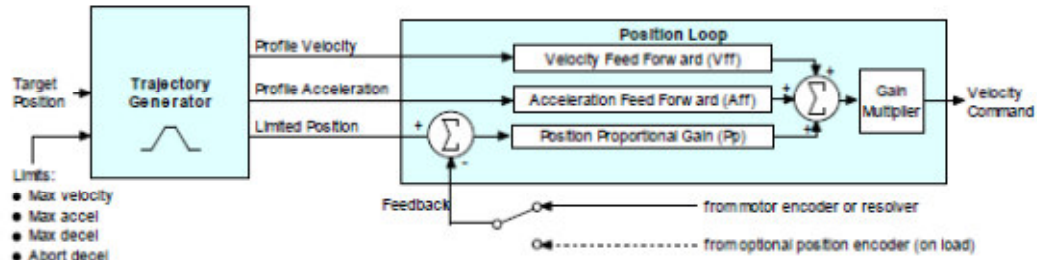


**Figure 5.7 Position loop diagram (Corp, 2008b)**

The amplifier receives position commands from the digital or analogue command inputs, over the CAN interface or serial bus or from the CVM control program. When using these, a trapezoidal or S-curve profile can be programmed. The trajectory generator updates the calculated profile in real time as the position commands are received. The output of the generator is an instantaneous position command. Also generated are the values for the instantaneous profile velocity and acceleration. The position loop processes these signals together with the actual position feedback in order to generate a velocity command. In the position mode, the limits which can be applied by the trajectory generator constrain the maximum velocity and acceleration and the maximum deceleration. The limits can be set by the user and are meant to generate the motion profile. If the motion is aborted, the 'abort deceleration' specifies the deceleration used by the trajectory generator. The position loop receives profile velocity and profile acceleration inputs from the trajectory generator. Another input received is the instantaneous commanded position of the profile. This is used with the actual

position feedback to generate a position error. The output of the position loop is a velocity command used as the input to the velocity loop.

### **CANopen Operation:**

In position mode, the amplifier can take instruction over a two-wire Controller Area Network (CAN). CAN specifies the data link and physical connection layers of a network. CANopen is a set of profiles built on a subset of the CAN application layer protocol. These protocols specify the different types of device that can use the can network efficiently. Xenus supports CANopen, which allows it to operate on profile torque, profile velocity, profile position, interpolated position and homing modes of operation. Figure 5.8 shows the architecture of the CANopen motion control system. The diagram shows that the control loops on the individual amplifiers are closed. Here the master application coordinates multiple devices, using the network to transmit commands and receive status information. Each device can transmit to the master or any other device in the network. CANopen provides the protocol for the mapping device and masters the internal commands to messages which can be shared across the network.

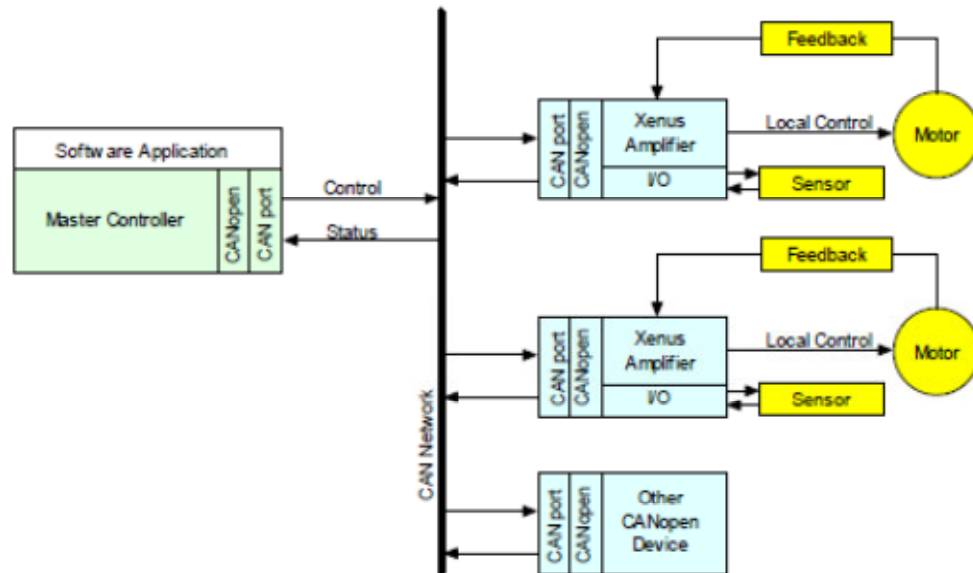


Figure 5.8 CANopen diagram (Corp, 2008b)

### Brake/Stop Sequences:

Disabling the amplifier by hardware or software command starts the following sequence of events: the motor begins to decelerate and at the same time, the *brake/stop delay time* count begins. The amplifier then slows the motor before applying the brake. When the motor slows to *brake/stop activation velocity* or the *brake/stop delay time* expires, the brake output is activated and the pulse width modulation delay brake/stop response time count begins. When the response time has passed, the amplifier's output stages are disabled.

### Servo Halbeck POSYS 1924

The POSYS 1924 as seen in Appendix 4 is an advanced motion control systems for brushed and brushless motors. They are system modules with 4 axes for servo and

stepper motors. The POSYS use a DSP in conjunction with ASIC. This provides a 16-bit DAC motor command, 10-bit pulse width modulation or pulse direction output. The POSYS can be used to control peripheral equipment using digital and analogue and programmable outputs. The actual status of each axis is given by the outputs for in-position, motion error and amplifier-enable signal.

**The System:**

The actual location of each axis is given by its own inputs. These inputs are produced using incremental encoder signals or a parallel-word input device. With incremental signals, data stream is digitally filtered and subsequently transferred to a high-speed up/down counter. The parallel word interface gives a direct binary-encoded position of up to 16-bits which is read by the POSYS. This position is used to maintain a 32-bit actual axis position counter.

The desired positions at each time interval are calculated by the trajectory generator. The bases for these calculations are the profile modes and profile parameters programmed by the host, together with the current system. The 32-bit error for the servo control is calculated by the output of the trajectory generator combined with the actual position encoder. This error is passed through a PID filter and the resultant value is output by the POSYS to an external amplifier using pulse width modulation or DAC signals.

Communication to/from the POSYS motion controllers is achieved by means of a parallel-bus microprocessor-style interface, an asynchronous serial port or a CAN interface. For CAN communications, the desired CAN data and CAN nodes address are selected by the user. This communication takes place through short commands travelling as a sequence of bytes and words, with an instruction code word which tells the POSYS the requested operations. The commands are sent by a host computer executing a supervisor program.

The POSYS act as the motion engine because they manage the high-speed dedicated motion functions such as trajectory generation and trajectory monitoring; meanwhile, the host software program provides the overall motion sequences. The POSYS also, using breakout function, monitor various signals, parameters or conditions and compare them against a set point condition value. Up to four POSYS parameters can be stored automatically in an on-board RAM chip, using the diagnostic parameter capture function. The motion error, tracking window and settle window functions monitor the difference between the desired position and the actual encoder position. If the motion travel is beyond the allowed range, the limit switch function allows the axis to be automatically stopped.



## 5.4.2 Connections

### Set Up Housing

The Xenus amplifiers are mounted in a housing case, in which the J1, J4 and J7 connections are wired up to so that the cables connecting to the POSYS and the power supplies can be easily connected. Schematic of connections is shown in Figure 5.10.

### Xenus and POSYS Connections

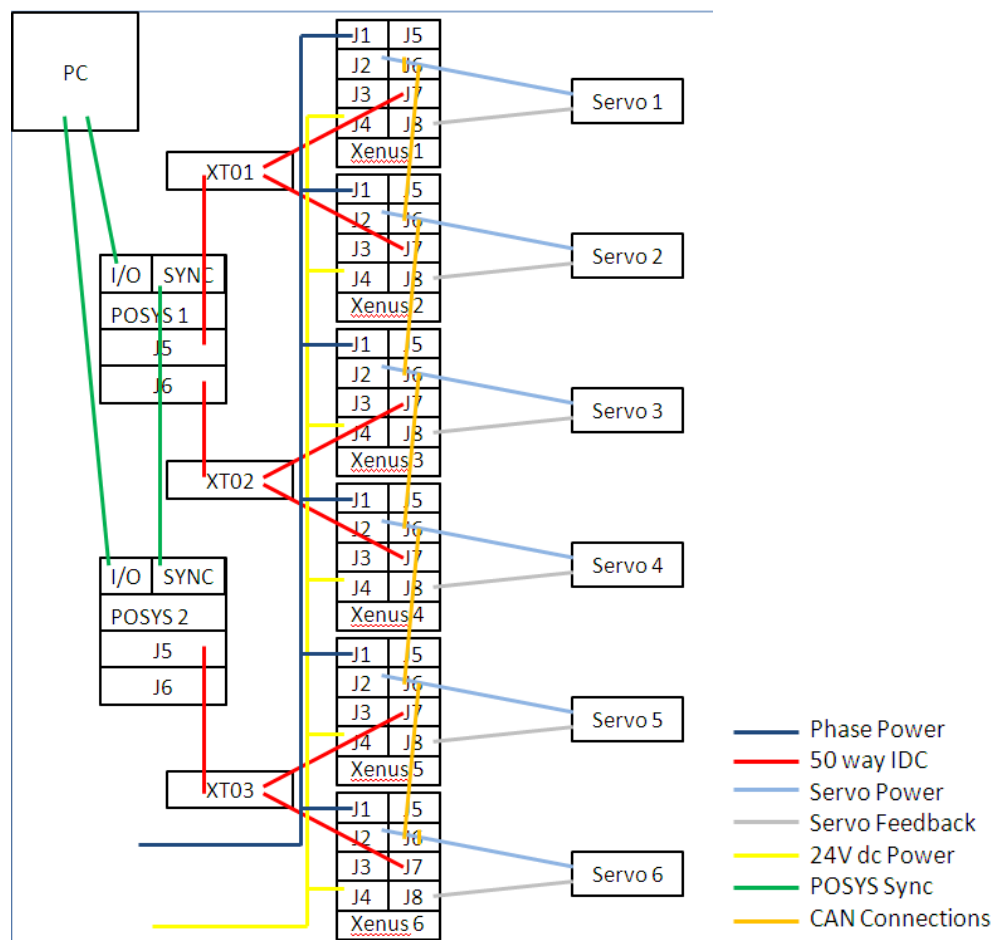


Figure 5.9 Schematic Diagram of Xenus and POSYS Connections

Each amplifier is connected as shown in the Figure 5.10. This shows the hardware connections of the rig to the computer and the power supply.

The J8 connections are as before. The XT connections are further described in the J7 section. It can be seen in this diagram that the J2 connection from the Xenus to the Servo is fitted with a trip switch on each of the phases and on the enable pin of the J7 for circuit protection. As expected, the earth connection is earthed. The J7 connections (apart from pin 1, which is the ground pin) are connected to the XT modules for connection to the POSYS; the corresponding pin configuration for this is given in the J7 section.

### **Xenus Housing**

The amplifiers were mounted in a cabinet where all the power connections, J7 connections and safety circuitry were set out for simple connection to the POSYS cards and servos.

### **Servo Connections**

Each servo requires one amplifier and has both of its connections to this amplifier. These are both screened cables.

The first connection is for powering the forcer; this connects to the Xenus J2 connection which provides a power supply from the mains. It has one pin for each phase and a common ground connection.

The second connection is the position sensor; this connects to the Xenus J8 connection which delivers commands to the servo and return feedback from it when queried. This connection provides commands using three phases of sinusoidal waves. It is made up of one pin for each of the three phases, four pins for the positive and negative sine and cosine waves used for position feedback, a positive 5V dc and ground power connection for the signals and a 5V dc and ground connection to the thermistor in the Xenus to protect against excessive temperatures. The J8 connection uses an analogue sin/cos converter to interpret the Xenus input for the servo and a digital encoder for feedback from it.

### **Amplifier Connections**

J1 is an earthed mains connection with a line filter used to provide the servo connection J2 with power. This circuitry is kept separate for safety from that used to power the Xenus. Instead the power used for this is a 24V dc source with a break connected at J4 with one pin for the break, one positive pin and one negative pin. For this application, the J4 connections are supplied in parallel; more details on this are given in the Power Supply section. The J3 connection is for regeneration and is not used here. J5 is an RJ45 computer connection for standalone operation. It contains one input pin, one output pin and one ground pin for each of these. It is not used for the main operation of the platform, but is used to tune each servo before use; in order that it is correctly configured. J6 has two sockets used for the CAN network connection for the simultaneous use of multiple amplifiers. Each J6 socket has a high, low and ground pin

for signals, a positive and ground pin for signalling and a shield. The nodes are connected together in series, using these ports with a terminus in the first and last amplifiers. Each amplifier is set an address on the CAN bus using the S1 switch. J7 is the connection used for interpreting special control signals; here this is used for the force feedback operation. It has eleven input pins plus one ground pin for them, three output pins plus one ground pin for them, one positive and one negative reference pin, a frame ground pin, a positive 5v dc pin and six encoder pins. Two Xenus drives are wired to one fifty-wire terminus in the housing. The J7 connection is further explained in the PCI Card Connection section.

### **PCI Card Connections**

The PCI cards connect to the J7 port of the Xenus amplifiers using three fifty-way IDC cables, one from each of the terminuses. They are four axis cards; one is used with four amplifiers and the other with two, in order to reduce wiring. This means that two of the cables go to one card (designated the master card) and the remaining cable go to the other card. One fifty-way connection can be made to either port J5, J6 or J9, where J9 is an optional connection. For the master card these will be J5 and J6, for the second card this will be J5. The cards are connected together using the sync I/O J4 port of the master card to the sync I/O J3 port of the second card. The master card is connected to the computer via RJ45, using the J2 connection. This port has a serial enable pin, an input pin, an output pin, a +5V pin and a ground pin. For the serial interface mode to be enabled, the JP4 setting needs to be switched to 2 - 3.

### **Power Supply**

The system was to be run from a three-phase 400V 32A 50Hz ac supply. Each phase has a positive; there is a communal earth for all the phases and an earth connection for the whole supply. Part of the first phase is stepped down to 24V dc and 4Amps and used to power the J4 Xenus connections in parallel. The remaining part of the first phase, the second and the third phases are used to power the J1 Xenus connections via a line filter. Each phase supplies the power for two of the servos. Each Xenus, the voltage step and the line filter are earthed.

All of the Xenus amplifiers have a common safety circuit. This is used to protect the circuitry from high currents. The circuit has a cut-out switch and reset switch for manual operation.

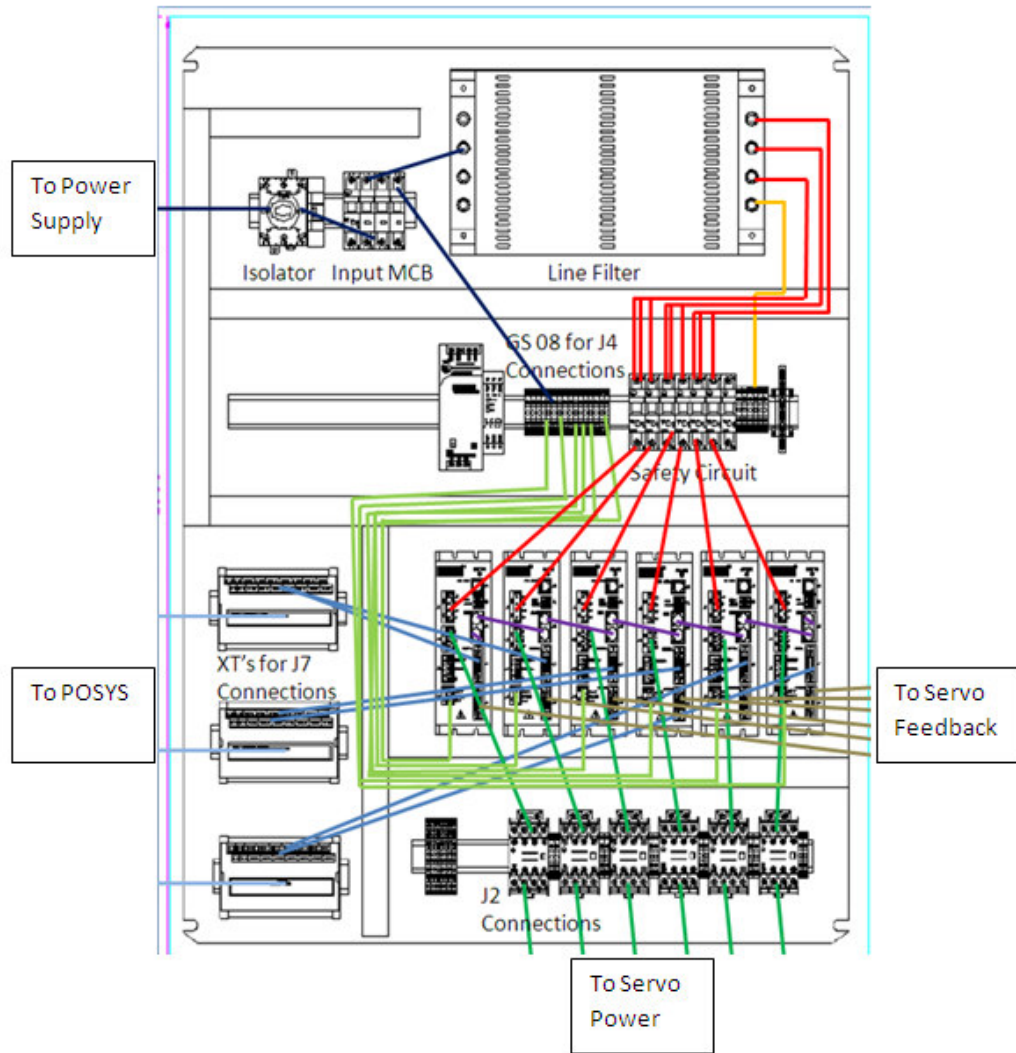


**Figure 5.10 Xenus Housing Cabinet, SCS Automation & Control**

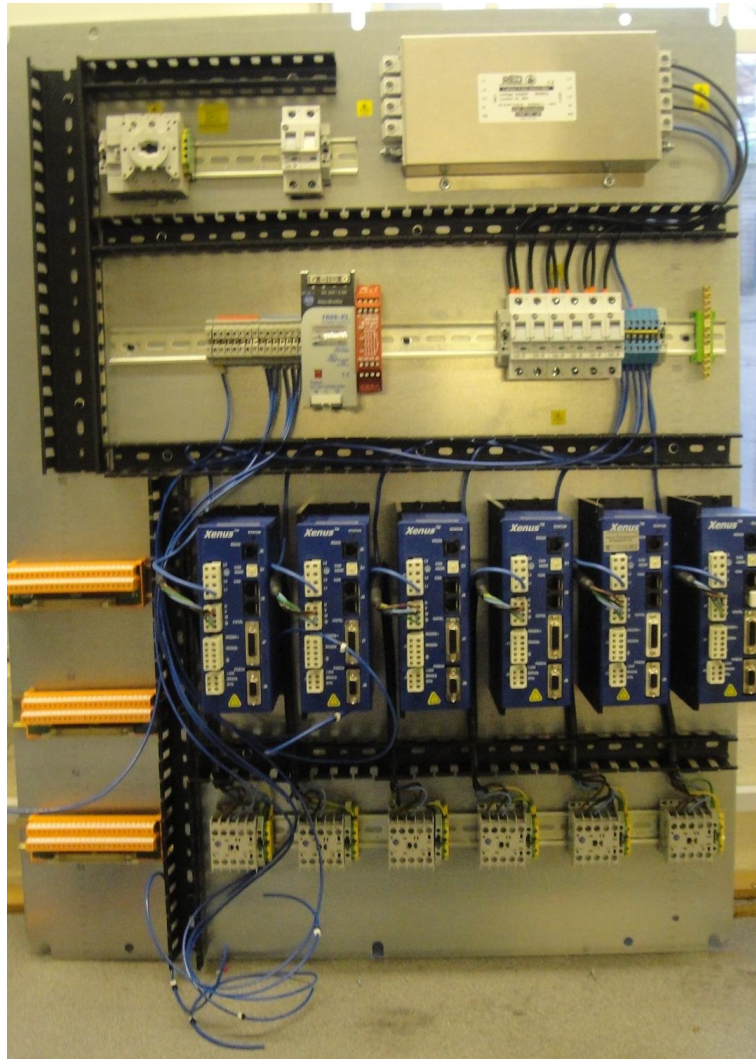


**Figure 5.11 Xenus Housing Setup**

As shown in Figure 5.11 the dimensions of the Xenus housing were 800mm by 1000mm. This diagram shows the isolator where the three phase power source was connected, the input MCB where the power was divided between the phases and distributed to the line filter and the GS08. The line filter distributes the connections for each phase and the neutral connection between the J1 connections via the safety circuit.

The J1 connections were two per phase, one per amplifier. The GS08 connection distributes the power source for the circuitry of the amplifiers in parallel along the rail. The XT connections were wired to the J7 connection as noted above in the layout described in the J7 section. Two of the XTs connected to one POSYS and the third connected to another POSYS before the POSYS were connected together. This connection was via a 50 way IDC cable connection for each XT. The first one was sent to J5 of the first POSYS, the second to J6 of the first POSYS and the third to J5 of the second POSYS. J2 connections contained the safety feature and were otherwise as normal, going from the Xenus amplifiers in the housing to the servos. The J8 connections were as normal, going from the amplifiers in the housing to the servos for the motor feedback.

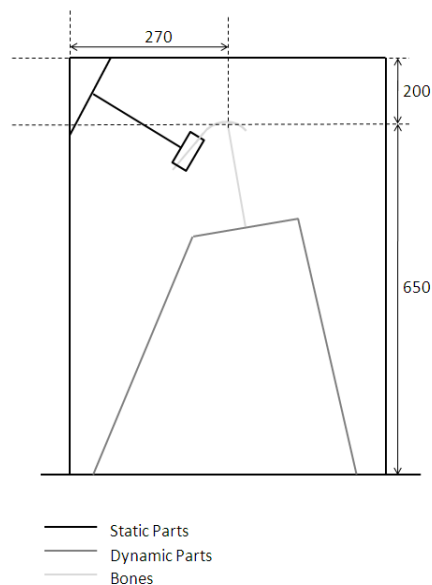


**Figure 5.12 Schematic Front View of Rig Showing Joint Interface Location and**

**Arc Size (all dimensions in mm)**



Figure 5.12 shows how the pelvis attachment, held in place by the pelvis holder, was attached to the frame using the corner piece so that the joint interface was fixed in the centre at a height of 650mm. The platform could move the femur bone around, keeping the top end of it in contact with the pelvis, thus simulating the movement of the joint.

The Xenus housing setup was hung by screw attachments in the wall to make the layout accessible and the connections easily made. The power was supplied from the three phase power source to the isolator. The POSYS and computer connection were made from the XT blocks in the housing and the servos were connected from their location in the rig to the Xenus amplifiers in the housing by connections 3m in length. The whole arrangement when set up was tidy and all contained within four main areas: the computer, the power source, the Xenus housing and the rig. The cables between the areas were few in number and grouped together.

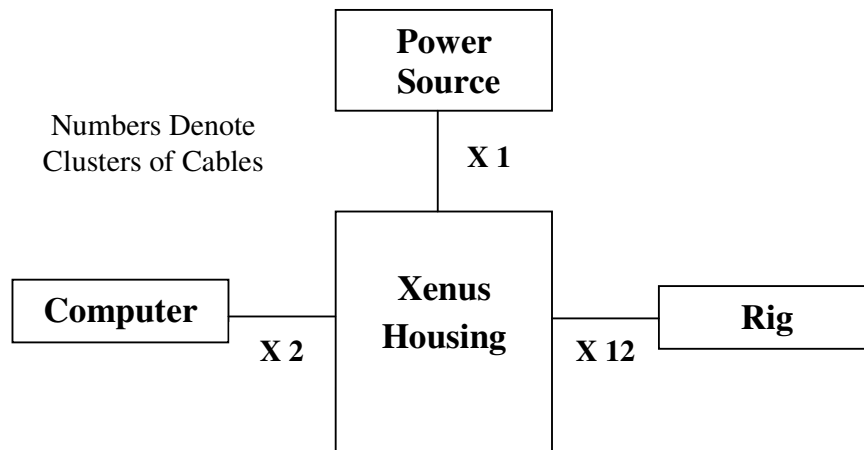


**Figure 5.13 Connections between Main Regions**

### 5.4.3 Assembling

The sub-chapter simply includes images of the final components and the final assembled rig.



**Figure 5.14 Actuator Holders, Bearing Holders, Bearing Holder Caps, Top and Bottom End Attachments**

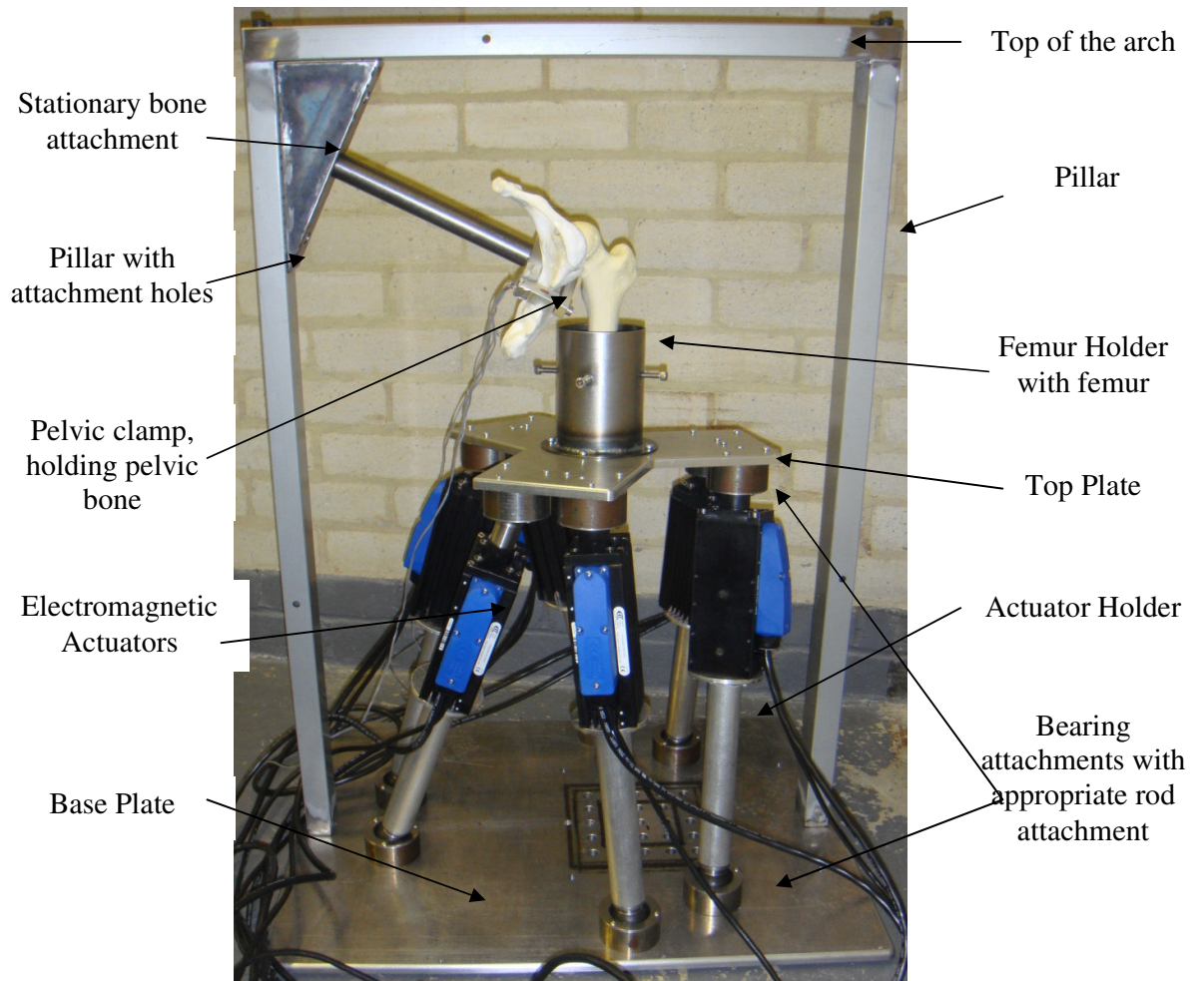


**Figure 5.15 Experimental Rig Set up**

## **Chapter 6. Experiment Procedure and Results**

### **6.1 Introduction**

This chapter presents the procedure used to obtain the results from the experiment, as well as a summary of results derived. The Stewart Platform was tested to see how accurately it could reproduce known data and facts of the human hip joint. For this procedure, a kinematic model of walking was derived from work produced by (Hamill and Knutzen, 2009). This data was used to position the Stewart Platform throughout the different stages of the experiment.

To find what force should be applied, (Bergmann et al., 2001) study into internal joint forces was used as a guide to what force per body weight should be applied at different sections of the gait cycle. This was scaled down appropriately to suite the maximum force applicable from the Stewart Platform.

For validation of the set up, the different of displacement of the femur head was measured from post force application compared to pre force application. It is known that this difference should be minimal and will therefore give a great understanding of what types of activities the machine can suitably handle. Each experiment in this chapter was performed 3 times and the average is displayed in the graphs.

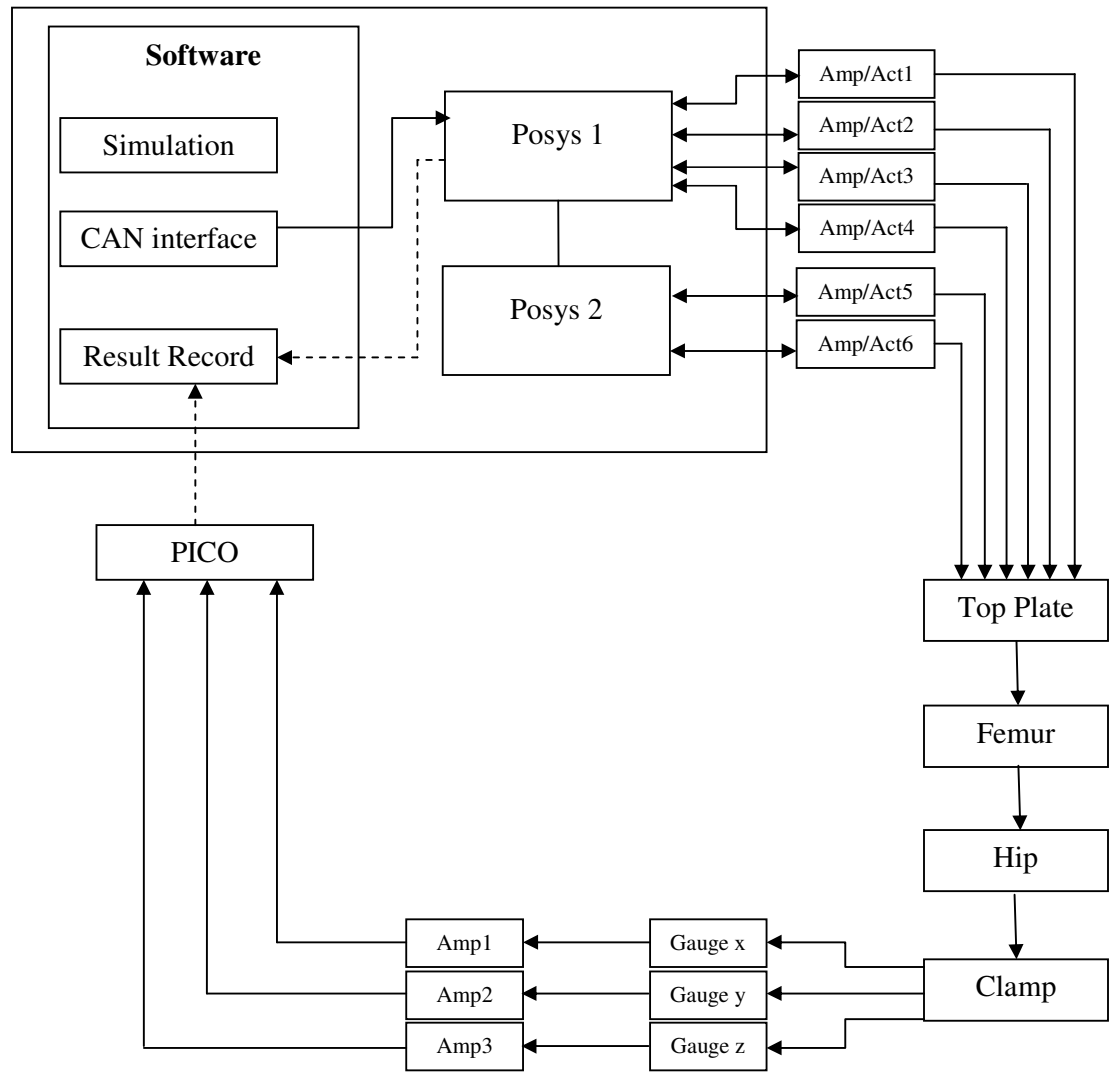


**Figure 6.1 Schematic of complete system**

## **6.2 Experiment Procedure**

This section will describe the procedure of how the experiment was to be carried out once everything was assembled and connected, other than the software programmed, which can be seen in the previous chapter.

### **Amplifier networking and tuning**

Firstly, each individual CAN address has to be allocated to each Xenus amplifier. This is performed by turning at CAN number dial on the face of each amplifier (next to the J4 connection). Each amplifier requires a separate number; however none can be set to number 0 as it is reserved for a bypass function.

Network configurations have to be established with the computer, the POSYS card and all 6 actuators. Upon opening this program, the software asks which method of connection is being used. For this project, the “CAN network” setting is used with the POSYS card drivers. This should automatically find all amplifiers on the control area network. If this fails, on the CME2 main screen, click on “Tools” in the menu bar and then “Communication Wizard”. In the drop down menu the two POSYS cards should be present. If not, then consult the POSYS manual about installation of the cards and drivers. In this case, POSYS channel 0 was selected as it is our master card. The bit rate is also an option based on the specifications of the card; in this case, 1Mbit/s was selected.

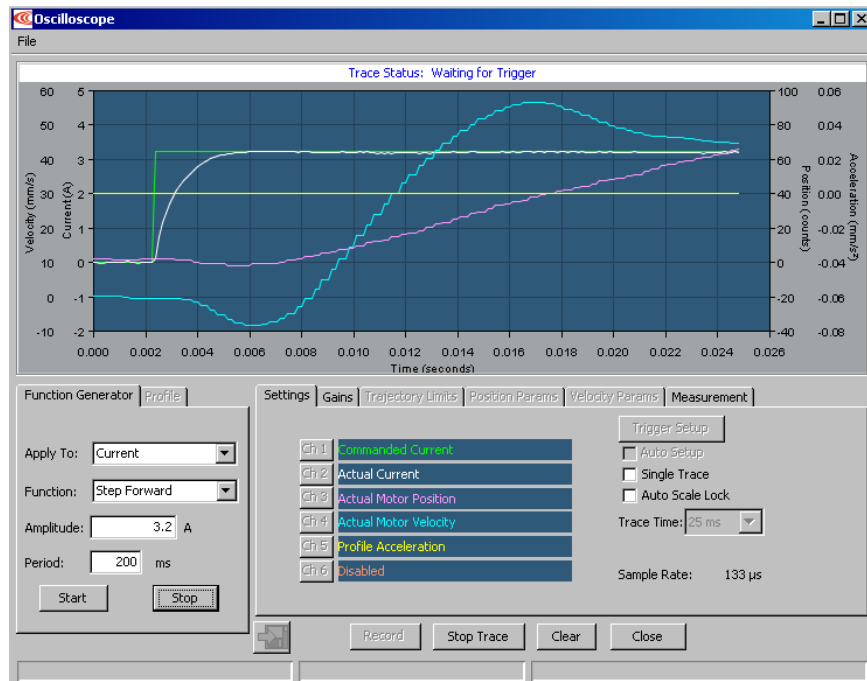
Then, the amplifiers have to be tuned, in turn, using the CME 2 software supplied by Copley Control, to synchronise the amplifiers and actuators. This is performed by selecting “Amplifier” from the CME2 main menu bar and then “Auto Tuning” from the dropped down box. The first step of this is the current loop calibration, as the positive initial position of the servo tube has to be determined. This is done by manually extending the tube (ensuring the amplifier is disabled) and then seeing the polarity of the position feedback, displayed in the window. If the displacement in counts is negative, this setting can be inverted in the same box. The bandwidth frequency is then determined.

The next calibration is for the velocity loop. The software then asks the user to place the servo tube in the middle of its range using the jog function. The jog function is an interval increase in current, which causes the tube to further extend. In this case, an extension to the mid-range is around 12cm. From this the gain values are determined.

### **Actuator configuration and observation**

Once the amplifier has been tuned, settings have to be loaded on them, regarding the actuator model. This is performed by going to the menu bar and again clicking on amplifier. Select basic set up from the drop down menu. A radio box should appear; asking which type of motor and model is being used, in this case, model STA (servo tube actuator) and the model 2504s. The software will then ask for the operating mode and command source. For this, position mode is selected and the command source is “CAN”.

Once all of the configurations have been set, the CME2 software can be used to look at the actuators response characteristics. Figure 6.2 and Figure 6.3 show various control functions with varying parameters operating at maximum current of 3.2A. Results show commanded and actual current (green and white lines, Ch1 and 2) to servo tube along with actual position and velocity of the thrust rod (pink and blue lines, Ch3 and Ch4) and profile acceleration which shows average acceleration throughout the time step (yellow line, Ch5).



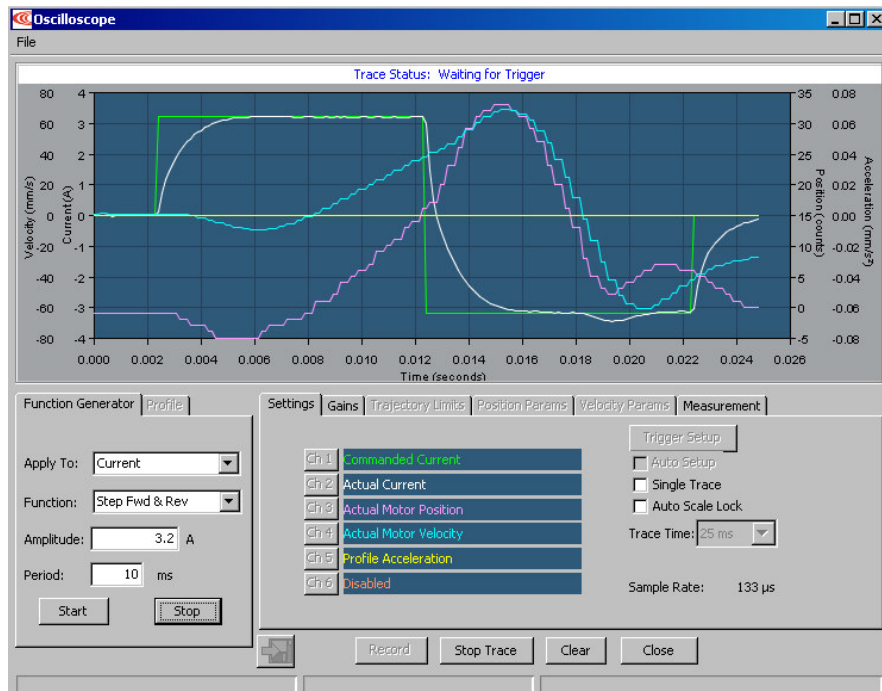
**Figure 6.2 Step forward function at 3.2A for 20ms**

Figure 6.2 shows that the command is followed quite accurately as the actual current follows the commanded current quite closely, only falling away slightly as the current is stepped up but this is quickly recovered. The position is shown to increase for the forward step during the time period. The velocity is shown to increase as the thrusters



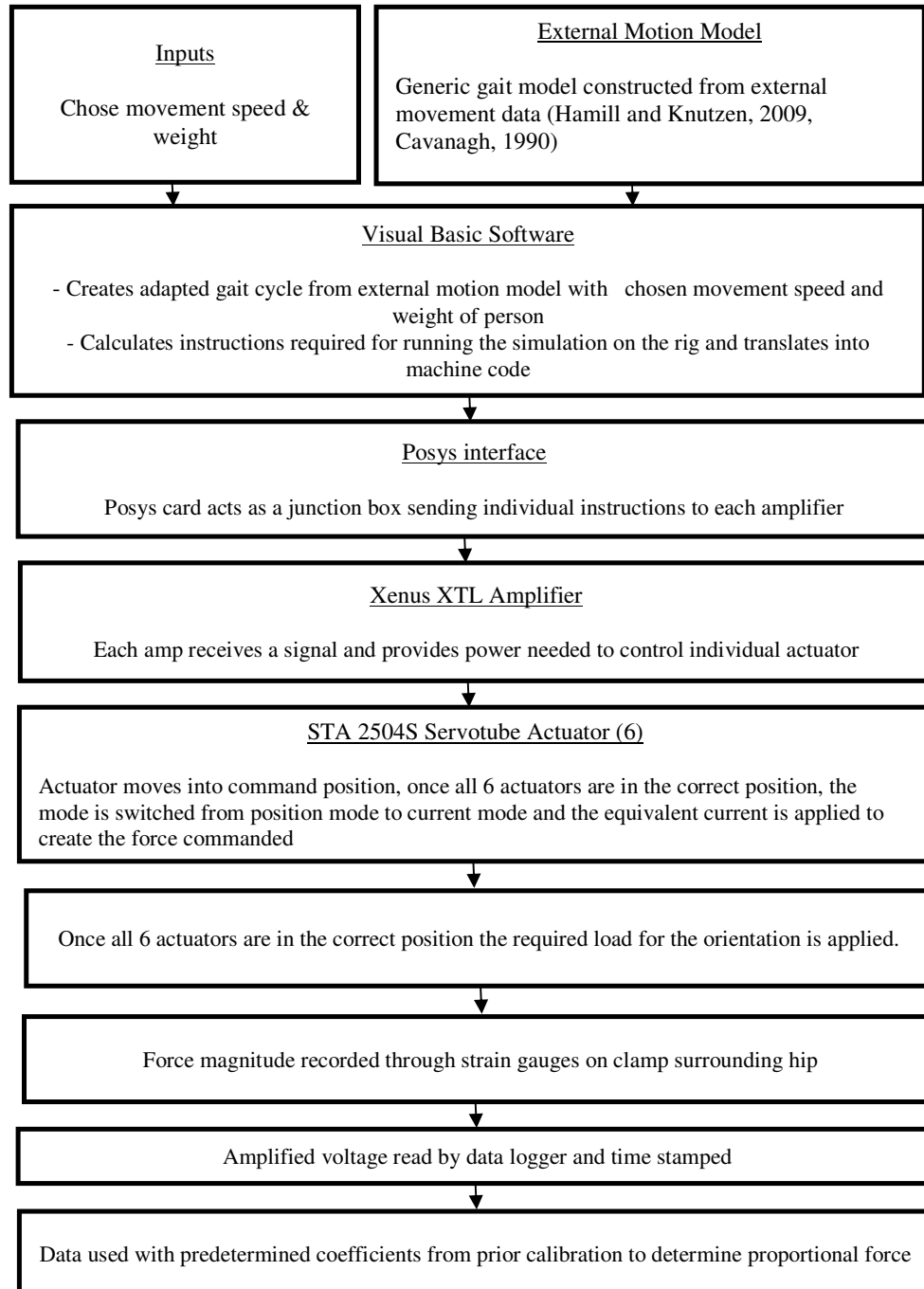
begins to move and then overshoots its intended final velocity for the move and corrects itself. For longer steps, velocity would continue at this rate but was here inhibited by loading. The initial position decreases slightly before the forward step is carried out, this is probably due to the electromagnetic solenoid being engaged by the current causing a shock.

Figure 6.3 shows the current increasing positively for the step forward and then negatively for the step back. The position and velocity increase to their peak at a slight delay to the current and then return backwards to their initial states. The second increase in position and velocity at the end are probably due to the attachment “bouncing” on the actuator body.



**Figure 6.3 Step forward and reverse function at 3.2A for 10ms**

A flow chart of how the whole set up:



**Figure 6.4 Process Flow Chart**

Various items of hardware and software were combined to form the foundation of the developed Stewart Platform joint simulator. The hardware consists of a PC and auxiliary devices. The auxiliary devices comprise PCI controllers (Servo Halbeck, POSYS 1924), connection cables, a power cabinet with the required forms of protection, such as fuses, amplifiers (Copley Control, Xenon) and actuators. Two PCI controllers were installed in PC. The first controller (POSYS1) was in charge of controlling four of the actuators, while the second was connected with the other two remaining actuators. It should be noted that actuators were not directly connected to the PC; however, the amplifiers provide the necessary power for the motor movements regarding the position and force required. The position and torque modes were regularly switched in the process of the experiment. The forces were measured by three strain gauges operating as a feedback mechanism to the system. The developed software calculates the values needed for a motion, i.e. the length of each actuator and the force needed to perform the walking. The controller sent the length of all six actuators each time and once they were in position the controller switched to force control and sent the required force for the movement. Afterwards it switched back again to position control recorded the new actuator position. It then repeated for the next orientation within the next step in the gait cycle.

**Table 2 Data from Software to POSYS Card**

Time	L1	L2	L3	L4	L5	L6	Force (N)
0	-	-	-	-	-	-	0
1	X11	X12	X13	X14	X15	X16	Y1
2	X21	X22	X23	X24	X25	X26	Y2
3	X31	X32	X33	X34	X35	X36	Y3

The table 2 represents the length of each actuator and the force at each time and these are the outputs of the software to the POSYS controller. At time zero, there were no position or force command values for the actuators to make any movement. For the first orientation, the first line of data from the software is used to place the platform into position. The POSYS controller ensures the actuators positions. Once the platform is in the correct position, the force (Y1) is applied. The force feedback clamp returns the force measured through the PICO data logger. The cycle continued through the further phases of the movement. As an instance, in time 3, L1 to L6 shows the position of actuators 1 to 6. Y3 represents a value for the force at stage 3.

### **6.3 Experimental Outcome:**

Since this study was designed to measure the force and displacement of the hip joints during three types of walking methods (slow, normal and fast walking) for three different weights, the obtained results are compared with a previous in vivo hip joint contact forces study (Bergmann et al., 2001) to see if a correlation existed between the results and Bergmann's data. How closely the Stewart Platform is at successful

replicating a scaled version of Bergmann's experiment, will be a guide to how successful the design and control system is.

#### About Bergmann's experiment

In Bergmann's experiment, instrumented total hip implants provided with telemetric data transmission were used to measure the hip contact forces. The instrumented implants provided the data regarding the contact force. It was transmitted by the acetabulum cup to the implant head; the angles of inclination of  $F$  in three planes are denoted as  $A_x$ ,  $A_y$ ,  $A_z$ . This study chose nine different daily activities to investigate. A Vicon system with six cameras and a sampling rate of 50 Hz was used to measure the positions of the body markers. In order to measure the ground reaction force, two Kistler plates were provided. By the use of a common marker signal, the data obtained from gait analysis and the readings from the instrumented implants were synchronized.

All the coordinates of the external markers on the legs and pelvis of the subjects, plus the coordinates of the ground reaction forces, were measured according to the fixed laboratory coordinate system. The marker positions relative to the bony landmarks on the patients were measured. The locations of the joint centre and additional reference points relative to these landmarks, used for calculating the rotations, were determined, using individual CT data. This allowed the calculation in relation to the laboratory coordinate system of the coordinates of the joint centre and reference points from the measured marker positions. These coordinates determined the positions and orientations of the body segments of pelvis, thighs, shanks and feet in space (Bergmann et al., 2001).

## Chapter 6

The force acting on the hip joint is known as contact force; it has three components. As shown on Figure 6.5, the Z-axis is assumed to be parallel to the midline of the femur, the X-axis is perpendicular to the femur midline and finally the Y-axis is perpendicular to the above axes.

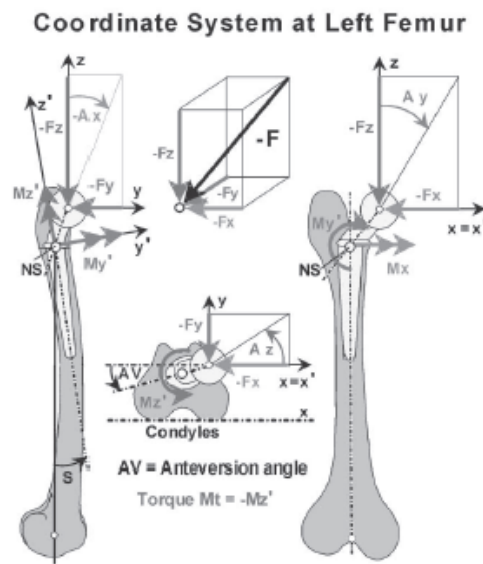


**Figure 6.5** Coordinate system for measured hip contact forces(Bergmann et al., 2001)

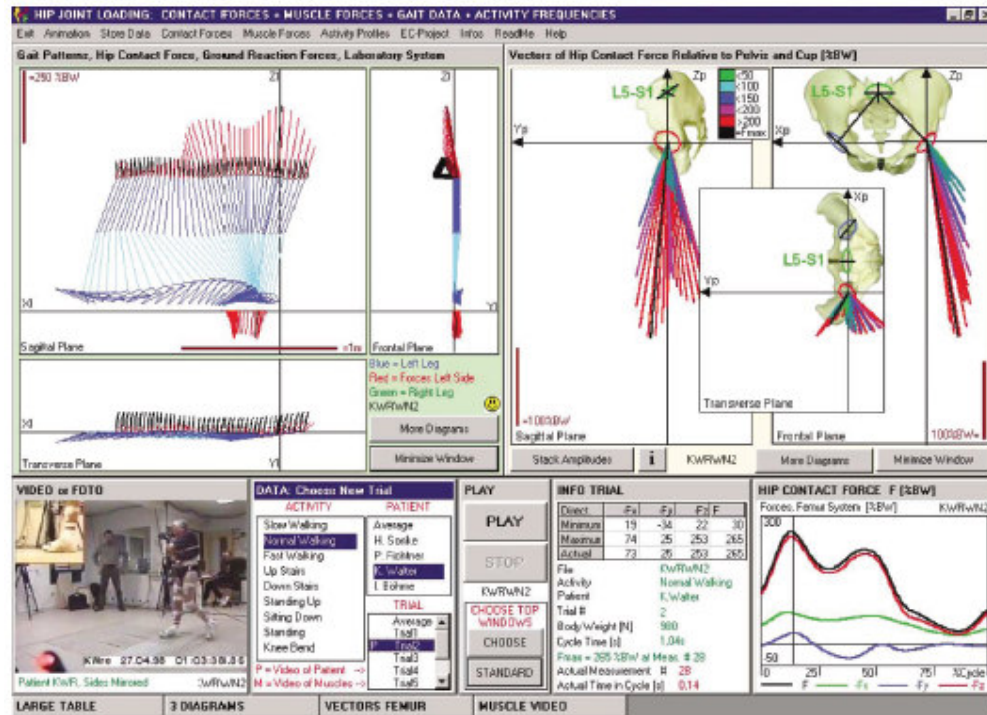


**Figure 6.6** Gait analysis data and calculated muscle forces (Bergmann et al., 2001)

Figure 6.6 displays the different steps taken in measuring the contact force on the hip joint. The picture on the top left hand side shows the gait patterns, hip contact force and ground reaction force in the sagittal plane. The picture on the right presents the different vectors of contact force on the pelvis and hip joint in all the planes. At the bottom left hand side of the figure, the patient is shown during the experiment, on the right are shown the different components of the contact force according to the body weight.

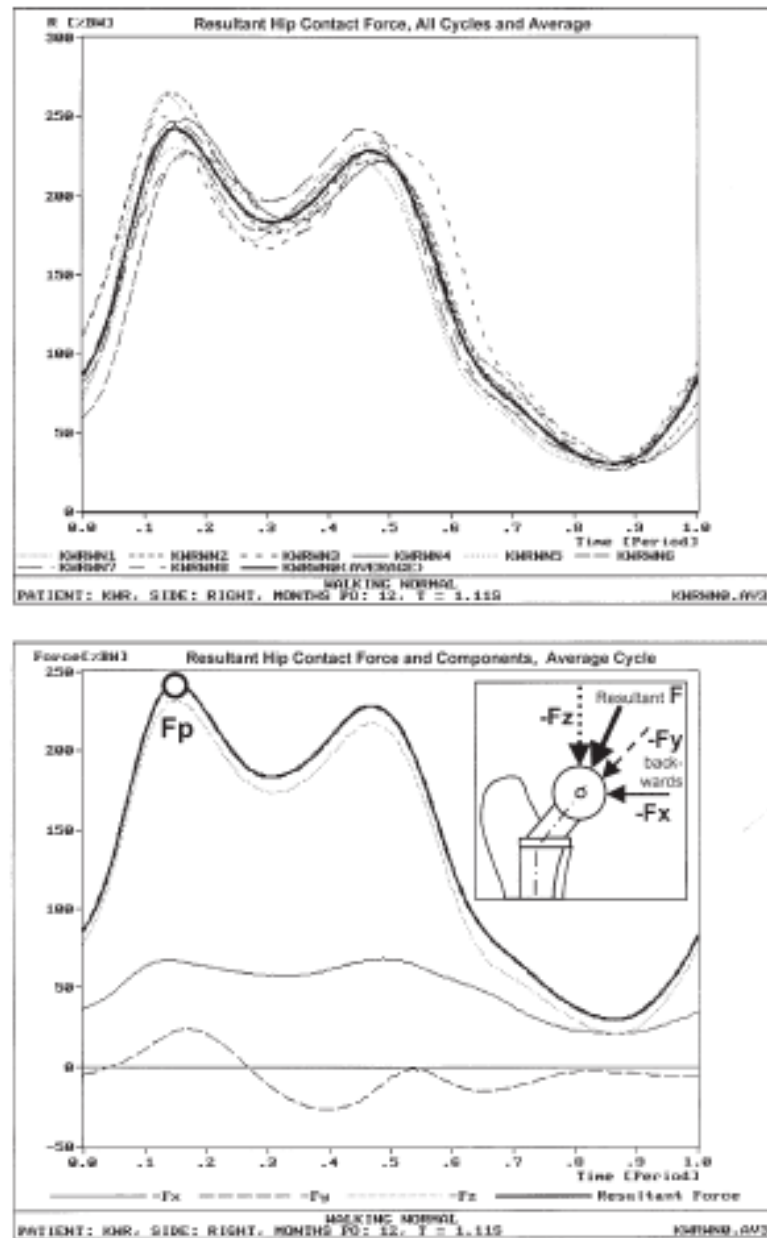


**Figure 6.7 Contact force on hip (Bergmann et al., 2001)**

Contact force  $F$  of a patient during normal walking shown in the above figure. Figure 6.7 shows at the top the results of eight trials of one of the participants and the thicker



line in this figure shows the average of all the trials. At the bottom of Figure 6.7, the average plus the components of the contact force are displayed.

The reference graphs from the above paper are provided in Appendix 1 together with personal information and the anatomical data of each participant. Finally, Appendix 1 contains a table displaying the peak loads of single and average patients and the cycle times and body weight of an average patient, which represent the data obtained from each participant during the recorded activities.

The walking speeds in the current study were 3.5 Km/h, 3.9 Km/h and 5.3 Km/h for slow, normal and fast walking respectively. The above speeds are chosen exactly the same as the experimental one in order to enable the user to compare them easily. All the movements of walking to obtain the calculated data are assumed to be on level ground. According to the paper the experiment was repeated for three different weights, light, normal and heavy, taken as 702 N for patient KWR, 860 N for HSR and 980 N for PFL respectively. Since the actuators of the rig have the limitation regarding the maximum force they are able to bear which is 312 N for each, the sample weights for the experimental have been chosen as 400 N, 490 N, and 560 N. it should be noticed that the proportion of the weights for experimental has been chosen in the way to be the same as the proportion of the experiment.

### **6.3.1 Force**

The main focus of this study was to create a machine that can closely replicate a human joint. This section will look at how well the internal forces can be replicated with this machine.

The following graphs present the trajectory of the contact force against the percentage of the walking stride. Each experiment took into account the individual speed of walking and weight of each patient. A comparison to the base study will be shown in the discussion chapter.

It is to be noted that the first 50% of the gait cycle is where the leg being examined takes the total body weight and the other foot is in 'flight'. Equally, in the latter 50% there is very little force shown as the weight is being transferred to the other leg and the leg being examined is in 'flight', until the weight transfers back again, as shown in all cases at around 85%.

The following three graphs (Figure 6.8 - Figure 6.10) represent the results from the Stewart Platform for the light weight in three different speeds. It can be seen that for all graphs two different peak points are observed and this is expected for a normal walking.

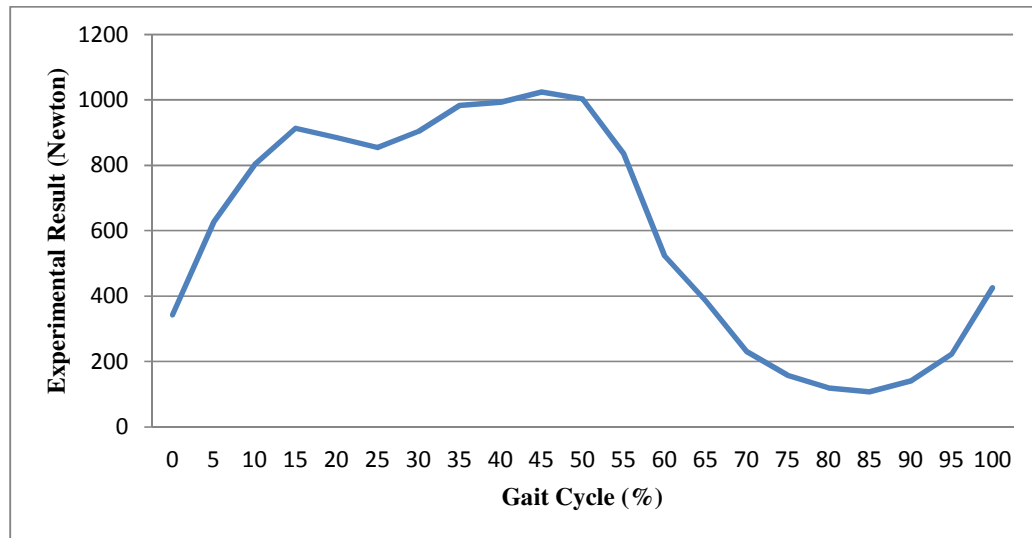


**Figure 6.8 Light Weight, Slow Walking Speed**

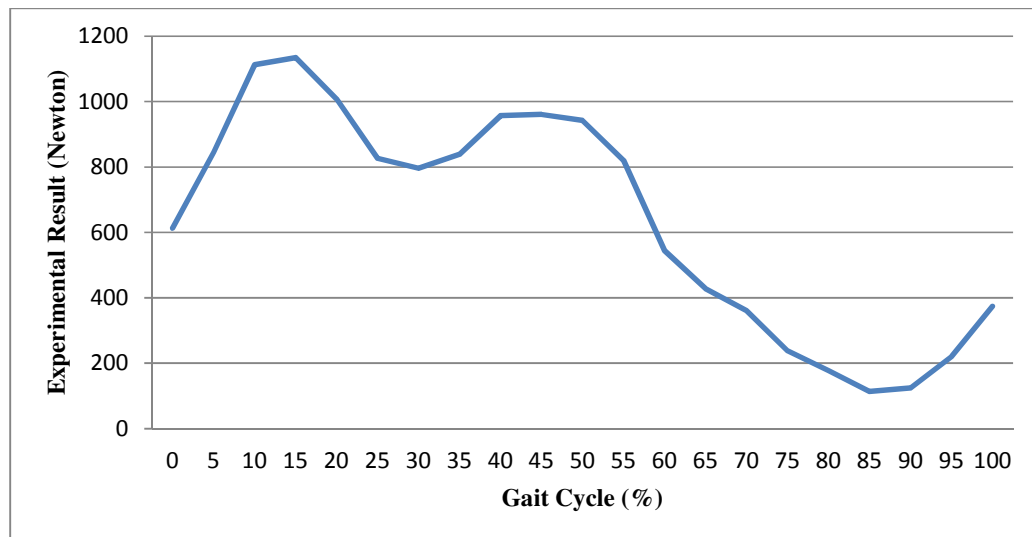


**Figure 6.9 Light Weight, Normal Walking Speed**

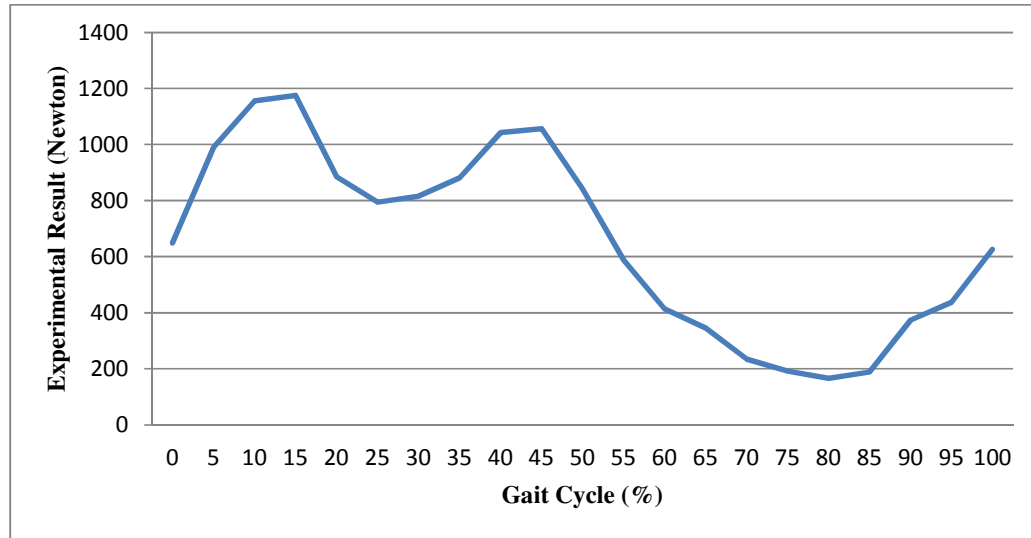


**Figure 6.10 Light Weight, Fast Walking Speed**

Figure 6.11 to Figure 6.13 represents the results taking from the Stewart Platform for the normal weight in slow, normal and fast speed. It is noted from the graphs that the peak contact forces acting on hip increases when the speed is increases.

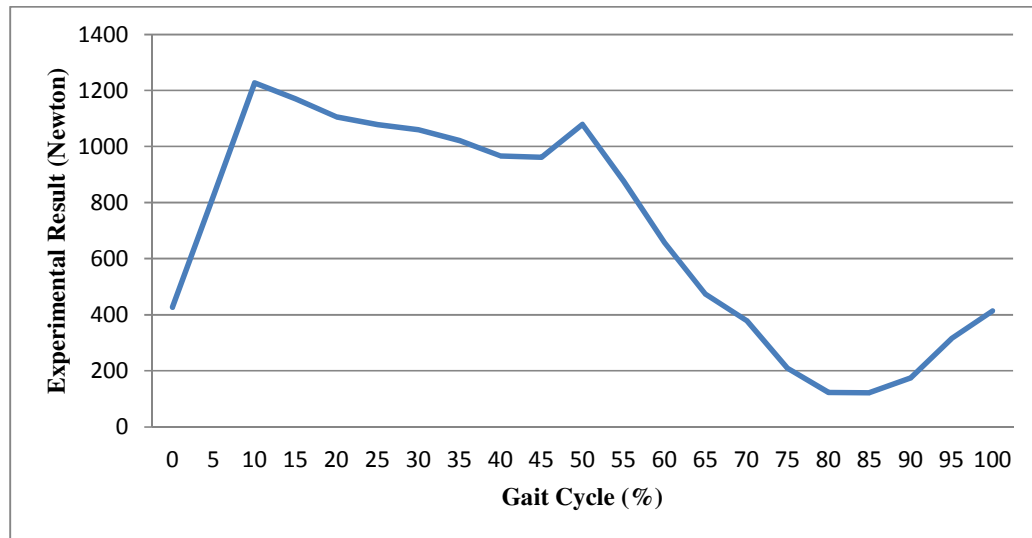


**Figure 6.11 Normal Weight, Slow Walking Speed**

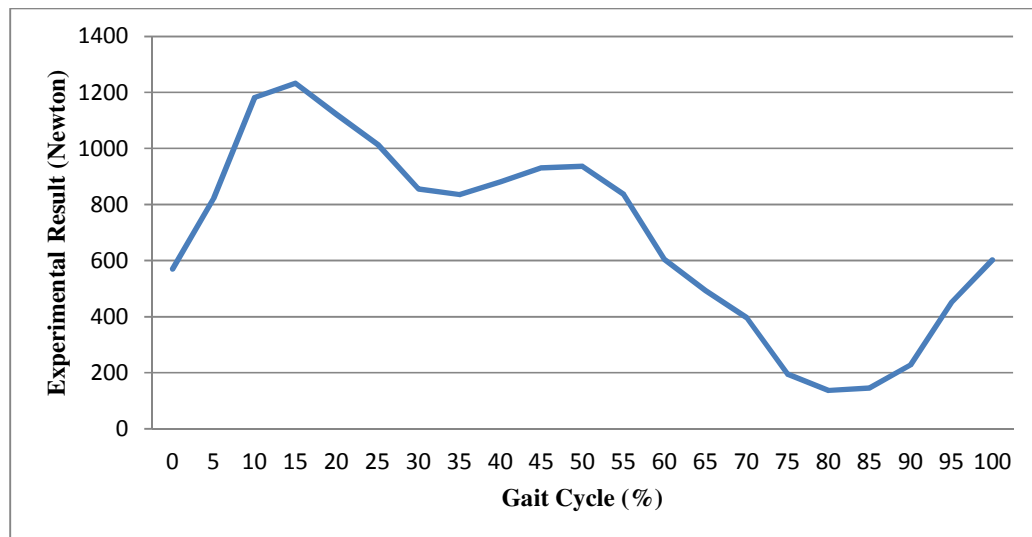


**Figure 6.12 Normal Weight, Normal Walking Speed**

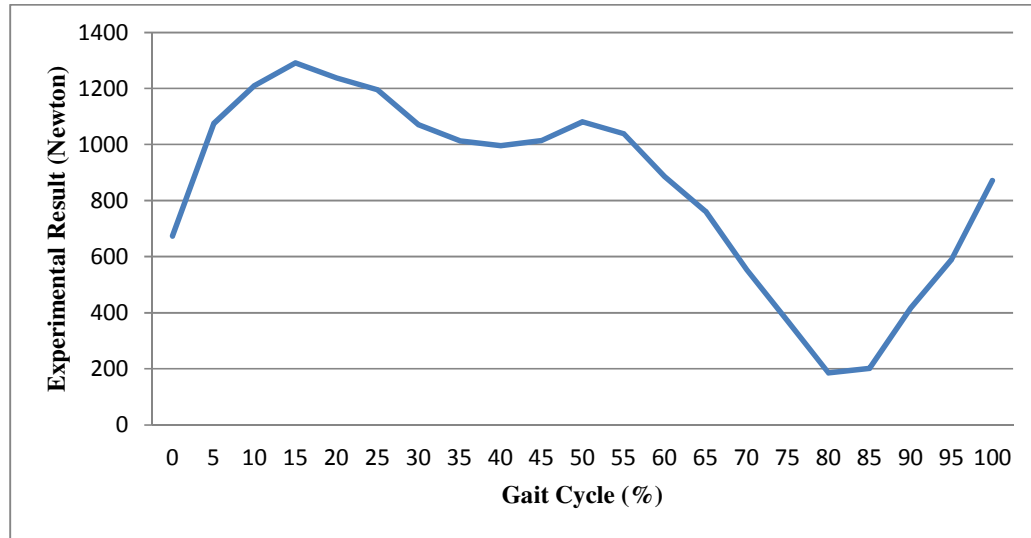


**Figure 6.13 Normal Weight, Fast Walking Speed**

The last three graphs in this section (Figure 6.14 - Figure 6.16) represent the experimental results from the universal human joint simulator, Stewart Platform, for the heavy weight in three different walking speeds. In these graphs we can notice only one peak contact force.

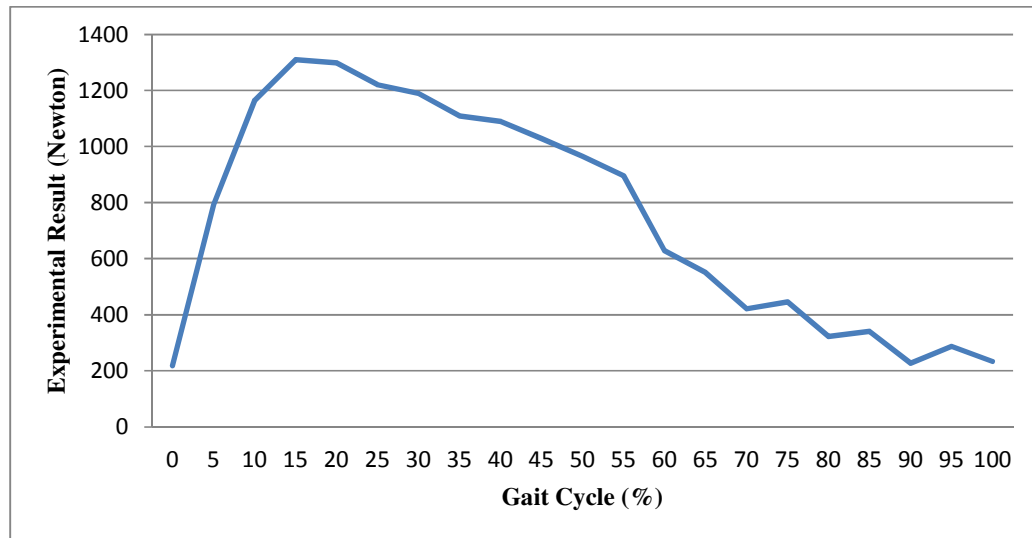


**Figure 6.14 Heavy Weight, Slow Walking Speed**

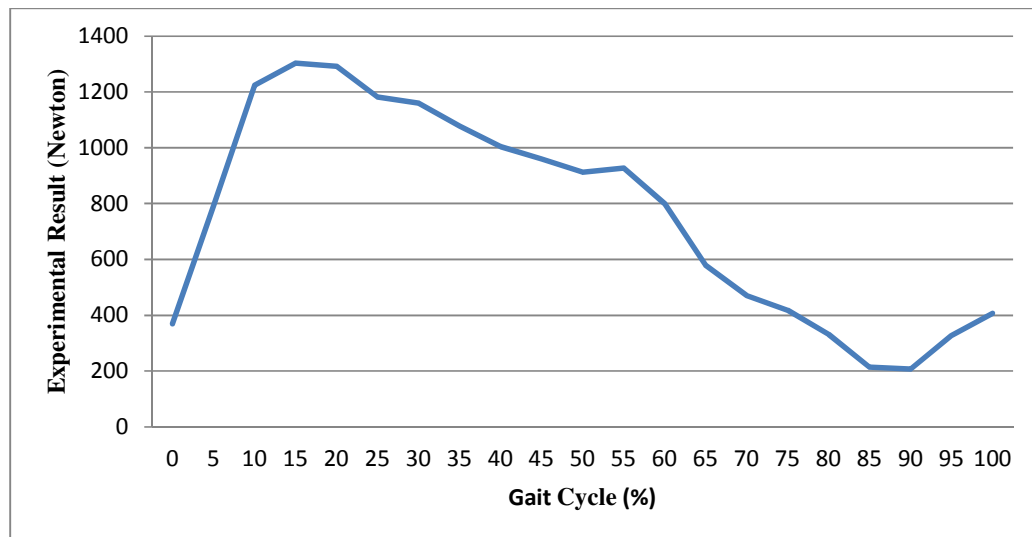


**Figure 6.15 Heavy Weight, Normal Walking Speed**

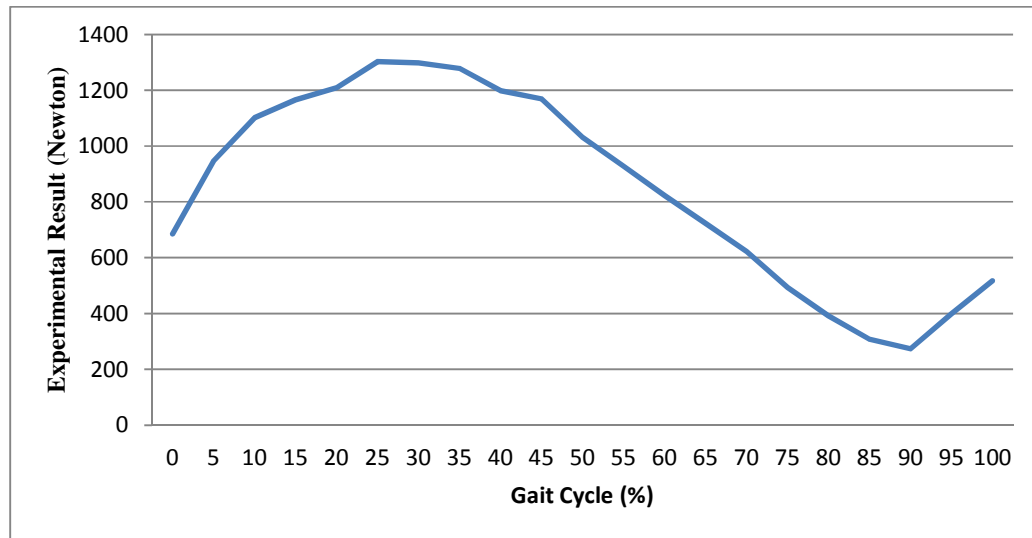


**Figure 6.16 Heavy Weight, Fast Walking Speed**



### **6.3.2 Displacement**

In addition to the force results, the displacement in the three dimensions of the hip joint was also obtained. This was performed by using an inverse equation of that used to calculate the actuator legs from the experimental.

In the following graphs displacement in millimeters of the hip joint during the stride according to the time are presented. Figure 6.17 to Figure 6.25 shows the difference in displacement of the femur head inside the joint in x, y, z directions during the force is applied.

The reason for obtaining these results was to observe the integrity of the design and build of the system. An ideal outcome would be neither too much nor too little displacement. But consistent readings are expected for all weights and activities.

The following first three graphs in Figure 6.17 to Figure 6.19 represents the displacement data of the platform in X, Y and Z plane for the light weight in three different speeds. These data is to verify whether the Stewart Platform is behaving as a real human hip would do or not.

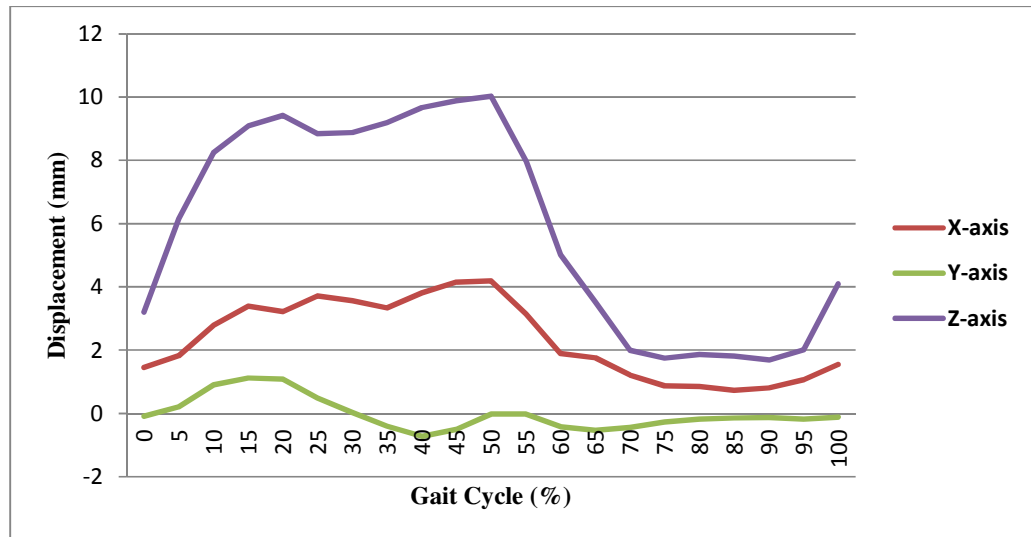


Figure 6.17 Light Weight, Slow Walking Speed

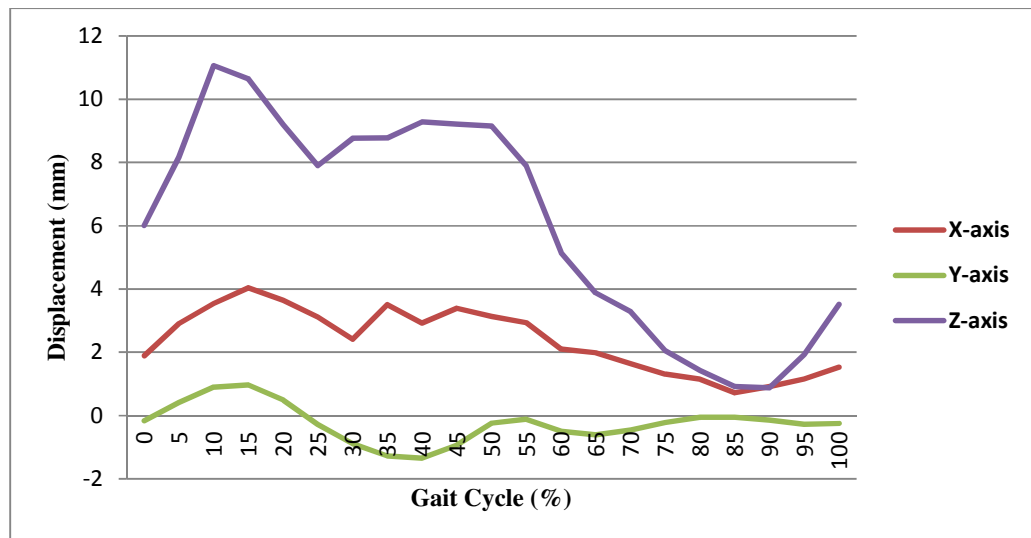
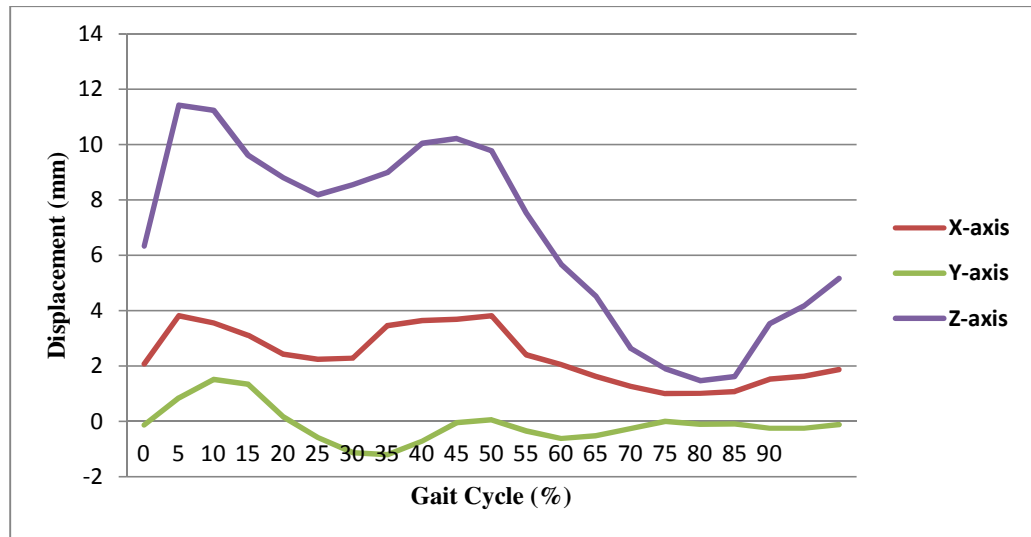


Figure 6.18 Light Weight, Normal Walking Speed



**Figure 6.19 Light Weight, Fast Walking Speed**

The next three graphs in Figure 6.20 to Figure 6.22 correspond to the displacement data for the normal weight in slow, normal and fast walking speeds. These data is to verify whether the Stewart Platform is behaving as a real human hip would do or not.

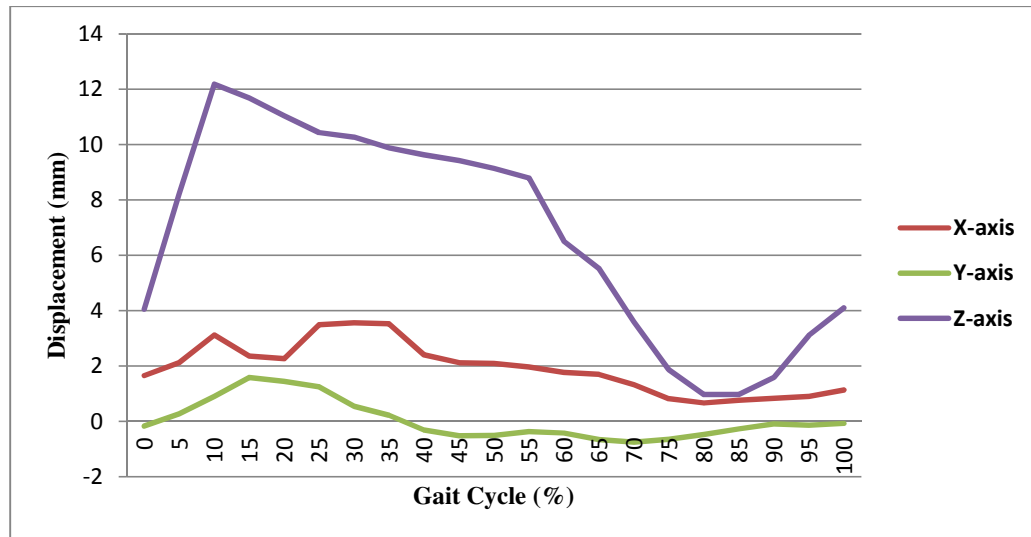


Figure 6.20 Normal Weight, Slow Walking Speed

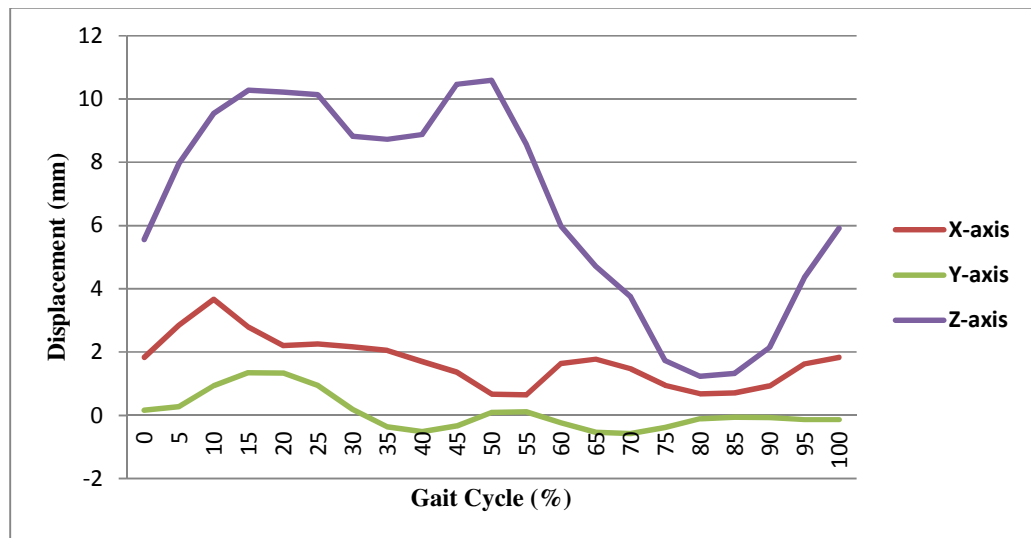
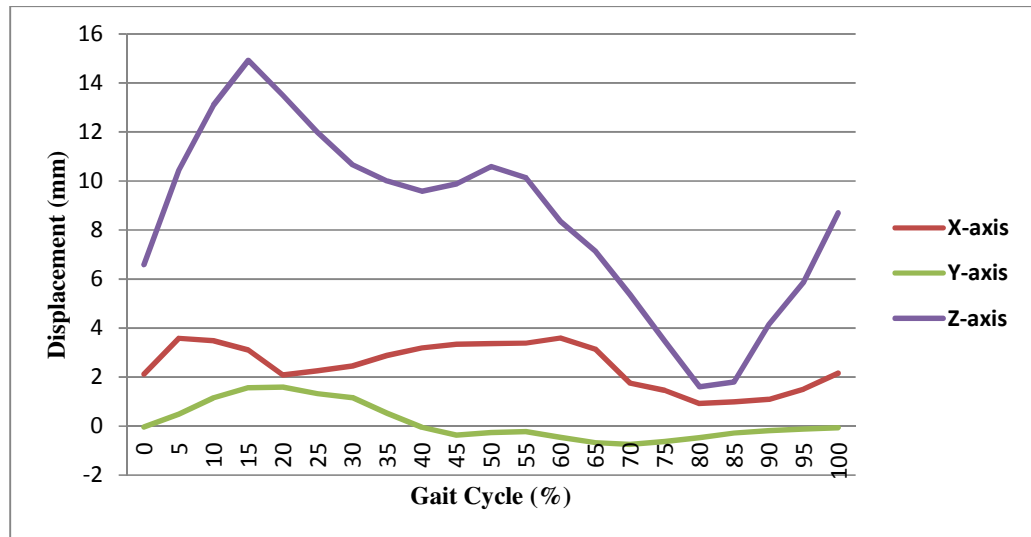


Figure 6.21 Normal Weight, Normal Walking Speed



**Figure 6.22 Normal Weight, Fast Walking Speed**

The last three graphs as shown in the following page (Figure 6.23 - Figure 6.25) stand for the displacement data of the platform for the heavy weight in different speeds. As in all the nine previous figures the most displacement occurs in the Z plane and that was due to the fact that the direction of the contact force mostly in Z direction.

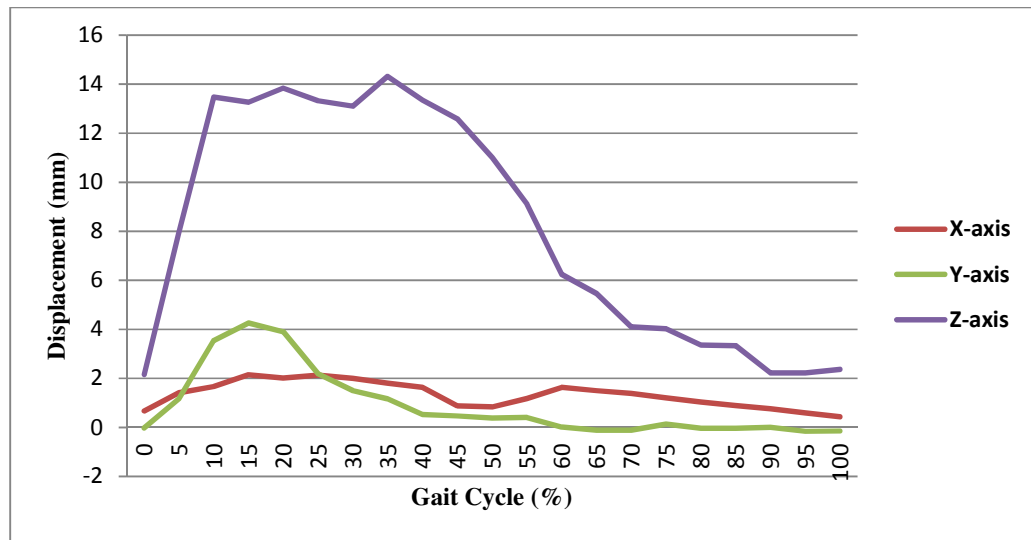


Figure 6.23 Heavy Weight, Slow Walking Speed

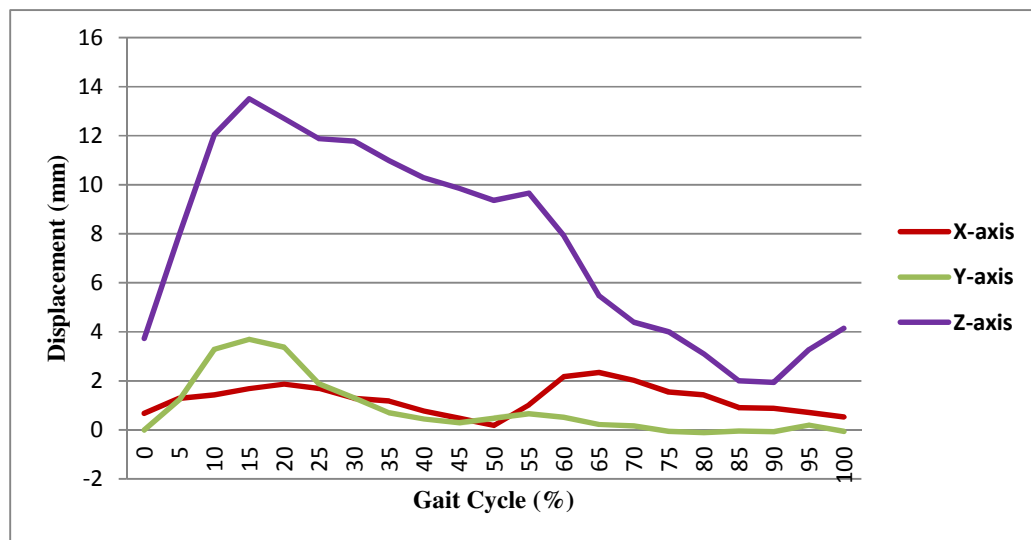
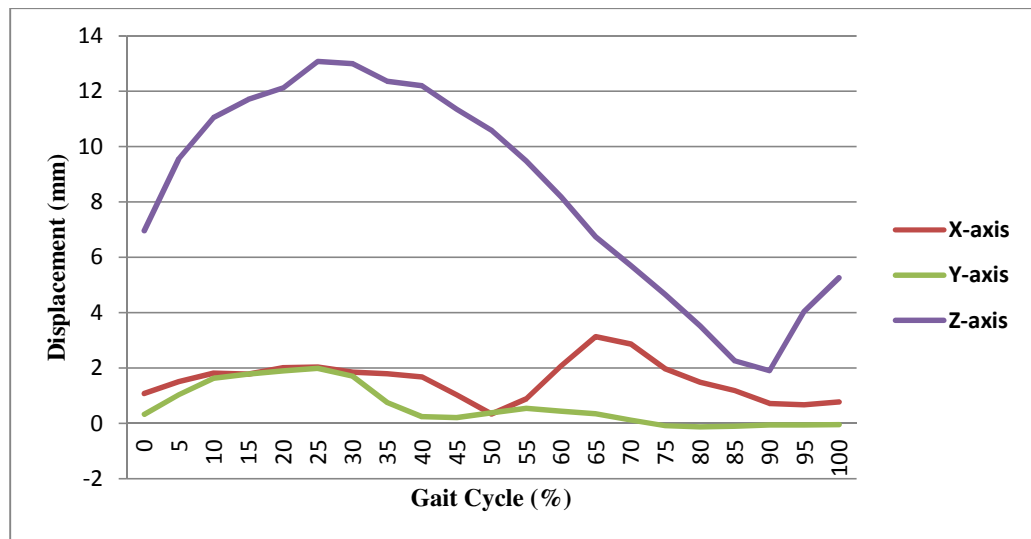


Figure 6.24 Heavy Weight, Normal Walking Speed



**Figure 6.25 Heavy Weight, Fast Walking Speed**

## **Chapter 7.      Evaluation of Results**

This chapter analyzes the results obtained from performing the experiment. It will look at whether the system was successful at fulfilling its requirement and if not, where improvements might be needed to make the simulation more realistic. A review of the system and notable experiments are also included.

The main objective of this thesis was to design and build a universal human joint simulator, using a Stewart Platform made with precision servo tubes. The Stewart Platform design was chosen for its ability to move the joint in all six degrees of freedom, which can be relatively small movements, but nevertheless an important fact in biomechanics. Having the ability to simulate joints with six degrees of freedom, allows the machine to be used for a large number of human joint investigations.

The topics under this study were the design and control of the Stewart Platform, human joints and their individual ranges of motion and the writing of a computer program to implementing these ranges of motion. Other topics for research were also the setting up and installation of the actuators' software and hardware.



### The Stewart Platform System

The system was designed in such a way as to simulate joint movement in a configurable manner. The case study used in this thesis is that of the hip joint. The system operated as expected during the simulation, with very little adjustments having to be made. For the heavier weight moving fast, some over-heating occurred, but just required a cool down period. This is to be expected when using the actuators constantly at their full potential.

The rig was designed to allow most of its components to be easily replaced if necessary. Most of the components were detachable, including the bearings, which could be replaced by universal or spherical joints and the bone holders, which could be replaced by other holders with the same functions or by more generic holders.

The method of pelvis attachment was suitable, as it enables the pelvis to be held tightly in place. However, the femur attachment could be improved by holding the bone more firmly as the screws simply press against the bone and can deflect slightly. The cylinder for the pelvic attachment itself was capable of fixing the femur and other similar bone shapes securely, but with other bones, including vertebrae, wrists and mandibles, it would be much less compatible; but since these are joints within the operating specification of the platform, an interchangeable attachment might improve the platform's usefulness.

The actuator cylinder holders were well designed because they were strong but had a low magnetic index and therefore interfered less with the magnetic thrust rods; they fitted well into the bearings, attached to the actuators easily and were easy to manufacture.

One of the important targets in this design was to minimizing the weight of the rig machine for the sake of transportation and mobility. A successful attempt to reduce the top plate was achieved and there were no serious suggestions for the re-thinking the design. However, options for materials should be considered further. Some components, such as the fixing pole, were made of steel, increasing the mass and stability because it is the arch that carries this weight; but it would be better to consider using aluminum. Moreover, if certain aspects of the design were to change, allowing greater freedom, the pillars would need to be positioned further apart from each other.

A matter of concern regarding the design of the Stewart Platform is the joints connecting the plates to the actuators. The bearings used were not adequate in terms of providing all the range of motions desired. Nevertheless, the motion which is permitted with these is enough to prove that the concept of the simulator articulating a human joint.

The positioning of each actuator to the base plate and top plate was based on existing Stewart Platform designs, but these should have been positioned closer to each other on the top plate to give more freedom. This would have made the design more generic, which, considering its purpose, would have improved it, as well as allowing it to be

used for automotive and aeronautical purposes (for other potential university laboratory projects). However, for the purpose of demonstrating human walking, this distance was seen as optimal.

The top plate was initially designed as a hexagon; the modification of the design involving removing excess material, thus improving the design by reducing the weight. This greatly improved the design of the simulators.

The Stewart Platform build was generally within the specifications. The system was able to obtain all positions successfully and retrieve data accordingly. However, there are two areas of improvements that the system would much benefit from, which will be explained in the data analysis part of this chapter.

#### Control System and Powering

The cabinet created to house the six Xenus amplifiers was designed to several specifications. First and foremost, safety was a large factor. A three-phase system operates at 420 volts which can be lethal if inappropriately used. Many safety guards were put into place, including a double lock to the cabinet, an on switch that would make the door inoperable once turned on and an extendable emergency stop switch with a 4 meter cable. The whole system was powered by a dedicated power supply that also had a circuit breaker and off switch. After the design phase, the technicians at Brunel University's Mechanical Engineering department reviewed the schematics and approved it for use in our laboratory.

Other than safety, the purpose of the Xenus housing cabinet was to allow easy connection to the rig, personal computer and three-phase power supply. This was all done via the gusset hole at the base of the cabinet. This setup was carefully connected, allowing the degree of control required.

The cabinet is a semi-permanent installation. This was decided based on various factors, but the largest being the requirement of a three-phase power supply outlet, which is not often readily available and in most cases, would have to be installed prior to the installation of the whole system. The limits in terms of movement were not the fault of the equipment but rather the design. Overall, the system proved to be an efficient, user-friendly system. Preventative measures were put into place if an electrical fault may emerge.

A Visual Basic program was created to virtually simulate the range of motion of human joint activities, translate this motion into machine command and then finally record two different sources of data for each set of command. This proved to work effectively. The Visual Basic code is modular and easy to modify to the demands of all operations with varying configuration parameters, such as attachment length, platform size and initial starting height using the Copley Control integrated library, CMO. The kinematics and loading were controlled using positioning mode and current mode respectively. Position data was easily acquired from the actuators and the PICO data logger allowed for the force readings from the clamp to be stored in sync.

## **7.1 Force**

The focus of the experiments presented in this study is to verify how well does the system designed and manufactured in this study perform in the task of emulating a real human hip. The way this was assessed is by comparing how well the machine could replicate existing known data and by how much displacement the femur head has under force. The assumption is that the femur head has minimum displacement (about 2 millimetres at most) in a x, y, z co-ordinate system and that most of the locomotion involves rotation around a fix point (ball/socket centre).

As previously mentioned, the input model of walking into the machine was made out of kinematic data from Hamill and Knutzen, with the load analysis taken from a study by Bergmann. The forces from Bergmann were scaled down to best fit the specifications allocated by the selection of the servo tube actuators. The scaling number is based on the Stewart Platform's maximum calculated force (as derived in chapter four) to the maximum force attained by Bergmann for each activity. The following section will compare the input force (scaled Bergman) to the actual forces recorded from notable graphs.

One of the main objectives of this study was to simulate the contact force of the hip in walking. Four graphs have been chosen to display in result chapter to see whether or not the obtained results from the Stewart Platform was successful.

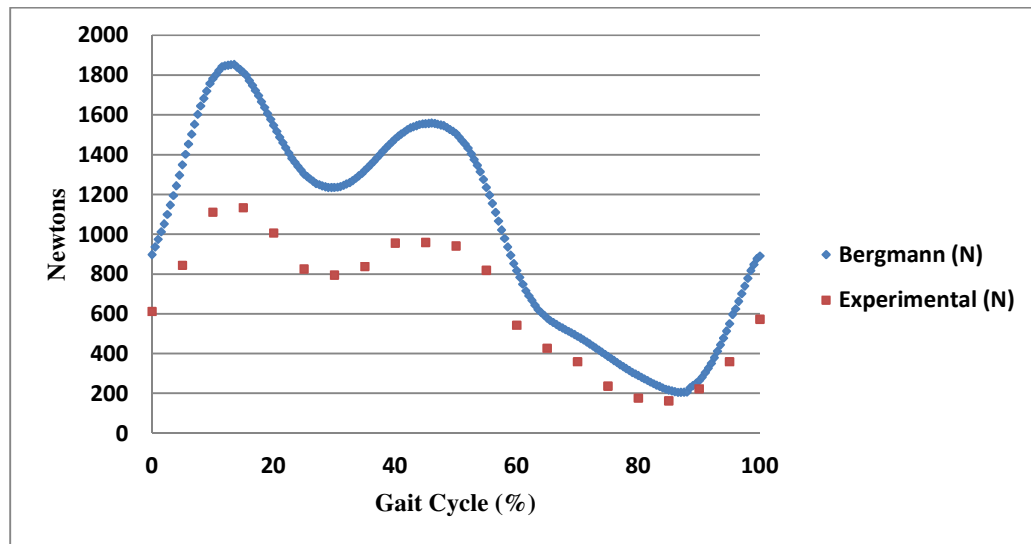


**Figure 7.1 Light Weight, Normal Walking Speed**

The graph in Figure 7.1 shows two matching trends, which suggests that this activity is well within the range of the simulator. This is obviously one of the least demanding activities, but it a good indication of what the system can successfully attain.

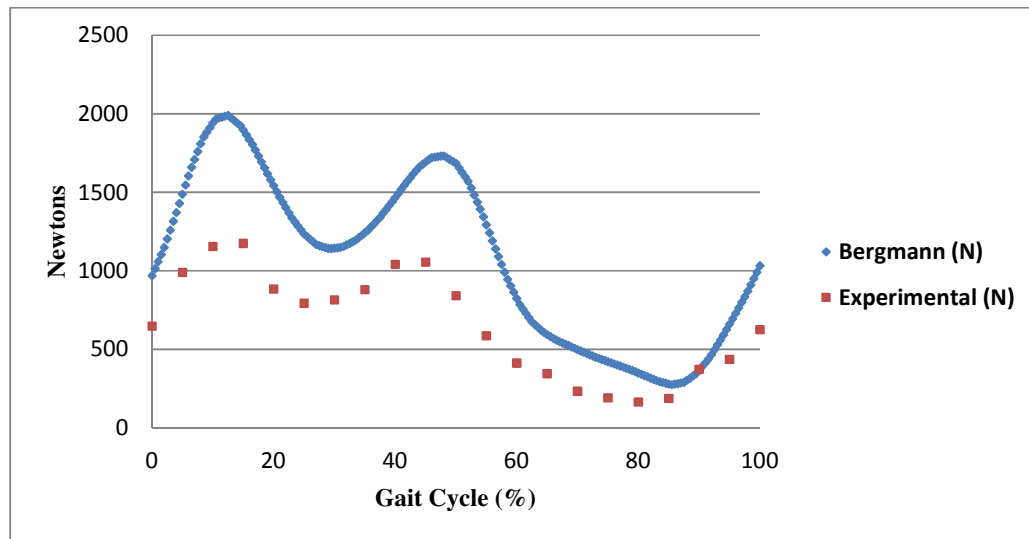


**Figure 7.2 Light Weight, Fast Walking Speed**

Similarly, the graph in Figure 7.2 shows two matching trends. However, at 90% of the gait cycle, the experimental is not matching the input result. This is a strange occurrence and could be due to the orientation of the femur head inside the acetabulum cup for that activity, as a faster walk suggests a longer stride and thus a greater angle. Such leg extension for creating a larger angle could result in causing an unrequited force on the pelvis. This anomaly will be noted and investigated in further in other graphs.

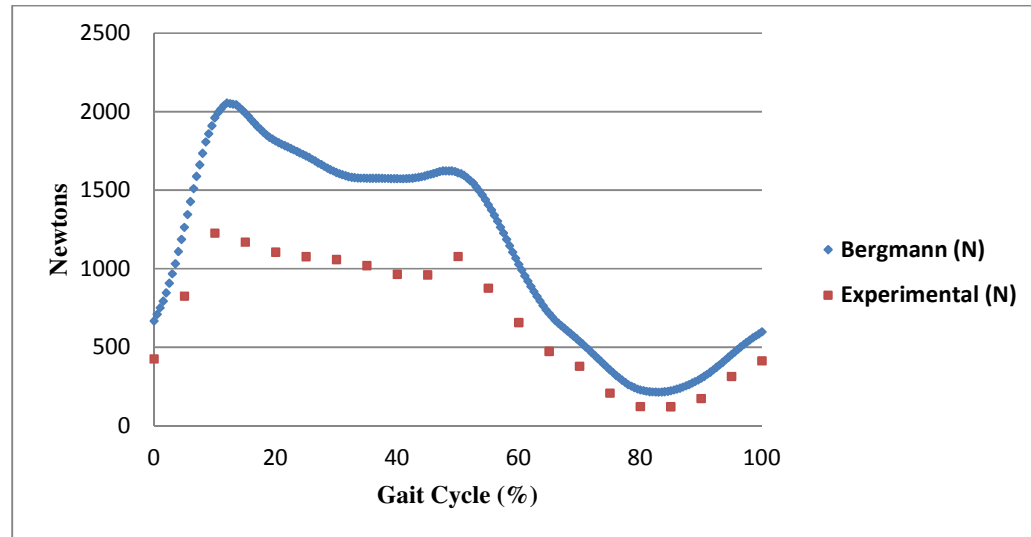


**Figure 7.3 Normal Weight, Slow Walking Speed**

These re-occurring matching profiles can be seen to slightly alter in Figure 7.3, with a clear larger difference in peak forces. This suggests that the machine can not accurately replicate forces over 1800N (or 1200N scaled). However, the rest of this graph is appropriate in matching as a scaled trend.



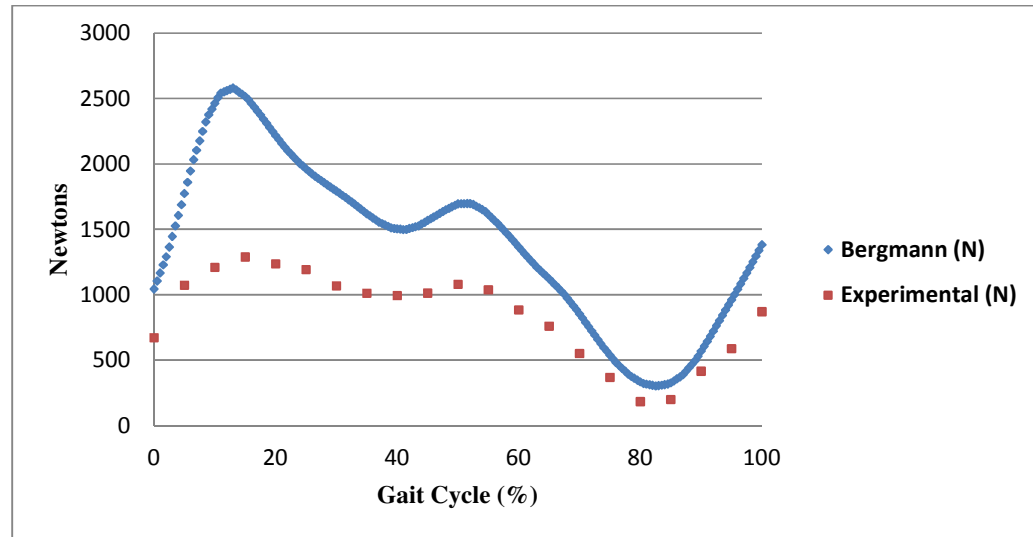


**Figure 7.4 Normal Weight, Fast Walking Speed**

The graph in Figure 7.4 further confirms the previous point of the machines inability to create forces over 1200N. A large misshape is obvious in the first quarter of the cycle. With real peak forces reaching above 2500N, the machine is plateauing at just under 1300N. This is below the theoretical maximum assumed by the six actuators and must be due to other system constraints, such as a current limit.

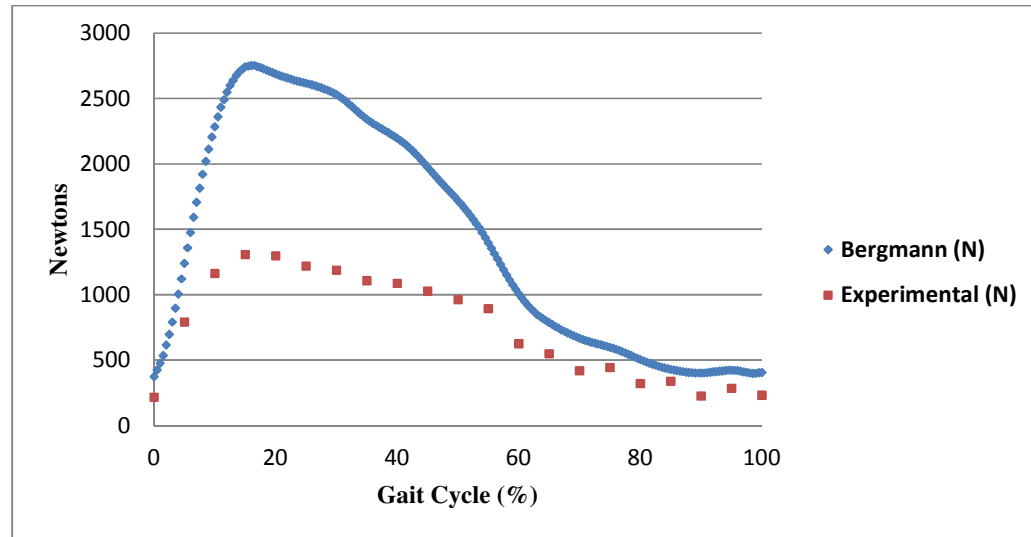


**Figure 7.5 Heavy Weight, Slow Walking Speed**

The final graph Figure 7.5 further highlights the shortcomings of the system with a clear lack of correlation in the first half of the cycle.

The selection shown in this section is a good representation of all 9 separate tests carried out. The general consensus is that the Stewart Platform is performing well until it is required to create a force larger than 1200N. This is 300N less than calculated and the machine has fallen short. However, this can be easily overcome scaling down the forces further, however, the relevance in doing so would hinder the use of the machine and any improvement should be focused on scaling the machine upwards to a one to one ratio. There is a suspicion that the current design could be more successful if the internal limits placed on the actuators could be tweaked, however this would certainly void any safety guarantee and could possibly cause damage and harm.

## 7.2 Displacement

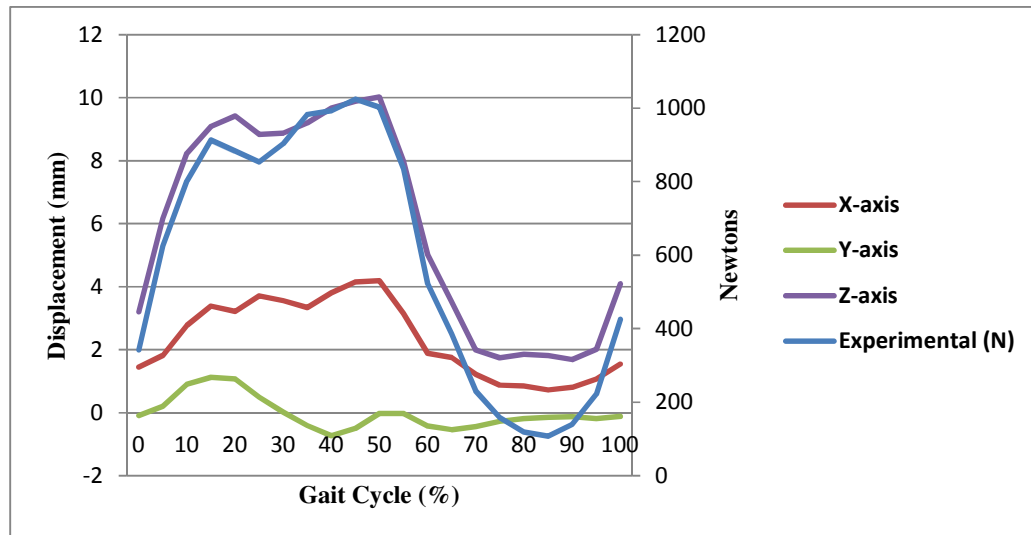


Figure 7.6 Light Weight, Slow Walking Speed

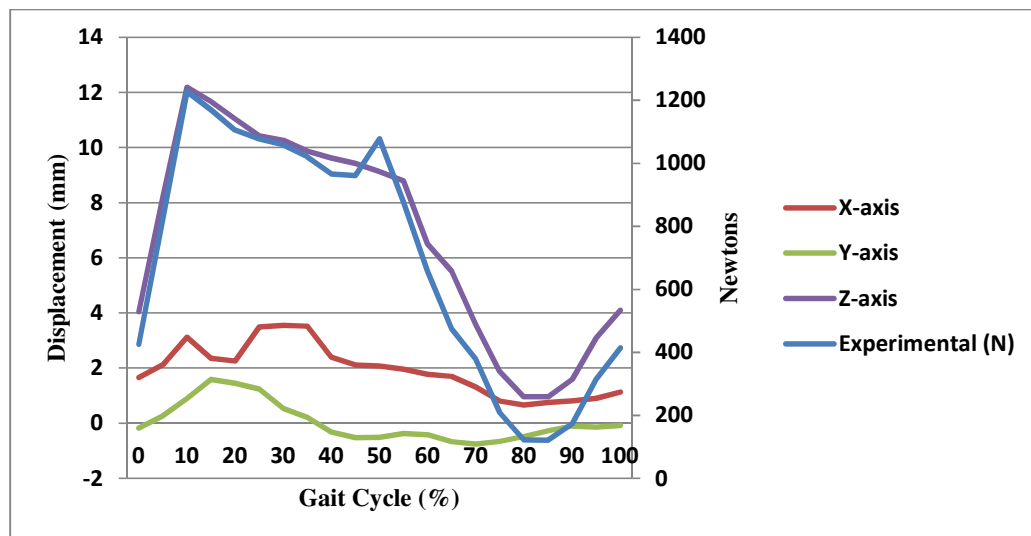
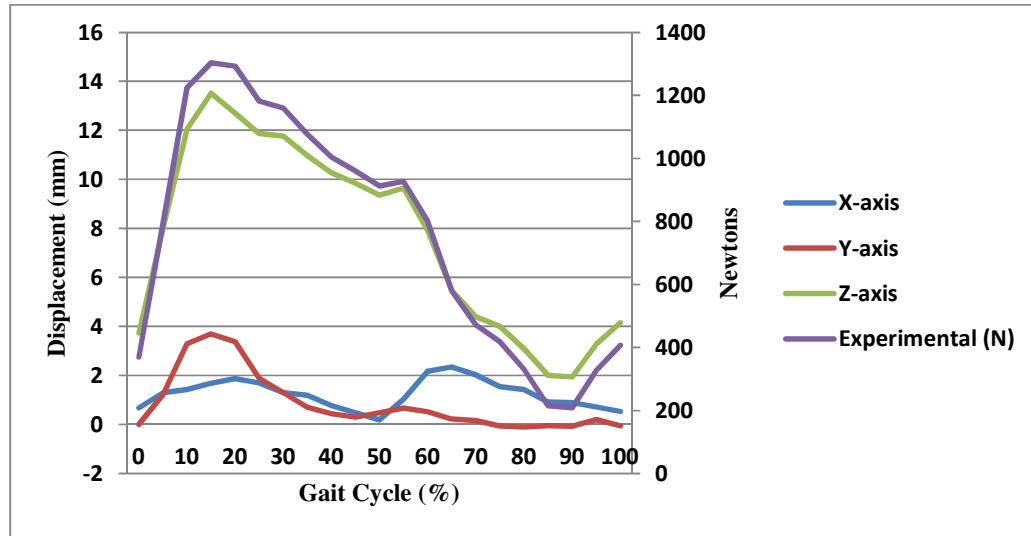


Figure 7.7 Normal Weight, Slow Walking Speed



**Figure 7.8 Heavy Weight, Normal Walking Speed**

The reason for observing the displacement of the platform is to verify that the Stewart Platform is behaving as a real human hip would do. As the hip joint can tentatively be seen as a ball and socket joint, the only mechanical ‘play’, would be dependent on the stiffness of the joint’s internal tissues, cartilage and non-conformity of fitting surfaces. For this reason, it is expected that the displacement in the three different planes would be at most 2 millimetres. From the results shown in chapter 6, this was clearly not the case for this joint simulator. This could be due for a number of reasons, however it is important to point out that the model in this study is only taking into account the bone on bone contact forces, which would not occur on a natural hip in real life.

Nevertheless, it was believed that the system would be stiff enough to prevent major displacement from occurring. This section shows comparisons of the displacement

graphs with the resultant force superimposed in blue. There is a running trend in all three graphs show of displacement in the Z-axis being proportional to the resultant force. This is to be expected, as walking is a vertical aligned activity. What is not to be expected is the large amount of displacement created in the Z-axis. This displacement created is consistently above 2 millimetres and can reach all the way to 12 millimetres. Reason for this will be examined further on in the section.

Regardless of this set back, the X and Y displacements occurred slightly higher than expected and also had negative displacements in the Y-axis. This is due to the sinuous model assumption made in the numerical model to account for the missing Y-axis in the data for the Visual Basics program. The amplitude for this clearly needs to be refined. The range of displacement for the X-axis was also considerably high, operating in a range of 1 millimetre to 4 millimetres.

There are several reasons why all displacements were greater than expected. The bone on bone contact nature of this hip joint meant there are no external factors of preventing the displacement, such as muscle or tendons. Also, no internal tissue could disperse the force around the cup, leading to a higher concentration in the upwards direction (the Z-axis).

Another factor could be that of the artificial bone deformation. Again, there is no other material present to represent the remainder of the musculoskeletal system. In a real body constraints and internal forces would be acting to hold the bone into joint, however in this case, the femur head could not be experiencing displacement, but the softness of the

material might be allowing for compression, which would contribute to the amount of displacement.

Two other possibilities exist that would cause such large results, and that regard the rigidity of the machine its self.

Firstly, the displacement could be due to looseness in the connection bar coming from the arch that suspense the hip clamp in place. This bar is far too solid to experience any bending, however as it only has a single studded rod and nut fastening it to the angular corner, it is possible this is a source of the error. This could be overcome by having multiple connections to the clamp.

The arch itself might also be allowing for the large displacements. The rapid movement of the actuators and would certainly cause a large amount of vibration that could amount to the fastenings becoming looser on the joining to the base plate. This would allow a freer movement of the pelvic half that would be less resistant to being moved by Stewart Platform.

The displacement comparison graphs have clearly showed that the system is not performing as first hoped and that much redesign and experimental inspection is required to achieve the goal of keeping the displacement within 2 millimetres. Further suggestions on how this could be done are available in the suggested further work section of the conclusion chapter.

## **Chapter 8. Conclusions**

### **8.1 Introduction**

The objective of this project was to create a joint simulator that could replicate a number of human joints. The device was successfully designed with a configurable control program written and proved to be very accurate in positioning. This part of the project can be deemed as a success.

However, judging from what has been discussed in chapter seven, a lot needs to be done to improve the performance of the machine and a few factors of the device will need to continue in the design process.

In conclusion, this project can be seen as a satisfactory proof of concept, as several of the activities tested did perform as hoped. This chapter will summarize the findings from the project and suggestions for improvement in further work.

#### **Summary:**

- The main contribution of this work is the development of a novel programmable/ configurable universal joint simulator.
- The study of human hip joint kinematics and load analysis have been simulated and analyzed.

- Such analyses are very useful to investigate the mobility and natural functionality as well as the motion variation due to replacement implant.
- The main challenge was developing a combined position and force feedback driven system. To achieve this the following tasks were performed:
  - A generic, configurable, programmable joint simulator driven by six electromagnetic actuators were designed and developed.
  - The developed Stewart Platform is a machine able simulating a number of human joint motions for different activities.
  - The platform has six degrees of freedom.
  - The developed software is capable of translating the kinematics and kinetics data of human joints to the actuator lengths.
- The simulator although has some weaknesses such as i) limited motion range, ii) inability to sustain realistic static load, but it has the ability to sustain realistic dynamic loads to follow required motion profiles.
- Initial tests are encouraging and areas of further development were identified.
- The device successfully simulated slow, normal and fast walking motion.
- A user friendly computer program. The program developed for this project allows for the weight and the activity to be selected of a person. Using existing data, this program can convert human movement data into a control command for driving the Stewart Platform. This software is also equipped to log both the forces recorded by the strain gauge and the actuator positions.



## 8.2 Recommendation for Future Study

This project is by no means in its final stage and it has lots of potential for many possible improvements and adaptation.

Below is a list of possible remedies to the short comings found in the verification process:

- The Stewart Platform failed to create its calculated maximum force of 1400N. Replacing the existing actuators with ones with a higher dynamics load could fix this problem. Similarly, investigating the limits imposed on the actuators by the safety features is a risk, but possible options
- Overall the system stiffness was very low and this was believed to be the cause of the large displacement readings. Having the clamp attached to a tetrahedron protruding out of a geodesic dome which would enclose the Stewart Platform. This would ensure maximum rigidity compared to both the ‘arch’ and the single member which is currently being used.

## References

- National Instruments [Online]. London. Available: <http://www.ni.com/> [Accessed 13/01/2011].
- Ahmed, A. M. 1983. A pressure distribution transducer for in-vitro static measurements in synovial joints. *J Biomech Eng*, 105, 309-14.
- An, K. N. & Chao, E. Y. 1984. Kinematic Analysis of Human Movement. *Annals of Biomedical Engineering*, 12, 585-597.
- Anderson, A. E., Ellis, B. J., Maas, S. A., Peters, C. L. & Weiss, J. A. 2008. Validation of finite element predictions of cartilage contact pressure in the human hip joint. *J Biomech Eng*, 130, 051008.
- Andriacchi, T. P., Ogle, J. A. & Galante, J. O. 1977. Walking Speed as a Basis for Normal and Abnormal Gait Measurements. *Journal of Biomechanics*, 10, 261-268.
- Azevedo, T. C. D., Enguica, R. & Freitas, P. 2008. Report on the Stewart platform problem.
- Bach, J. M. & Hull, M. L. 1995. A new load application system for in vitro study of ligamentous injuries to the human knee joint. *J Biomech Eng*, 117, 373-82.
- Bachtar, F., Chen, X. & Hisada, T. 2006. Finite element contact analysis of the hip joint. *Medical & Biological Engineering & Computing*, 44, 643-651.
- Bajekal, R. *Biomechanics of the hip* [Online]. Available: [http://www.bartsandthelondon.nhs.uk/docs/bajekal\\_hip\\_biomechanics.pdf](http://www.bartsandthelondon.nhs.uk/docs/bajekal_hip_biomechanics.pdf) [Accessed 16/01/2011].
- Barkmann, R., Dencks, S., Laugier, P., Padilla, F., Brixen, K., Ryg, J., Seekamp, A., Mahlke, L., Bremer, A., Heller, M. & Gluer, C. C. 2010. Femur ultrasound (FemUS)-first clinical results on hip fracture discrimination and estimation of femoral BMD. *Osteoporosis International*, 21, 969-976.
- Bean, J. C., Chaffin, D. B. & Schultz, A. B. 1988. Biomechanical Model Calculation of Muscle-Contraction Forces - a Double Linear-Programming Method. *Journal of Biomechanics*, 21, 59-66.
- Bergmann, G., Deuretzbacher, G., Heller, M., Graichen, F., Rohlmann, A., Strauss, J. & Duda, G. N. 2001. Hip contact forces and gait patterns from routine activities. *Journal of Biomechanics*, 34, 859-871.

## References

---

- Bergmann, G., Graichen, F. & Rohlmann, A. 1993. Hip joint loading during walking and running, measured in two patients. *Journal of Biomechanics*, 26, 969-90.
- Bergmann, G., Graichen, F., Rohlmann, A. & Linke, H. 1997. Hip joint forces during load carrying. *Clin Orthop Relat Res*, 190-201.
- Bergmann, G., Graichen, F., Siraky, J., Jendrzynski, H. & Rohlmann, A. 1988. Multichannel strain gauge telemetry for orthopaedic implants. *Journal of Biomechanics*, 21, 169-76.
- Bergmann, G., Kniggeendorf, H., Graichen, F. & Rohlmann, A. 1995. Influence of shoes and heel strike on the loading of the hip joint. *Journal of Biomechanics*, 28, 817-27.
- Berns, G. S., Hull, M. L. & Patterson, H. A. 1990. Implementation of a five degree of freedom automated system to determine knee flexibility in vitro. *J Biomech Eng*, 112, 392-400.
- Brand, R. A., Pedersen, D. R., Davy, D. T., Kotzar, G. M., Heiple, K. G. & Goldberg, V. M. 1994. Comparison of hip force calculations and measurements in the same patient. *J Arthroplasty*, 9, 45-51.
- Brown, C. 2009-2010. Advanced Solid Body Mechanics notes.
- Brown, T. D. & Shaw, D. T. 1982. A technique for measuring instantaneous in vitro contact stress distributions in articular joints. *Journal of Biomechanics*, 15, 329-33.
- Brown, T. D. & Shaw, D. T. 1983. In vitro contact stress distributions in the natural human hip. *Journal of Biomechanics*, 16, 373-84.
- Burgess, I. C., Kolar, M., Cunningham, J. L. & Unsworth, A. 1997. Development of a six station knee wear simulator and preliminary wear results. *Proc Inst Mech Eng H*, 211, 37-47.
- Calonius, O. & Saikko, V. 2003. Force track analysis of contemporary hip simulators. *Journal of Biomechanics*, 36, 1719-1726.
- Carlson, K. L. *Human hip joint mechanics : An investigation into the effects of femoral head endoprosthesis replacements using in vivo and in vitro pressure data*. Massachusetts Institute of Technology.
- Cavanagh, P. R. 1990. *Biomechanics of distance running*, Champaign, Ill., Human Kinetics Books.
- Corp, C. C. 2008a. Models STA2504-2510 Servo Tube Actuator.
- Corp, C. C. 2008b. Xenus XTL™ User Guide.

## References

---

- Crowinshield, R. D., Brand, R. A. & Johnston, R. C. 1978. The effects of walking velocity and age on hip kinematics and kinetics. *Clin Orthop Relat Res*, 140-4.
- Crowninshield, R. D. & Brand, R. A. 1981. A physiologically based criterion of muscle force prediction in locomotion. *Journal of Biomechanics*, 14, 793-801.
- Currey, J. D. 2002. *Bones : structure and mechanics*, Princeton, N.J. ; Oxford, Princeton University Press.
- Daniel, M., Antolic, V., Iglic, A. & Kralj-Iglic, V. 2001. Determination of contact hip stress from nomograms based on mathematical model. *Medical Engineering & Physics*, 23, 347-357.
- Dasgupta, B. & Mruthyunjaya, T. S. 2000. The Stewart platform manipulator: a review. *Mechanism and Machine Theory*, 35, 15-40.
- Davy, D. T., Kotzar, G. M., Brown, R. H., Heiple, K. G., Goldberg, V. M., Heiple, K. G., Berilla, J. & Burstein, A. H. 1988. Telemetric Force Measurements across the Hip after Total Arthroplasty. *Journal of Bone and Joint Surgery-American Volume*, 70A, 45-50.
- Dostal, W. F. & Andrews, J. G. 1981. A three-dimensional biomechanical model of hip musculature. *Journal of biomechanics*, 14, 803-807, 809-812.
- Dowson, D., Seedhom, B. B., and Johnson, G. R. 1981. *Bio-mechanics of the lower limb. In: An introduction to the bio-mechanics of joints and joint replacement*, London, Mechanical Engineering Publications Ltd.
- Drake, R. L., Vogl, W., and Mitchell, A. W. M 2005. *Gray's anatomy for students*, Toronto, Elsevier Churchill Livingstone.
- Duda, G. N., Schneider, E. & Chao, E. Y. 1997. Internal forces and moments in the femur during walking. *Journal of Biomechanics*, 30, 933-41.
- Dumbleton, J. H. 1981. *Tribology of natural and artificial joints*, Amsterdam ; Oxford, Elsevier Scientific.
- Dunning, C. E., Gordon, K. D., King, G. J. & Johnson, J. A. 2003. Development of a motion-controlled in vitro elbow testing system. *J Orthop Res*, 21, 405-11.
- Ferguson, S. J., Bryant, J. T., Ganz, R. & Ito, K. 2000. The influence of the acetabular labrum on hip joint cartilage consolidation: a poroelastic finite element model. *Journal of biomechanics*, 33, 953-960.
- Ferguson, S. J., Bryant, J. T., Ganz, R. & Ito, K. 2003. An in vitro investigation of the acetabular labral seal in hip joint mechanics. *Journal of Biomechanics*, 36, 171-8.

## References

---

- Fong, T. W. 1990. *Design and testing of a Stewart Platform Augmented Manipulator for space applications*. Massachusetts Institute of Technology.
- Foundation, A. *Types of Replacement Parts* [Online]. Available: <http://www.arthritis.org/types-replacement-parts.php> [Accessed 14/01/2011].
- Frayssé, F., Dumas, R., Cheze, L. & Wang, X. 2009. Comparison of global and joint-to-joint methods for estimating the hip joint load and the muscle forces during walking. *Journal of Biomechanics*, 42, 2357-62.
- Gillison, D. B. 1991. *Reconfiguration of the Wrist Joint Motion Simulator*. Syracuse University.
- Gmbh, S. H. 2008. User's and Programmer's Manual POSYS® 7xx/8xx/8xx-B/9xx/18xx/19xx.
- Gray, H. *Anatomy of the human body* [Online]. Available: [www.bartleby.com/107](http://www.bartleby.com/107) [Accessed 04/07/2010].
- Hamill, J. & Knutzen, K. 2009. *Biomechanical basis of human movement*, Philadelphia, Pa. ; London, Lippincott Williams & Wilkins.
- Hatze, H. 1980. A Mathematical-Model for the Computational Determination of Parameter Values of Anthropomorphic Segments. *Journal of Biomechanics*, 13, 833-843.
- Hay, J. G., Reid, J. G., Hay, J. G. A. & Mechanical Bases of Human, M. 1988. *Anatomy, mechanics and human motion*, Prentice Hall.
- Heller, M. O., Bergmann, G., Deuretzbacher, G., Durselen, L., Pohl, M., Claes, L., Haas, N. P. & Duda, G. N. 2001. Musculo-skeletal loading conditions at the hip during walking and stair climbing. *Journal of Biomechanics*, 34, 883-893.
- Hicks, J. H. 1953. The mechanics of the foot. I. The joints. *J Anat*, 87, 345-57.
- Hodge, W. A., Carlson, K. L., Fijan, R. S., Burgess, R. G., Riley, P. O., Harris, W. H. & Mann, R. W. 1989. Contact pressures from an instrumented hip endoprosthesis. *Journal of Bone and Joint Surgery-American Volume*, 71, 1378-86.
- Hodge, W. A., Fijan, R. S., Carlson, K. L., Burgess, R. G., Harris, W. H. & Mann, R. W. 1986. Contact pressures in the human hip joint measured in vivo. *Proc Natl Acad Sci U S A*, 83, 2879-83.
- Iglic, A., Antolic, V. & Srakar, F. 1993. Biomechanical analysis of various operative hip joint rotation center shifts. *Arch Orthop Trauma Surg*, 112, 124-6.
- Iglic, A., Kralj-Iglic, V., Daniel, M. & Macek-Lebar, A. 2002. Computer determination of contact stress distribution and size of weight bearing area in the human hip joint. *Comput Methods Biomech Biomed Engin*, 5, 185-92.

## References

---

- Ipavec, M., Brand, R. A., Pedersen, D. R., Mavcic, B., Kralj-Iglic, V. & Iglic, A. 1999. Mathematical modelling of stress in the hip during gait. *Journal of Biomechanics*, 32, 1229-35.
- Jensen, R. K. 1978. Estimation of the biomechanical properties of three body types using a photogrammetric method. *Journal of Biomechanics*, 11, 349-58.
- Johnston, R. C., Brand, R. A. & Crowninshield, R. D. 1979. Reconstruction of the hip. A mathematical approach to determine optimum geometric relationships. *Journal of Bone and Joint Surgery-American Volume*, 61, 639-52.
- Jonsson, K., Buckwalter, K., Helvie, M., Niklason, L. & Martel, W. 1992. Precision of hyaline cartilage thickness measurements. *Acta Radiol*, 33, 234-9.
- Kapandji, I. A. 1987. *The physiology of the joints : annotated diagrams of the mechanics of the human joints*, Edinburgh, Churchill Livingstone.
- Keller, M. S. & Nijs, E. L. 2009. The role of radiographs and US in developmental dysplasia of the hip: how good are they? *Pediatr Radiol*, 39 Suppl 2, S211-5.
- Kidshealth.Org. *Bones Muscles and Joints* [Online]. Available: <http://health.msn.com/kids-health/articlepage.aspx?cp-documentid=100151209> [Accessed 14/01/2011].
- King, G. J. W., Itoi, E., Risung, F., Niebur, G. L., Morrey, B. F. & An, K. N. 1993. Kinematics and Stability of the Norway Elbow - a Cadaveric Study. *Acta Orthopaedica Scandinavica*, 64, 657-663.
- Kotzar, G. M., Davy, D. T., Goldberg, V. M., Heiple, K. G., Berilla, J., Heiple, K. G., Jr., Brown, R. H. & Burstein, A. H. 1991. Telemeterized in vivo hip joint force data: a report on two patients after total hip surgery. *J Orthop Res*, 9, 621-33.
- Lewis, J. L., Lew, W. D. & Schmidt, J. 1988. Description and error evaluation of an in vitro knee joint testing system. *J Biomech Eng*, 110, 238-48.
- Li, G., Rudy, T. W., Sakane, M., Kanamori, A., Ma, C. B. & Woo, S. L. 1999. The importance of quadriceps and hamstring muscle loading on knee kinematics and in-situ forces in the ACL. *Journal of Biomechanics*, 32, 395-400.
- Lipshitz, H. & Glimcher, M. J. 1979. Invitro Studies of the Wear of Articular-Cartilage .2. Characteristics of the Wear of Articular-Cartilage When Worn against Stainless-Steel Plates Having Characterized Surfaces. *Wear*, 52, 297-339.
- Macwilliams, B. A., Wilson, D. R., Desjardins, J. D., Romero, J. & Chao, E. Y. 1999. Hamstrings cocontraction reduces internal rotation, anterior translation, and anterior cruciate ligament load in weight-bearing flexion. *J Orthop Res*, 17, 817-22.

## References

---

- Maletsky, L. P. & Hillberry, B. M. 2005. Simulating Dynamic Activities Using a Five-Axis Knee Simulator. *Journal of Biomechanical Engineering*, 127, 123-133.
- Martin, P. E., Mungiole, M., Marzke, M. W. & Longhill, J. M. 1989. The use of magnetic resonance imaging for measuring segment inertial properties. *Journal of Biomechanics*, 22, 367-76.
- Mavcic, B., Pompe, B., Antolic, V., Daniel, M., Iglic, A. & Kralj-Iglic, V. 2002. Mathematical estimation of stress distribution in normal and dysplastic human hips. *J Orthop Res*, 20, 1025-30.
- McLean, C. A. & Ahmed, A. M. 1993. Design and development of an unconstrained dynamic knee simulator. *J Biomech Eng*, 115, 144-8.
- Medlineplus. Bethesda USA. Available: <http://www.nlm.nih.gov/medlineplus/> [Accessed 08/10 2009].
- Morrell, K. C., Hodge, W. A., Krebs, D. E. & Mann, R. W. 2005. Corroboration of in vivo cartilage pressures with implications for synovial joint tribology and osteoarthritis causation. *Proc Natl Acad Sci U S A*, 102, 14819-24.
- Mow, V. C., And Huiskes, R. 2005. *Basic orthopaedic biomechanics and mechanobiology*, Lippincott Williams & Wilkins.
- Mow, V. C. & Lai, W. M. 1980. Recent Developments in Synovial Joint Biomechanics. *Siam Review*, 22, 275-317.
- Mungiole, M. & Martin, P. E. 1990. Estimating segment inertial properties: comparison of magnetic resonance imaging with existing methods. *Journal of Biomechanics*, 23, 1039-46.
- Naish, J. H., Xanthopoulos, E., Hutchinson, C. E., Waterton, J. C. & Taylor, C. J. 2006. MR measurement of articular cartilage thickness distribution in the hip. *Osteoarthritis and Cartilage*, 14, 967-973.
- Nakanishi, K., Tanaka, H., Sugano, N., Sato, Y., Ueguchi, T., Kubota, T., Tamura, S. & Nakamura, H. 2001. MR-based three-dimensional presentation of cartilage thickness in the femoral head. *European Radiology*, 11, 2178-2183.
- Palastanga, N., Field, D., and Soames, R 2006. *The lower limb. In: Anatomy and human movement: Structure and function*, Philadelphia, Elsevier.
- Pappas, M. J., And Buechel, F.F., 1979. New Jersey Knee Simulator. *Proceedings of the 11th International Biomaterials Symposium*.
- Park, S., Krebs, D. E. & Mann, R. W. 1999. Hip muscle co-contraction: evidence from concurrent in vivo pressure measurement and force estimation. *Gait Posture*, 10, 211-22.

## References

---

- Patts. *The Skeleton: Skeletal System* [Online]. Available: <http://webschoolsolutions.com/patts/systems/skeleton.htm> [Accessed 30/11/2009].
- Paul, J. P. 1966. Biomechanics. The biomechanics of the hip-joint and its clinical relevance. *Proc R Soc Med*, 59, 943-8.
- Paul, J. P. 1970. Effect of Walking Speed on Force Actions Transmitted at Hip and Knee Joints. *Proceedings of the Royal Society of Medicine-London*, 63, 200-&.
- Paul, J. P. 1976. Approaches to Design - Force Actions Transmitted by Joints in Human Body. *Proceedings of the Royal Society of London Series B-Biological Sciences*, 192, 163-172.
- Pedersen, D. R., Brand, R. A. & Davy, D. T. 1997. Pelvic muscle and acetabular contact forces during gait. *Journal of Biomechanics*, 30, 959-65.
- Physiotherapy, W. *Artificial Hip Joint* [Online]. Available: <http://www.wepphysio.co.uk/article.php?aid=328> [Accessed 15/05 2010].
- Rappoport, D. J., Carter, D. R. & Shcurman, D. J. 1985. Contact Finite-Element Stress-Analysis of the Hip-Joint. *Journal of Orthopaedic Research*, 3, 435-446.
- Rastegar, J., Miller, N. & Barmada, R. 1980. An apparatus for measuring the load-displacement and load-dependent kinematic characteristics of articulating joints-application to the human ankle joint. *J Biomech Eng*, 102, 208.
- Richard L. Drake, E. A. 2010. *Gray's anatomy for students* Churchill Livingstone/Elsevier
- Rohrle, H., Scholten, R., Sigolotto, C., Sollbach, W. & Kellner, H. 1984. Joint forces in the human pelvis-leg skeleton during walking. *Journal of Biomechanics*, 17, 409-24.
- Rushfeldt, P. D., Mann, R. W. & Harris, W. H. 1981. Improved techniques for measuring in vitro the geometry and pressure distribution in the human acetabulum. II Instrumented endoprosthesis measurement of articular surface pressure distribution. *Journal of Biomechanics*, 14, 315-23.
- Rydell, N. W. 1966. Forces acting on the femoral head-prosthesis. A study on strain gauge supplied prostheses in living persons. *Acta Orthop Scand*, 37, Suppl 88:1-132.
- Sarfaty, O. & Ladin, Z. 1993. A video-based system for the estimation of the inertial properties of body segments. *Journal of Biomechanics*, 26, 1011-6.
- Schopfer, A., Diangelo, D., Hearn, T., Powell, J. & Tile, M. 1994. Biomechanical comparison of methods of fixation of isolated osteotomies of the posterior acetabular column. *Int Orthop*, 18, 96-101.



## References

---

- Seireg, A. & Arvikar, R. J. 1973. A mathematical model for evaluation of forces in lower extremities of the musculo-skeletal system. *Journal of Biomechanics*, 6, 313-26.
- Seireg, A. & Arvikar, R. J. 1975. Prediction of Muscular Load Sharing and Joint Forces in Lower-Extremities during Walking. *Journal of Biomechanics*, 8, 89-102.
- Sharkey, N. A. & Hamel, A. J. 1998. A dynamic cadaver model of the stance phase of gait: performance characteristics and kinetic validation. *Clin Biomech (Bristol, Avon)*, 13, 420-433.
- Shaw, J. A. & Murray, D. G. 1973. Knee-Joint Simulator. *Clinical Orthopaedics and Related Research*, 15-23.
- Stansfield, B. W., Nicol, A. C., Paul, J. P., Kelly, I. G., Graichen, F. & Bergmann, G. 2003. Direct comparison of calculated hip joint contact forces with those measured using instrumented implants. An evaluation of a three-dimensional mathematical model of the lower limb. *Journal of Biomechanics*, 36, 929-936.
- Stroeve, S. 1997. A learning feedback and feedforward neuromuscular control model for two degrees of freedom human arm movements. *Human Movement Science*, 16, 621-651.
- Swanson, S. A., Freeman, M. A. & Heath, J. C. 1973. Laboratory tests on total joint replacement prostheses. *J Bone Joint Surg Br*, 55, 759-73.
- Szklar, O. & Ahmed, A. M. 1987. A Simple Unconstrained Dynamic Knee Simulator. *Journal of Biomechanical Engineering-Transactions of the Asme*, 109, 247-251.
- Treharne, R. W., Young, R. W. & Young, S. R. 1981. Wear of artificial joint materials III: simulation of the knee joint using a computer-controlled system. *ARCHIVE: Engineering in Medicine 1971-1988 (vols 1-17)*, 10, 137-142.
- Ulucay, O. 2006. *Design and Control of a Stewart Platform*. Sabancı University.
- Walker, P. S., Blunn, G. W., Broome, D. R., Perry, J., Watkins, A., Sathasivam, S., Dewar, M. E. & Paul, J. P. 1997. A knee simulating machine for performance evaluation of total knee replacements. *Journal of Biomechanics*, 30, 83-9.
- Wang, M. J. J., Wu, W. Y., Lin, K. C., Yang, S. N. & Lu, J. M. 2007. Automated anthropometric data collection from three-dimensional digital human models. *International Journal of Advanced Manufacturing Technology*, 32, 109-115.
- Woodford, C. *How strain gauges work: Measuring strain with mechanical, electrical, and piezoelectric gages* [Online]. Available: <http://www.explainthatstuff.com/straingauge.html> [Accessed 15/09/2010].

## *References*

---

- Wuelker, N., Wirth, C. J., Roetman, B. & Plitz, W. 1995. A Dynamic Shoulder Model - Reliability Testing and Muscle Force Study. *Journal of Biomechanics*, 28, 489-499.
- Yang, T. 2003. *A three-dimensional biphasic finite element formulation for hydrated soft tissue*.
- Yoshida, H., Faust, A., Wilckens, J., Kitagawa, M., Fetto, J. & Chao, E. Y. S. 2006. Three-dimensional dynamic hip contact area and pressure distribution during activities of daily living. *Journal of Biomechanics*, 39, 1996-2004.

## Appendix 1 – Force Data used in Experiments

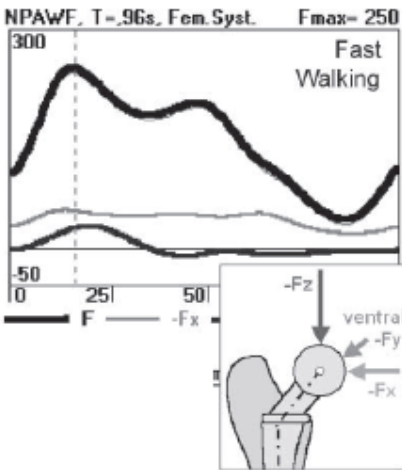
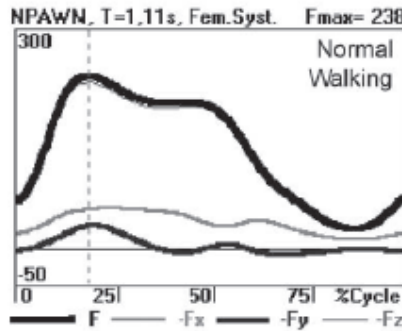
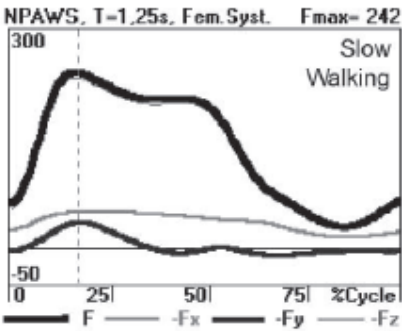
The following data, table, and graphs are from (Bergmann et al., 2001).

Personal data and anatomical parameters of patients				
Patient	HSR	PFL	KWR	IBL
Gender	Male	Male	Male	Female
Age at implantation (years)	55	51	61	76
Operated joint	Right	Left	Right	Left
Measurement (months postoperatively)	14	11	12	31
Weights at measurement (N)				
Total body (BW)	860	980	702	800
Thigh	75.7	80.2	62.2	98.4
Shank	39.1	53.9	36.5	43.0
Foot	9.2	12.3	9.9	7.2
Lengths (cm)				
Body height	174	175.0	165.0	170
Thigh	43.3	41.0	39.3	47.5
Shank	38.1	41.0	40.0	40.9
Foot	30.0	27.5	29.0	26
Angles (degree)				
AV= Anteversion	4	23	-2	14
S= Femur shaft—implant shaft	10	7	9	9

Peak loads of single and average patients, cycle times and body weight of average patient<sup>a</sup>

Patient and activity	Peak hip contact force $F_p$ (% BW)					Peak torsional implant moment $M_{tp}$ (% BW m)					Cycle time (s)	Body weight (N)
	HSR	PFL	KWR	IBL	NPA	HSR	PFL	KWR	IBL	NPA		
Patient	HSR	PFL	KWR	IBL	NPA	HSR	PFL	KWR	IBL	NPA	NPA	NPA
Slow walking	239	255	244	—	242	1.72	1.65	1.71	—	1.64	1.25	847
Normal walking	248	211	242	285	238	1.82	1.25	1.64	1.55	1.52	1.11	836
Fast walking	279	218	275	—	250	1.91	1.21	1.94	—	1.54	0.96	847
Up stairs	265	227	272	(314)	251	2.25	1.82	2.96	(2.92)	2.24	1.59	847
Down stairs	263	226	316	—	260	1.83	1.63	2.33	—	1.74	1.46	847
Standing up	181	208	182	220	190	1.18	0.77	1.03	1.01	0.88	2.49	836
Sitting down	176	153	149	(199)	156	0.91	0.37	0.65	(0.75)	0.47	3.72	847
Standing on 2-1-2 legs	253	223	(369)	—	231	1.64	0.96	(1.55)	—	1.17	6.72	920
Knee bend	177	117	147	—	143	0.67	0.58	0.83	—	0.51	6.67	847

<sup>a</sup> Peak hip contact forces  $F_p$  in % BW and peak torsional implant moments  $M_{tp}$  in % BW m. HSR, PFL, KWR, IBL are 'individual' averages from several trials of the patients, NPA is the 'typical' average from 2 to 4 patients (Table 3). Data in parentheses were not used for calculating NPA. The body weight of NPA depends on the number of averaged patients (Table 3).



## Appendix 2 – Data used in Creating Generic Movement Model for the Software

Data modified from (Hamill and Knutzen, 2009).

time (ms)	Heel x	Heel y	IC x	IC y	Hip x	Hip y	Knee x	Knee y	Ankle x	Ankle y	hip	foot	shin	thigh	d Hip
0	139.1965	33.7988	-117.039	960.8488	-138.875	817.3138	71.2735	500.174	184.3008	122.2974	145.186456	99.3297543	394.418427	380.447164	497.677475
42	148.5699	43.9356	-52.6116	962.8947	-73.3523	819.4881	129.2452	498.5237	207.234	117.4741	144.898687	94.0711837	388.948648	379.557496	498.710659
83	155.896	51.7004	17.5514	970.124	-2.7509	827.6524	187.6139	499.6091	225.2517	114.0165	143.910876	93.238991	387.425163	379.27716	500.305432
125	159.3292	55.7181	86.2856	981.7078	64.2766	840.0502	232.4894	500.3617	234.7272	112.6339	143.357147	94.468337	387.734258	379.056491	503.060254
167	160.1514	57.4574	152.7498	994.3636	126.837	852.7439	263.7166	499.954	239.1157	112.8897	143.970874	96.4784979	387.8453	378.413449	506.709466
208	160.3755	58.4427	216.7429	1004.68	185.9522	863.2155	286.9158	499.2408	241.4929	113.8631	144.776628	98.2418104	388.045373	377.718454	510.287194
250	160.8529	59.4857	278.657	1010.693	243.1287	870.1817	306.195	498.382	243.271	115.0613	144.933383	99.4051836	388.451012	377.110561	513.050584
292	161.7948	61.0952	339.3495	1011.391	299.3745	872.5881	324.3649	497.2322	244.8999	116.5255	144.444611	99.8948237	388.911658	376.186884	514.377109
333	163.2748	63.873	400.2315	1006.404	356.091	870.3273	344.8206	495.1796	246.8816	118.4002	143.056814	99.8163942	389.300352	375.316958	514.218587
375	165.5426	68.8445	462.1389	996.3943	413.9826	864.1425	371.3921	491.4435	250.1318	121.2689	140.746467	99.5170863	389.529581	375.12464	513.040244
417	169.8648	78.7167	525.6751	983.8261	474.0093	855.6371	407.674	486.0878	256.5635	126.7479	138.20917	99.1143822	389.81989	375.455799	511.534627
458	180.063	98.2425	592.4363	972.2856	538.252	847.139	456.9072	480.1456	269.9636	137.6026	136.373054	98.139367	390.235335	375.900428	510.460495
500	204.0059	131.9451	664.3104	965.0532	608.6337	840.4378	522.5499	474.5135	296.3716	156.2711	136.487702	95.5153224	390.429057	375.913572	510.612609
542	253.2933	179.9845	739.5354	963.5039	684.5092	836.0806	608.3036	469.1397	343.8152	182.9895	138.796902	90.5717638	389.661457	374.770487	511.485823
583	214.0742	223.1561	812.5442	966.3945	761.0693	833.5012	714.9302	464.1787	419.58	214.0742	142.514191	205.70638	387.019381	372.193398	511.614311
625	447.8179	272.7165	878.788	971.8138	832.9578	832.94	836.2902	463.3738	524.0245	241.4812	146.240691	82.3595158	383.074658	369.581224	510.212991
667	575.1624	284.145	938.4812	979.5927	899.553	836.4076	961.4648	472.5408	651.5061	255.2193	148.382538	81.6397982	378.553867	369.096355	507.572532
708	713.675	264.9703	996.5345	989.1932	964.6761	844.1692	1080.867	490.9622	795.7294	248.9548	148.482047	83.6027559	373.993359	371.827258	505.317821
750	865.6452	220.7872	1057.667	997.5264	1031.78	852.5717	1189.301	510.7773	953.0286	224.8342	147.248096	87.4770644	370.928704	376.345954	504.234267
792	1034.357	163.5488	1121.961	1001.063	1100.919	856.8826	1284.958	524.0499	1121.452	191.5556	145.707767	91.4873614	370.522117	380.326123	504.092769
833	1217.372	108.6481	1187.999	998.0358	1170.755	854.426	1367.583	526.7247	1295.866	161.1292	144.641385	94.4223167	372.56328	382.268758	504.365508
875	1399.436	69.8418	1255.297	989.0475	1239.162	845.2944	1438.988	519.5977	1462.701	143.2082	144.655771	96.8765378	377.135734	382.11094	504.108617
917	1552.409	50.923	1321.962	977.1038	1304.218	832.7062	1503.167	508.3945	1600.078	137.1185	145.483732	98.4987197	383.715533	380.47179	502.517323
958	1650.026	43.1152	1379.255	966.8234	1359.058	822.0975	1558.207	499.833	1689.076	133.6909	146.128385	98.6349833	388.827381	378.833383	500.103841
1000	1685.193	39.8256	1407.57	962.3362	1385.993	817.5894	1586.15	496.5313	1722.682	130.679	146.346175	98.2841056	390.498262	378.339964	498.86373

## Appendix

d Knee	d Ankle	th Knee	th Hip	th Ankle	th Knee ef	th Hip ef	th Ankle ef	Force Hip (%BW)	Sine	phi Knee	phi Hip	phi Ankle
766.47922	471.295407	0.29456589	0.73618006	0.76198825	0.369501467	-0.273524679	0.070677704	0.3	0	0.001	0.05	0.01
756.010799	454.998664	0.36117563	0.70668863	0.87523751	0.302891721	-0.244033249	-0.042571558	0.35	0.261799	0.004235	0.060353	0.022941
749.173801	449.03032	0.42850912	0.66735886	0.93611258	0.235558237	-0.204703472	-0.103446623	0.4	0.523599	0.00725	0.07	0.035
747.119723	450.622176	0.4540265	0.61393325	0.92995626	0.210040859	-0.15127787	-0.097290309	0.55	0.785398	0.009839	0.078284	0.045355
748.325293	454.454609	0.43358412	0.55108447	0.89526248	0.230483232	-0.088429088	-0.062596522	0.7	1.047198	0.011825	0.084641	0.053301
751.407871	458.601584	0.38791311	0.48490261	0.85410178	0.276154242	-0.022247224	-0.021435825	1.65	1.308997	0.013074	0.088637	0.058296
755.120413	462.335688	0.33072896	0.41568441	0.81481486	0.333338395	0.04697097	0.017851092	2.6	1.570796	0.0135	0.09	0.06
758.022518	465.450878	0.27225552	0.34688979	0.77679391	0.391811832	0.11576559	0.055872042	2.7	1.832596	0.013074	0.088637	0.058296
759.816463	467.957542	0.22427574	0.2836371	0.7385765	0.43979161	0.179018287	0.094089454	2.8	2.094395	0.011825	0.084641	0.053301
760.728776	470.068007	0.20277772	0.23542098	0.69941913	0.461289638	0.227234404	0.133246829	2.7	2.356194	0.009839	0.078284	0.045355
760.632725	471.703751	0.22046029	0.20551597	0.6668142	0.443607061	0.25713941	0.165851758	2.6	2.617994	0.00725	0.07	0.035
758.564808	471.691307	0.28145067	0.19047361	0.65854291	0.382616687	0.272181774	0.174123046	2.45	2.879793	0.004235	0.060353	0.022941
752.058304	467.785622	0.38682914	0.1891307	0.69539956	0.277238213	0.273524679	0.137266398	2.3	3.141593	0.001	0.05	0.01
736.614137	457.867932	0.54131167	0.2028807	0.7915331	0.12275569	0.259774685	0.041132853	2.2	3.403392	-0.00224	0.039647	-0.00294
707.322239	555.831473	0.74387401	0.24526012	0.74680139	-0.079806651	0.217395264	0.085864568	2.1	3.665191	-0.00525	0.03	-0.015
667.280523	432.736564	0.9620157	0.32777636	1.006789	-0.297948346	0.134879021	-0.174123046	2	3.926991	-0.00784	0.021716	-0.02536
631.907513	429.79358	1.12784761	0.43399257	0.97365912	-0.463780259	0.028662817	-0.140993163	1.9	4.18879	-0.00983	0.015359	-0.0333
618.727056	431.163894	1.18484401	0.53405116	0.89651964	-0.520776655	-0.071395781	-0.063853688	1.8	4.45059	-0.01107	0.011363	-0.0383
632.658005	434.565685	1.12242037	0.60857603	0.83394813	-0.458353019	-0.14592065	-0.001282178	1.7	4.712389	-0.0115	0.01	-0.04
665.643767	439.046586	0.96213361	0.65002239	0.80264345	-0.298066254	-0.187367009	0.030022505	1.55	4.974188	-0.01107	0.011363	-0.0383
704.495007	444.242488	0.73458958	0.66038756	0.78775111	-0.070522221	-0.197732173	0.044914847	1.4	5.235988	-0.00983	0.015359	-0.0333
736.813896	451.491655	0.48739351	0.66208483	0.77451717	0.176673841	-0.19942945	0.058148784	1.25	5.497787	-0.00784	0.021716	-0.02536
755.893768	460.11406	0.29492593	0.67252048	0.76049381	0.369141424	-0.209865095	0.072172143	1.1	5.759587	-0.00525	0.03	-0.015
763.423557	465.85607	0.21025053	0.69218423	0.75032799	0.453816823	-0.229528849	0.082337961	0.95	6.021386	-0.00224	0.039647	-0.00294
764.987177	467.321744	0.2002871	0.70544651	0.74853006	0.463780259	-0.242791131	0.084135895	0.8	6.283185	0.001	0.05	0.01



## Appendix

Time (ms)	Heel x	Heel y	IC x	IC y	Hip x	Hip y	Knee x	Knee y	Ankle x	Ankle y	hip	foot	shin	thigh	d Hip	i
0	30.8	5.91	67.68	121.83	57.68	101.83	37.47	60	32.44	13.39	22.3606798	7.65767589	46.880625	46.4563559	68.815645	
25	38.58	5.33	68.11	119.8	58.11	99.8	38.01	58.39	38.01	11.85	22.3606798	6.54486822	46.54	46.0304041	68.3900439	
50	48.01	5.68	68.98	118.02	58.98	98.02	37.82	57.25	46.68	12.21	22.3606798	6.66406783	45.903172	45.9340669	68.2930341	
75	58.31	5.74	70.19	117.51	60.19	97.51	40.47	55.71	56.2	12.41	22.3606798	6.99578444	46.0686759	46.2181609	68.5749109	
100	68.31	5.81	70.3	117.58	60.3	97.58	45.74	53.53	65.97	12.41	22.3606798	7.0025424	45.8269277	46.3939231	68.5973476	
125	78.58	6.07	71.78	117.73	61.78	97.73	52.16	52.39	75.92	12.62	22.3606798	7.06951908	46.3269954	46.3493258	68.2221372	
150	88.93	6.94	73	118.23	63	98.23	60.14	51.89	85.87	13.76	22.3606798	7.47502508	45.999237	46.4281725	67.5749599	
175	98.65	9.28	73.17	119.26	63.17	99.26	67.37	53.35	95.19	16.34	22.3606798	7.8622643	46.300027	46.1017147	66.1647043	
200	107.18	13.32	72.31	120.78	62.31	100.78	73	56.2	102.91	19.73	22.3606798	7.70201272	47.1663969	45.8437837	64.583686	
225	114.03	18.16	71.53	122.47	61.53	102.47	76.69	59.12	108.02	23.47	22.3606798	8.01973815	47.4604193	45.9243737	63.5597994	
250	119.36	24.7	70.53	124.02	60.53	104.02	78.99	61.67	112.2	27.8	22.3606798	7.80228172	47.4350187	46.198421	62.9213326	
275	123.81	31.04	69.6	124.84	59.6	104.84	78.99	62.98	116.68	33.37	22.3606798	7.50105326	47.9300344	46.1327617	62.5686159	
300	127.16	37.8	68.66	125.43	58.66	105.43	77.8	63.1	120.29	39.6	22.3606798	7.10189411	48.5556392	46.4560922	62.9965753	
325	128.13	44.9	67.43	124.92	57.43	104.92	75.41	62	121	45.9	22.3606798	7.19978472	48.349334	46.5339317	63.4240238	
350	125.67	52	66.45	123.74	56.45	103.74	72.29	59.9	119	51.09	22.3606798	6.73179025	47.5335692	46.613852	64.1065613	
375	121.83	57.06	65.6	121.6	55.6	101.6	67.73	57.14	114.43	54.87	22.3606798	7.71725988	46.7551377	46.0850138	64.495182	
400	116.09	60.2	65.16	118.16	55.16	98.16	62.6	53.97	108.84	57.62	22.3606798	7.69538173	46.3838345	44.811937	64.2410282	
425	109.12	61	65.06	115.52	55.06	95.52	57.02	51.35	102.14	58.01	22.3606798	7.59345113	45.6088807	44.2134651	64.6717133	
450	102.15	59.47	64.47	114.27	54.47	94.27	49.7	50.43	94.91	56.85	22.3606798	7.6994805	45.6635577	44.0987358	65.5263191	
475	95.24	55.79	64.01	113.69	54.01	93.69	42.11	51.4	88.16	54.05	22.3606798	7.29067898	46.1261856	43.932381	66.0276768	
500	88.73	50.2	63.6	114.84	53.6	94.84	35.55	54.51	81.83	49.87	22.3606798	6.9078868	46.51202	44.184968	66.5320329	
525	81.83	43.37	61.91	117.06	51.91	97.06	30.22	58.54	75.05	44.69	22.3606798	6.90730049	46.9206927	44.2068603	66.5495793	
550	73.87	35.77	60.27	119.8	50.27	99.8	26.54	62.49	67.27	38.64	22.3606798	7.19700632	47.1991038	44.2170668	66.4992406	
575	64.09	27.94	58.63	122.65	48.63	102.65	24.29	65.23	57.95	32.45	22.3606798	7.61837909	46.9842952	44.6395789	66.905097	
600	52.62	20.57	57.7	124.88	47.7	104.88	23.47	66.66	48.23	26.43	22.3606798	7.32200109	47.2388664	45.2533015	67.5371105	
625	40.63	14.35	57.3	126.15	47.3	106.15	24.24	66.38	38.38	21.49	22.3606798	7.48612717	47.0643358	45.9719099	68.3038542	
650	29.57	10.71	57.04	125.88	47.04	105.88	26.6	64.61	29.16	18.06	22.3606798	7.36142649	46.62034	46.0543863	68.4149582	
675	21.78	9.02	57.09	125.11	47.09	105.11	28.8	62.82	23.46	16.35	22.3606798	7.52005984	46.7758111	46.0756791	68.4132166	
700	19.33	8.2	57.5	124.06	47.5	104.06	30.25	61.56	21.64	15.44	22.3606798	7.59958552	46.916804	45.8673359	68.1822008	
725	21.6	6.19	57.38	122.81	47.38	102.81	30.8	59.94	23.42	13.6	22.3606798	7.63023591	46.9239811	45.9644787	68.2578442	

# Appendix

d Knee	d Ankle	th Knee	th Hip	th Ankle	th Knee ef	th Hip ef	th Ankle ef	Force hip (% bw)	phi Knee	phi Hip	phi Ankle	sine
91.9711433	54.4996972	0.34257306	0.01357383	0.10833537	0.70921761	0.43703628	0.08833247	0.2	0.001	0.05	0.01	0
90.2175842	53.0630615	0.45189145	0.01175616	0.08720161	0.59989922	0.43885394	0.10946622	0.2	0.006374261	0.060748522	0.022898226	0.21666156
86.6870584	52.5671095	0.67297295	0.01509136	0.00669305	0.37881772	0.43551875	0.18997479	0.3	0.011497228	0.070994455	0.035193346	0.43332312
85.1934863	53.059085	0.78926566	0.02283769	0.04207467	0.26252501	0.42777242	0.15459316	0.6	0.016129355	0.080258711	0.046310453	0.64998469
85.3585251	52.7882875	0.77643537	0.14441903	0.11648832	0.2753553	0.30619107	0.08017951	0.8	0.020054051	0.088108103	0.055729723	0.86664625
86.2766	53.3250298	0.74760563	0.2545735	0.15277171	0.30418504	0.1960366	0.04389612	1	0.023087801	0.094175602	0.063010723	1.08330781
87.5112438	53.3794586	0.65524958	0.40200805	0.17185406	0.39654109	0.04860205	0.02481377	1.2	0.02508875	0.0981775	0.067813	1.29996937
88.8876077	54.0426063	0.55335163	0.55487701	0.18889684	0.49843904	-0.1042669	0.00777099	1.5	0.025963335	0.099926671	0.069912005	1.51663093
90.6502206	54.8358168	0.45154322	0.69899745	0.09925056	0.60024745	-0.24838734	0.09741727	1.6	0.025670663	0.099341326	0.069209591	1.7332925
91.6641702	55.4256006	0.38457259	0.80006552	0.12616647	0.66721808	-0.34945542	0.07050136	2.2	0.024224418	0.096448836	0.065738603	1.94995406
92.0829914	54.7404585	0.36450002	0.87470707	0.38664262	0.68729065	-0.42409696	-0.18997479	3.6	0.021692225	0.09138445	0.05966134	2.16661562
91.4663178	55.0363153	0.4711002	0.89743309	0.35006222	0.58069047	-0.44682298	-0.15339438	4.3	0.018192487	0.084384973	0.051261968	2.38327718
90.1767476	55.4662023	0.64094811	0.88829766	0.24894949	0.41084256	-0.43768755	-0.05228165	4.6	0.013888847	0.075777693	0.040933232	2.59993874
86.7439064	55.4238974	0.83461149	0.86035627	0.20013264	0.21717918	-0.40974617	-0.00346481	4.5	0.008982538	0.065965077	0.029158092	2.81660031
81.7589445	53.9614158	1.03765751	0.81036583	0.32201521	0.01413316	-0.35975572	-0.12534738	4.3	0.003702976	0.055405951	0.016487141	3.03326187
75.1309643	54.1000591	1.25587921	0.72999481	0.33630325	-0.20408854	-0.27938471	-0.13963542	4	-0.00170298	0.044594049	0.003512859	3.24992343
67.268373	53.8515831	1.48276941	0.63044718	0.26311493	-0.43097874	-0.17983707	-0.0664471	2.7	-0.00698254	0.034034924	-0.00915809	3.46658499
60.1957349	52.9861539	1.67299959	0.50799253	0.25817068	-0.62120892	-0.05738242	-0.06150285	2.2	-0.01188885	0.024222307	-0.02093323	3.68324655
55.0967331	53.2233417	1.82023559	0.3552692	0.20615666	-0.76844492	0.0953409	-0.00948883	2	-0.01619249	0.015615027	-0.03126197	3.89990812
52.3216217	53.3110589	1.90257663	0.18935005	0.18350392	-0.85078596	0.26126005	0.01316391	1.9	-0.01969222	0.00861555	-0.03966134	4.11656968
53.0964575	53.3543672	1.89169197	0.0428266	0.14771504	-0.8399013	0.40778351	0.04895279	1.8	-0.02222442	0.003551164	-0.0457386	4.33323124
57.2544889	53.7933174	1.7839866	0.04918546	0.10735792	-0.73219593	0.40142465	0.08930991	1.7	-0.02367066	0.000658674	-0.04920959	4.5498928
63.4787019	54.3515161	1.60754594	0.10283877	0.11955402	-0.55575527	0.34777133	0.07711381	1.5	-0.02396334	7.33293E-05	-0.049912	4.76655436
70.8159756	54.5397479	1.37533695	0.11304691	0.13862884	-0.32354628	0.33756319	0.058039	1.4	-0.02308875	0.00182225	-0.047813	4.98321593
78.4517903	54.53449	1.1167279	0.10136983	0.09124435	-0.06493723	0.34924027	0.10542348	1.3	-0.0210878	0.005824398	-0.04301072	5.19987749
85.1286203	54.5504629	0.83061334	0.061812	0.00012176	0.22117733	0.38879811	0.19654607	1.1	-0.01805405	0.011891897	-0.03572972	5.41653905
89.6216871	53.9817645	0.51479977	0.00378713	0.00078527	0.5369909	0.44682298	0.19588256	0.7	-0.01412936	0.019741289	-0.02631045	5.63320061
91.8515895	54.2560633	0.29378655	0.05545005	0.11089277	0.75800412	0.39516006	0.08577506	0.5	-0.00949723	0.029005545	-0.01519335	5.84986217
92.3160008	54.4659159	0.20100471	0.07808055	0.12428838	0.85078596	0.37252956	0.07237946	0.3	-0.00437426	0.039251478	-0.00289823	6.06652374
92.3715633	54.5316651	0.21110123	0.09461501	0.08291509	0.84068944	0.35599509	0.11375275	0.2	0.001	0.05	0.009999999	6.2831853



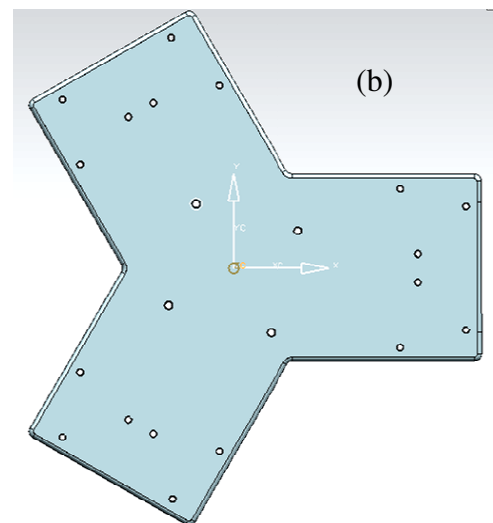
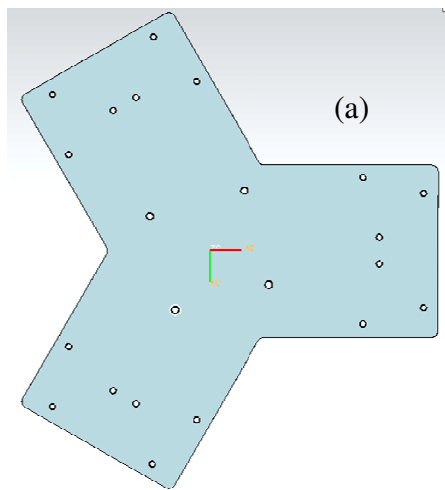
# Appendix

Real Data										Counts					
Time Instant	Time	t1	t2	t3	t4	t5	t6	Force	F/6	u1	u2	u3	u4	u5	u6
0	0	27.3	27.1	27.3	27.3	27.1	27.3	0	0	814254195	808288963	814254195	814254195	808288963	814254195
1	42	15.3	15.2	67.8	75.5	21	37.5	206	34.3333	456340263	453357647	2022213715	2251875155	626349381	1118481037
2	83	12.1	16	61.1	71.6	21.7	40.3	240	40	360896548	477218576	1822378437	2135553127	647227693	1201994288
3	125	8.9	18.4	52.3	67	22.5	44.3	275	45.8333	265452832	548801362	1559908220	1998352787	671088622	1321298932
4	167	6.6	24.9	40.8	62.5	23.6	51.2	387	64.5	196852662	742671408	1216907368	1864135062	703897399	1527099443
5	208	7.7	40.3	29.1	63	26.1	65	481	80.1667	229661439	1201994288	867941285	1879048143	778462802	1938700465
6	250	12.4	25	26.2	36.3	31.3	45.2	1133	188.833	369844396	745654025	781445418	1082689644	933558839	1348142477
7	292	34.3	13.7	41.6	15.8	56.2	32.8	1785	297.5	1023037322	408618405	1240768297	471253343	1676230248	978298080
8	333	44.1	17.5	42.5	9.7	70.1	37.8	1854	309	1315333700	521957817	1267611842	289313761	2090813886	1127428885
9	375	42.3	26.1	27.5	4.6	68.7	45.6	1923	320.5	1261646610	778462802	820219427	137200340	2049057260	1360072941
10	417	44.7	34.4	19.5	2.1	69.8	51.8	1854	309	1333229396	1026019938	581610139	62634938	2081866037	1544995139
11	458	47.5	40.5	15.1	1.1	70.4	55.3	1785	297.5	1416742647	1207959520	450375031	32808777	2099761734	1649386703
12	500	49.4	44.6	12.4	0.8	69.7	56.7	1682	280.333	1473412353	1330246780	369844396	23860928	2078883421	1691143328
13	542	50	46.7	10.7	1.1	67.5	56.1	1579	263.167	1491308050	1392881718	319139922	32808777	2013265867	1673247632
14	583	48.9	46.5	10	2	63.6	53.4	1511	251.833	1458499272	1386916486	298261610	59652322	1896943839	1592716997
15	625	44.8	42.3	11.4	4.2	56.6	47.1	1442	240.333	1336212012	1261646610	340018235	125269876	1688160712	1404812183
16	667	38.1	32.9	17.8	9.5	46.8	36.7	1373	228.833	1136376734	981280696	530905665	283348529	1395864334	1094620108
17	708	42.4	19.1	40.4	16	47.2	22.7	1305	217.5	1264629226	569679675	1204976904	477218576	1407794799	677053854
18	750	19.2	25.2	33.4	41.2	20.7	30.6	1236	206	572662291	751619257	996193777	1228837833	617401532	912680526
19	792	20.1	19.4	47	50.3	19	26.5	1167	194.5	599505836	578627523	1401829567	1500255898	566697059	790393266
20	833	20.2	17.9	54.3	57.1	18.2	26.5	164	27.3333	602488452	533888281	1619560542	1703073793	542836130	790393266
21	875	19.5	17.5	55.7	59.3	18.3	27.7	961	160.167	581610139	521957817	1661317167	1768691347	545818746	826184659
22	917	18	17.5	55.4	60.3	18.5	29.5	858	143	536870898	521957817	1652369319	1798517508	551783978	879871749
23	958	16.4	17.1	56.6	63	19	31.9	755	125.833	489149040	510027353	1688160712	1879048143	566697059	951454535
24	1000	15.2	16.4	59.6	67.2	19.7	34.5	652	108.667	453357647	489149040	1777639195	2004318019	587575371	1029002554

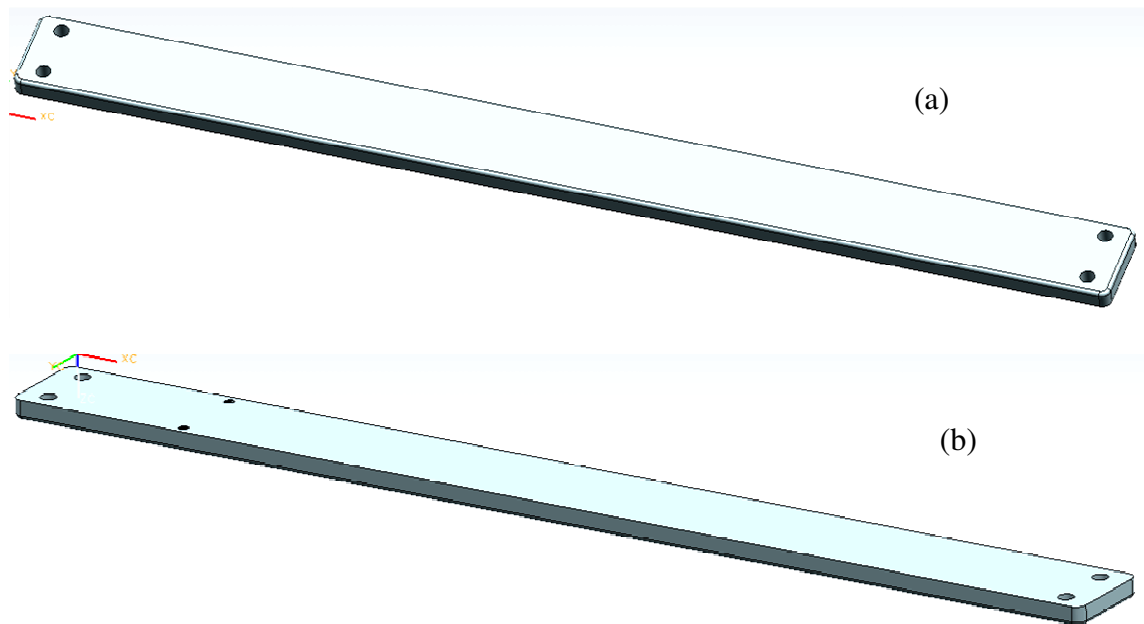
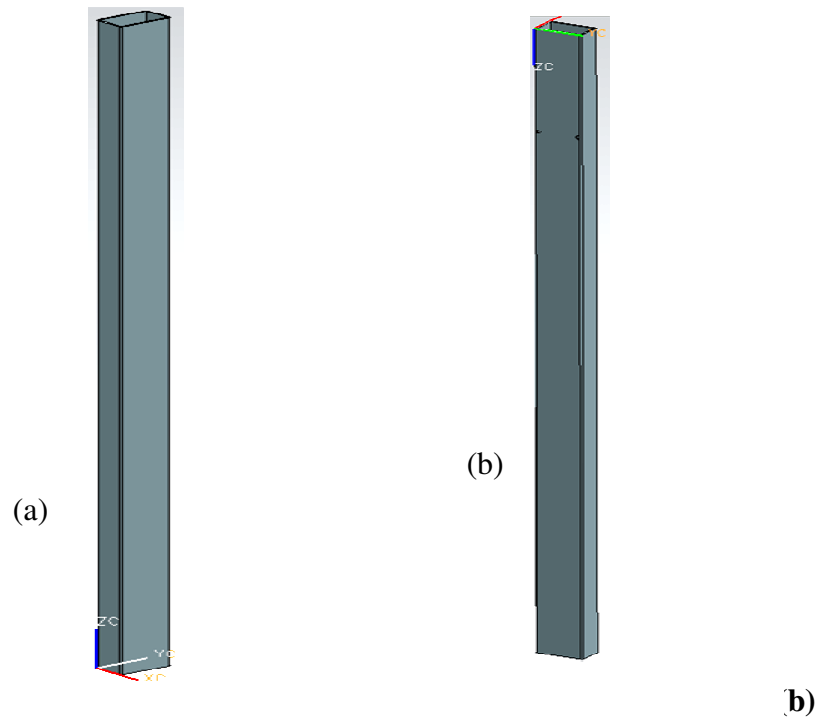
### Appendix 3 – CAD Plans of Stewart Platform



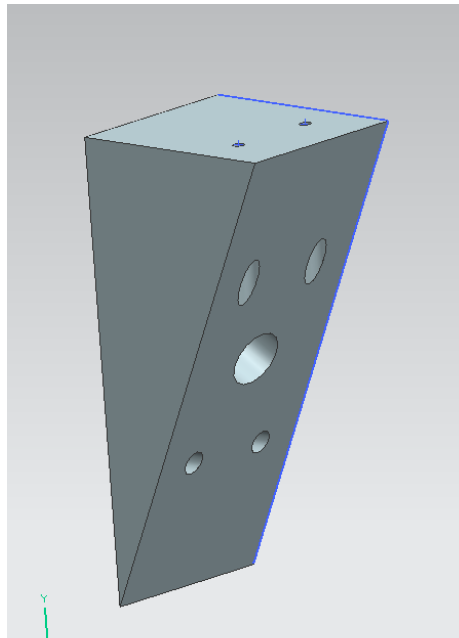
**Base Plate**



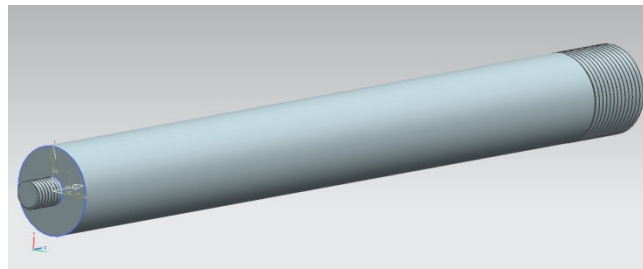
**m view**



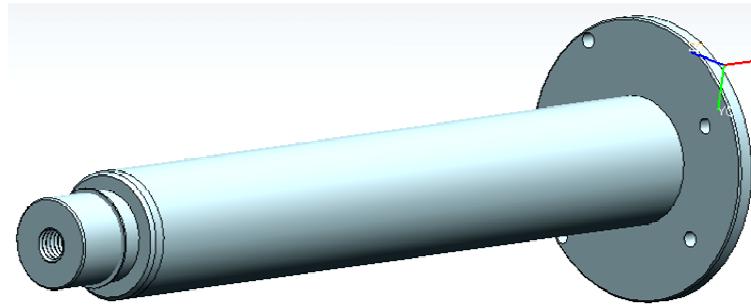
**Top of the Arch, a view from above (a) and below (b)**



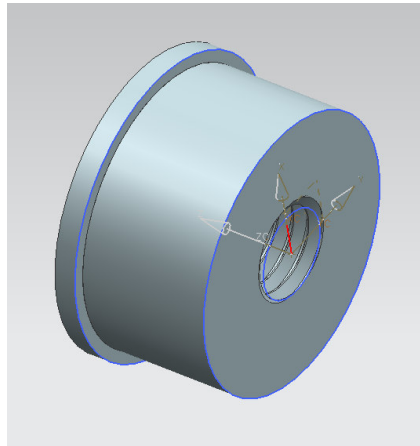
**View of the Corner Pole Attachment**



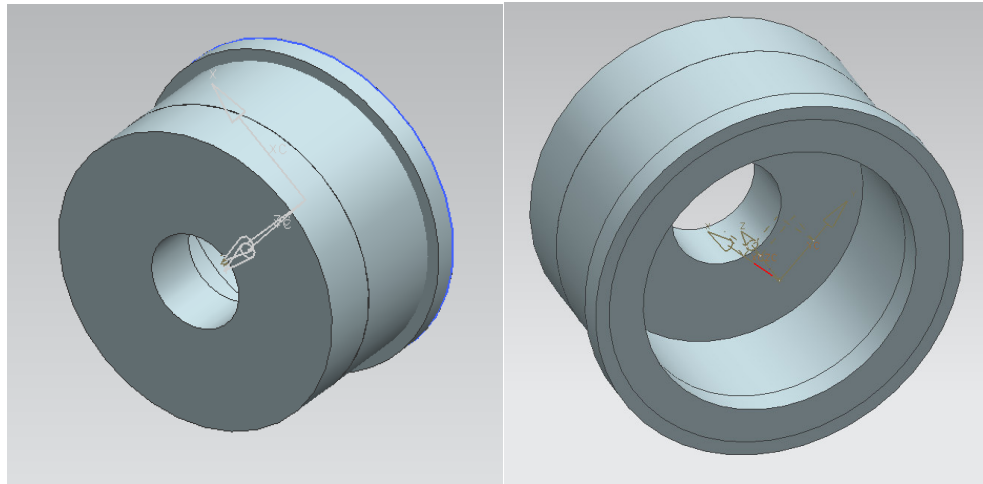
**View of the Fixing Pole Modelling**



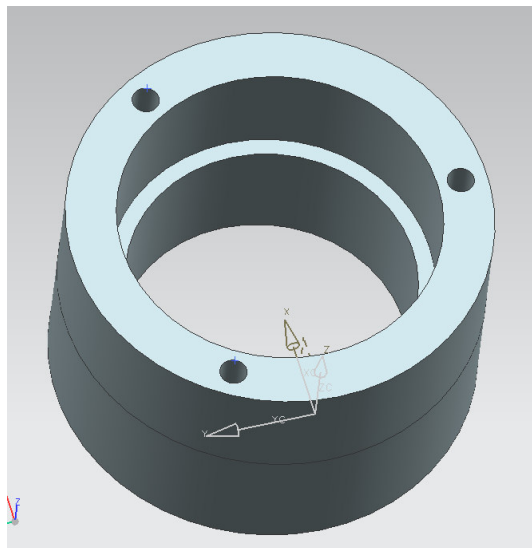
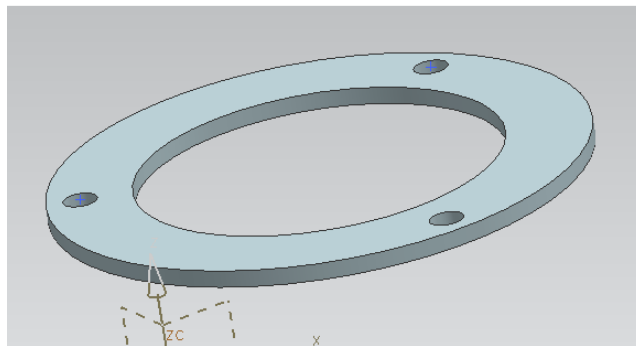
**Actuator holder**



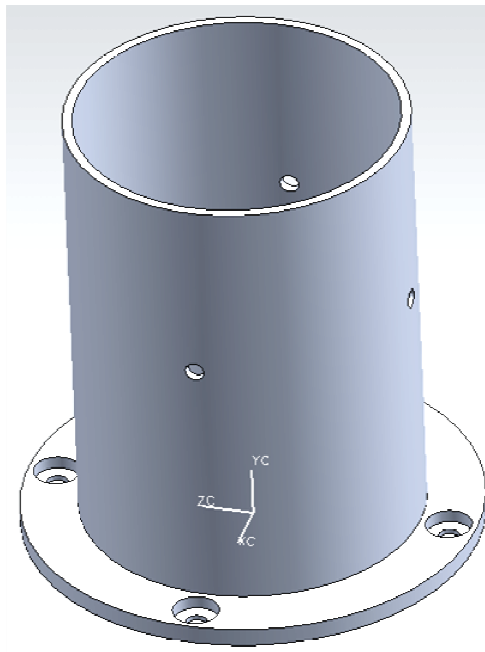
**Top Rod Attachment**



**Bottom Attachment Modelling**



**Bearing Attachment**



**Femur Holder**

## Appendix 4 – Parts and Equipments used

Images of the final components.



**Actuator Holders, Bearing Holders, Bearing Holder Caps, Top and Bottom End Attachments**





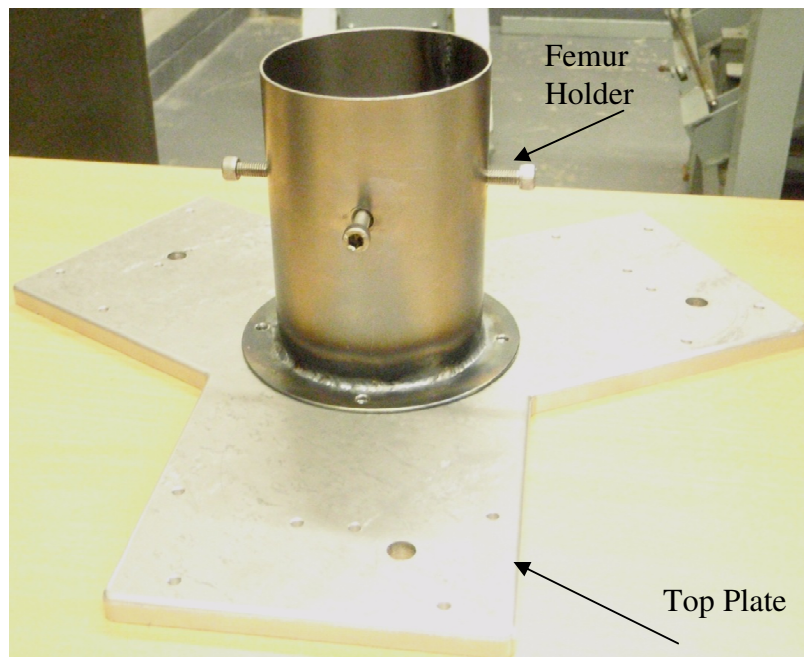
**Bearing Holder with Bearing and Bearing Holder Cap**



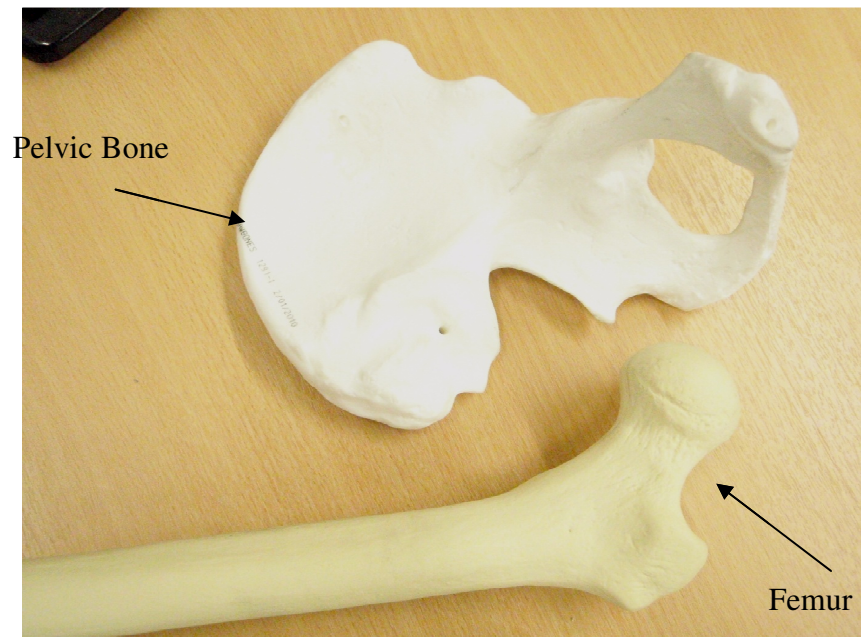
**Actuator Cylinder Holder**



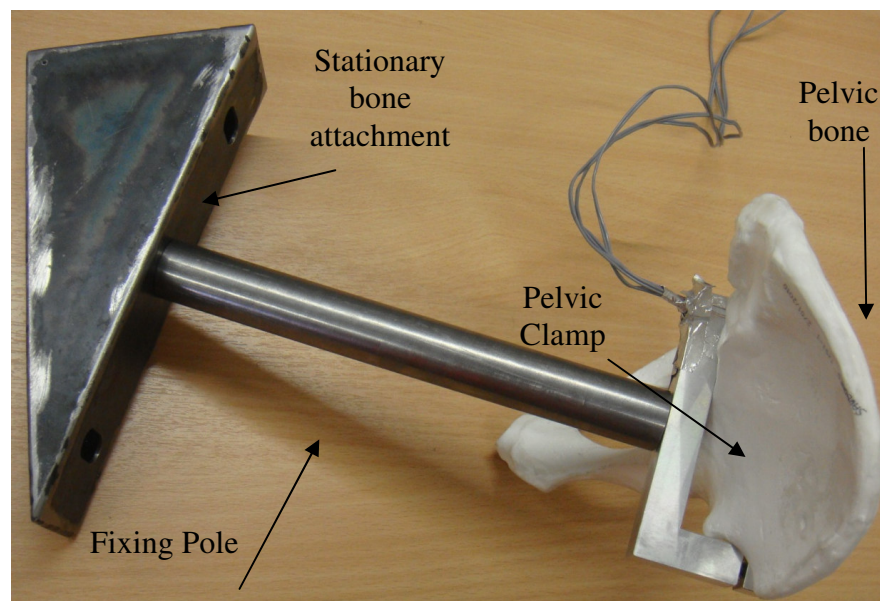
**Top Plate**



**Moving Plate with Femur Holder**



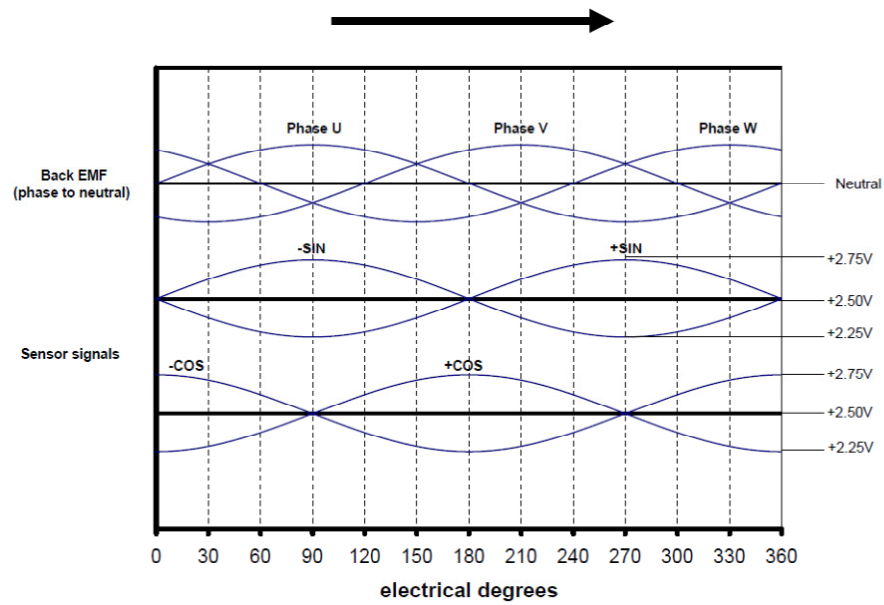
**Pelvis and Femur**



**Stationary bone attachment, fixing pole, pelvic clamp and pelvic bone assembled**



**Servo Tube Acuator Copley STA25 (Corp, 2008a)**

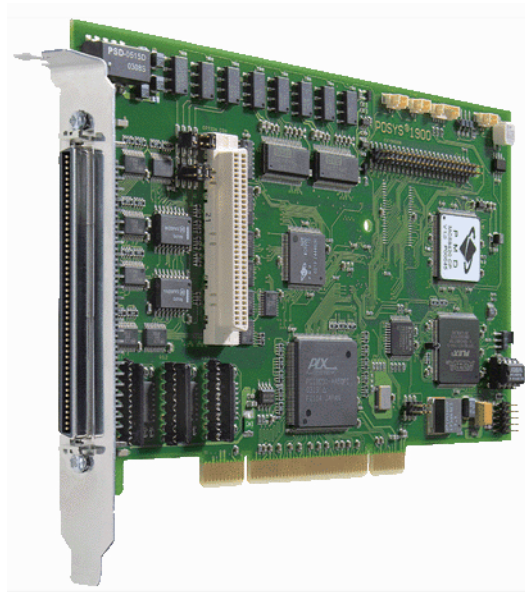


**Forcer phase back EMF and position sensor outputs. (Corp, 2008a)**





**Xenus XTL Amplifier Copley (Corp, 2008b)**



**POSYS 1924 (GmbH, 2008)**

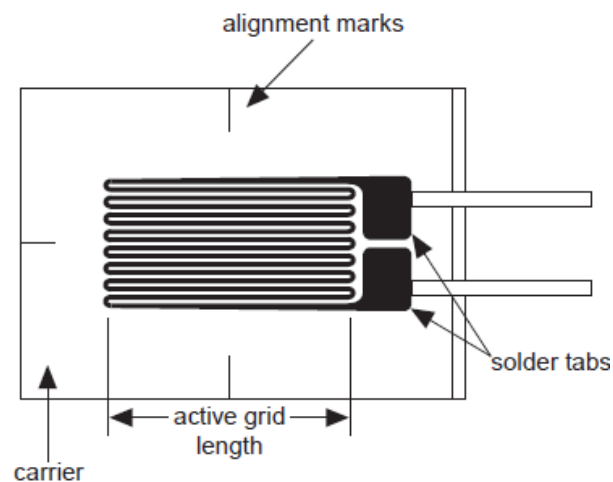
## **Appendix 5 – Strain Gauges**

Stress is caused by external forces being applied to an object; it is dependent on the force and the area it is acting on; the force can be either tensile or compressive. If the stress is great enough to deform the shape, the body experiences strain. The magnitude of the strain is dependent on the level of deformation. This was the case for the artificial bones being tested, because they experienced compression when pushed against each other as well as shear stress at the points where they made contact. If the bone returned to its original shape, the deformation was called elastic. When a body exceeds a certain level of stress, it does not return to its original shape and this is called plastic deformation. It is important that the bones and artificial joints do not experience any form of plastic deformation and minimal elastic deformation. How much the material deforms depends on the Poisson Ratio of the materials (Woodford, Brown, 2009-2010).

It should be noted that there is no device to measure stress directly; it is with the use of strain gauges that strain can be measured and also be applied to calculate stress. Strain gauges have only the ability to measure the strain on the surface of the material being tested; it is very difficult to determine the stress and strain within a body (Brown, 2009-2010).

There are three types of strain gauges available: piezoelectric (or semi-conductive), mechanical and metallic. Piezoelectric strain gauges are a semi-conductive and generate

electrical voltages when under strain the strain can be calculated using the measured voltage. Mechanical gauges are used when a brittle, transparent lacquer layer is applied to the outer surface of a body. When under load, the surface produces ridges according to the level of strain. Metallic strain gauges work by measuring the change in length with the use of optical sensors. Optical sensors are accurate sources of measurement and are sensitive and thus able to pick up discrete changes. They have optical flats which produce interference fringes and this can be used to measure the strain. A strain gauge is a transducer and is therefore able to measure strain by converting the strain acting on the gauge into an electric signal. The relationship between strain and electrical resistance is used to calculate the strain. Although other relationships can also be used to calculate the strain, electrical resistance is the most efficient and is more applicable to this case. The values of strain obtained in most cases are extremely small and, for this reason, the unit of measurement is a micro-strain (Woodford).



**Metallic strain gauge (Woodford)**

The strain gauge comprises a nonconductive case so that there is interference with the strain gauge and the surface it is placed on. Within the case is a resistive wire grid, usually made of foil as shown in the above figure. The grid is extremely thin, approximately 0.025mm, and is applied to the surface with the use of an adhesive which transmits the strain well but also insulates the gauge from the surface. The strain gauge stretches and increase in length, giving a positive value of strain; it also shrinks, resulting in a negative strain value, depending on the force acting on the bone, which change the electrical resistance within the strain gauge. Strain gauges are used widely in industry because they are needed to measure the stress in new designs involved in machinery, aerospace or automotive design. Every strain gauge has different gage factors: the higher the gage factor, the more sensitive it is. It is very important that the temperature of the strain gauge is kept constant because any fluctuations can affect the results. It was expected that thermal expansion would occur and as a result resistance would increase and in turn affect the degree of strain detected. For this reason the sensitivity of strain gauges to temperature needs to be low, by compensating for the thermal expansion (Brown, 2009-2010). If the temperature is constant, the initial relationship is:

$$R = \frac{l\rho}{A}$$

where:

R is the resistance of the semi-conductive gauge element

l is the length of the element

$\rho$  is the resistivity



A is the area of the element

When the element is under strain, this causes a change in resistance and therefore the relationship becomes:

$$\frac{\Delta R}{R} = \frac{\Delta l}{l} + \frac{\Delta \rho}{\rho} - \frac{\Delta A}{A}$$

The above equations indicate that the change in resistance is due to the change in length, density and area of the element.

### **Half Bridge**

The Half Bridge comprises of two strain gauges and two discrete resistors. The output voltage is:

$$V_O = V_{EX} \times \frac{X}{2}$$

Additional errors can result if the temperature of the resistors and strain gauges are not of equal value.

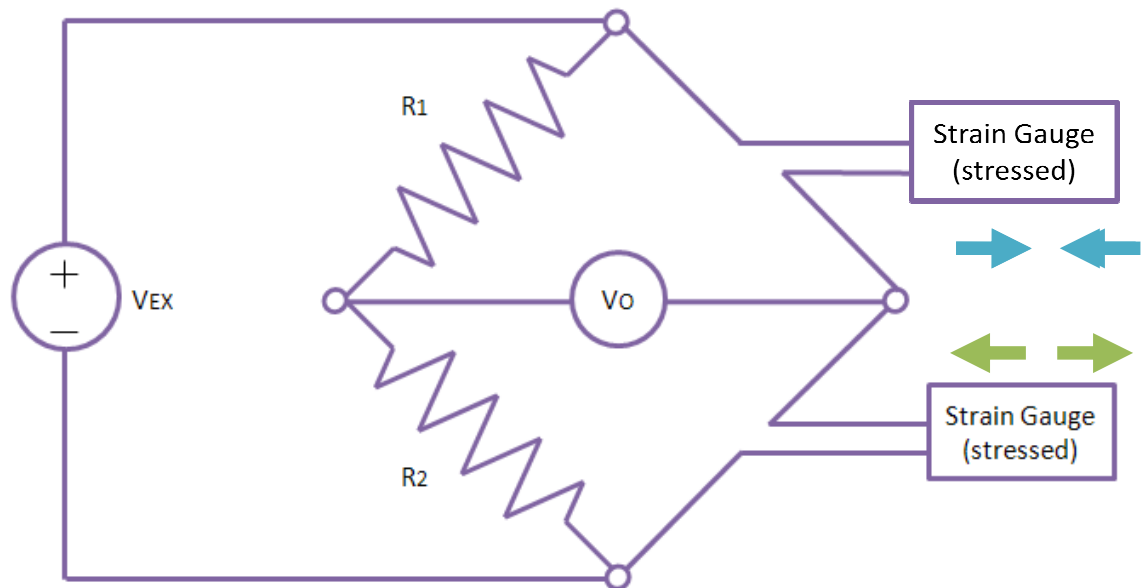
### **Data logger**

To record the difference in voltage from the strain gauge arrangement, a data logger was required. The Pico ADC-11 model was selected for its ease of use with a USB interface and 12 channels availability. The data is saved in a Pico-log format which is easily exportable and combined with the position data from the Stewart Platform's actuators.

In order to ensure accuracy of the readings, an amplifier was used to increase the voltage difference from the force clamp. The Pico ADC-11 claims to be accurate to 0.5%.



**Data logger (Pico ADC-11 model) (Technology)**



**Half Bridge**

The set up shows that the strain gauges have replaced two non-parallel resistors; this is why, when one gauge is experiencing compression, the other is under tension, as can be seen more clearly with the arrows. The Half Bridge minimises the error found in a Quarter Bridge, because there are two active strain gauges and therefore the resistance is proportional to the change in temperature. It can therefore be cancelled out and reduce the effect of thermal expansion.

For the purpose of this project, the strain gauges were used to measure bending in the device holding the bones. It was not necessary to determine torsion or shear strain and thus a Half Bridge was sufficient and was cheaper than a Full Bridge, although more accurate than a Quarter Bridge and was temperature compensated.

Another factor to be considered was the directions in which the readings had to be taken. The strain could be measured linearly in one direction, either perpendicularly or using strain gauge rosettes; with these, measurements could be taken from a combination of angles. Because the strain gauges were to be applied to the device holding the pelvic bone, they mainly experienced compression and there was no need to take measurements from different angles; therefore linear strain gauges were used. The positioning of the strain gauges could be displayed on the pelvic clamp and three strain gauges altogether were used.

## Appendix 6 – Visual Basic Code for Kinematic Simulation

```

'Routine for hip walk
Private Sub Timer_hip_walk_Tick(ByVal sender As System.Object,
ByVal e As System.EventArgs) Handles Timer_hip_walk.Tick
    Dim x(16), y(16), z(16), l(2), a, b, s(6), scx(6), scy(6),
scz(6), psi, th, phi As Single
    l(1) = Val(TextBox_l1.Text)
    x(14) = Val(Label_x14.Text)
    y(14) = Val(Label_y14.Text)
    z(14) = Val(Label_z14.Text)
    y(16) = y(14)
    x(16) = x(14) - l(1) * System.Math.Sin(2.678937271 -
System.Math.PI / 2)
    z(16) = z(14) + l(1) * System.Math.Cos(2.678937271 -
System.Math.PI / 2)
    Label_time.Text = Val(Label_time.Text) + 1
    If CheckBox1.Checked = False Then
        If Label_time.Text = 1000 Then Label_time.Text = 0
    End If
    If Label_time.Text = 1000 Then
        th = -0.242791131
        phi = 0.049999999
        Label_force.Text = Val(TextBox_weight.Text) * 9.81 * 0.8
        Form2.Label145.Text = Label_t1.Text
        Form2.Label146.Text = Label_t2.Text
        Form2.Label147.Text = Label_t3.Text
        Form2.Label148.Text = Label_t4.Text
        Form2.Label149.Text = Label_t5.Text
        Form2.Label150.Text = Label_t6.Text
        Form2.Label207.Text = Label_time.Text
    End If
    If Label_time.Text < 1000 Then
        th = -0.229528849
        phi = 0.039647237
        Label_force.Text = Val(TextBox_weight.Text) * 9.81 * 0.95
        Form2.Label139.Text = Label_t1.Text
        Form2.Label140.Text = Label_t2.Text
        Form2.Label141.Text = Label_t3.Text
        Form2.Label142.Text = Label_t4.Text
        Form2.Label143.Text = Label_t5.Text
        Form2.Label144.Text = Label_t6.Text
        Form2.Label208.Text = Label_time.Text
    End If
    If Label_time.Text < 958 Then
        th = -0.209865095
        phi = 0.029999999
        Label_force.Text = Val(TextBox_weight.Text) * 9.81 * 1.1
        Form2.Label133.Text = Label_t1.Text
        Form2.Label134.Text = Label_t2.Text
        Form2.Label135.Text = Label_t3.Text
        Form2.Label136.Text = Label_t4.Text
        Form2.Label137.Text = Label_t5.Text
        Form2.Label138.Text = Label_t6.Text
        Form2.Label209.Text = Label_time.Text
    End If
End Sub

```

```
End If
If Label_time.Text < 917 Then
    th = -0.19942945
    phi = 0.021715728
    Label_force.Text = Val(TextBox_weight.Text) * 9.81 * 1.25
    Form2.Label1127.Text = Label_t1.Text
    Form2.Label1128.Text = Label_t2.Text
    Form2.Label1129.Text = Label_t3.Text
    Form2.Label1130.Text = Label_t4.Text
    Form2.Label1131.Text = Label_t5.Text
    Form2.Label1132.Text = Label_t6.Text
    Form2.Label210.Text = Label_time.Text
End If
If Label_time.Text < 875 Then
    th = -0.197732173
    phi = 0.015358984
    Label_force.Text = Val(TextBox_weight.Text) * 9.81 * 1.4
    Form2.Label1121.Text = Label_t1.Text
    Form2.Label1122.Text = Label_t2.Text
    Form2.Label1123.Text = Label_t3.Text
    Form2.Label1124.Text = Label_t4.Text
    Form2.Label1125.Text = Label_t5.Text
    Form2.Label1126.Text = Label_t6.Text
    Form2.Label211.Text = Label_time.Text
End If
If Label_time.Text < 833 Then
    th = -0.187367009
    phi = 0.011362967
    Label_force.Text = Val(TextBox_weight.Text) * 9.81 * 1.55
    Form2.Label1115.Text = Label_t1.Text
    Form2.Label1116.Text = Label_t2.Text
    Form2.Label1117.Text = Label_t3.Text
    Form2.Label1118.Text = Label_t4.Text
    Form2.Label1119.Text = Label_t5.Text
    Form2.Label1120.Text = Label_t6.Text
    Form2.Label212.Text = Label_time.Text
End If
If Label_time.Text < 792 Then
    th = -0.14592065
    phi = 0.01
    Label_force.Text = Val(TextBox_weight.Text) * 9.81 * 1.7
    Form2.Label1109.Text = Label_t1.Text
    Form2.Label1110.Text = Label_t2.Text
    Form2.Label1111.Text = Label_t3.Text
    Form2.Label1112.Text = Label_t4.Text
    Form2.Label1113.Text = Label_t5.Text
    Form2.Label1114.Text = Label_t6.Text
    Form2.Label213.Text = Label_time.Text
End If
If Label_time.Text < 750 Then
    th = -0.071395781
    phi = 0.011362967
    Label_force.Text = Val(TextBox_weight.Text) * 9.81 * 1.8
    Form2.Label1103.Text = Label_t1.Text
    Form2.Label1104.Text = Label_t2.Text
    Form2.Label1105.Text = Label_t3.Text
    Form2.Label1106.Text = Label_t4.Text
```

```
Form2.Label1107.Text = Label_t5.Text
Form2.Label1108.Text = Label_t6.Text
Form2.Label214.Text = Label_time.Text
End If
If Label_time.Text < 708 Then
    th = 0.028662817
    phi = 0.015358984
    Label_force.Text = Val(TextBox_weight.Text) * 9.81 * 1.9
    Form2.Label197.Text = Label_t1.Text
    Form2.Label198.Text = Label_t2.Text
    Form2.Label199.Text = Label_t3.Text
    Form2.Label1100.Text = Label_t4.Text
    Form2.Label1101.Text = Label_t5.Text
    Form2.Label1102.Text = Label_t6.Text
    Form2.Label215.Text = Label_time.Text
End If
If Label_time.Text < 667 Then
    th = 0.134879021
    phi = 0.021715729
    Label_force.Text = Val(TextBox_weight.Text) * 9.81 * 2
    Form2.Label191.Text = Label_t1.Text
    Form2.Label192.Text = Label_t2.Text
    Form2.Label193.Text = Label_t3.Text
    Form2.Label194.Text = Label_t4.Text
    Form2.Label195.Text = Label_t5.Text
    Form2.Label196.Text = Label_t6.Text
    Form2.Label216.Text = Label_time.Text
End If
If Label_time.Text < 625 Then
    th = 0.217395264
    phi = 0.03
    Label_force.Text = Val(TextBox_weight.Text) * 9.81 * 2.1
    Form2.Label185.Text = Label_t1.Text
    Form2.Label186.Text = Label_t2.Text
    Form2.Label187.Text = Label_t3.Text
    Form2.Label188.Text = Label_t4.Text
    Form2.Label189.Text = Label_t5.Text
    Form2.Label190.Text = Label_t6.Text
    Form2.Label217.Text = Label_time.Text
End If
If Label_time.Text < 583 Then
    th = 0.259774685
    phi = 0.039647239
    Label_force.Text = Val(TextBox_weight.Text) * 9.81 * 2.2
    Form2.Label179.Text = Label_t1.Text
    Form2.Label180.Text = Label_t2.Text
    Form2.Label181.Text = Label_t3.Text
    Form2.Label182.Text = Label_t4.Text
    Form2.Label183.Text = Label_t5.Text
    Form2.Label184.Text = Label_t6.Text
    Form2.Label218.Text = Label_time.Text
End If
If Label_time.Text < 542 Then
    th = 0.273524679
    phi = 0.05
    Label_force.Text = Val(TextBox_weight.Text) * 9.81 * 2.3
    Form2.Label173.Text = Label_t1.Text
```

```
Form2.Label74.Text = Label_t2.Text
Form2.Label75.Text = Label_t3.Text
Form2.Label76.Text = Label_t4.Text
Form2.Label77.Text = Label_t5.Text
Form2.Label78.Text = Label_t6.Text
Form2.Label219.Text = Label_time.Text
End If
If Label_time.Text < 500 Then
    th = 0.272181774
    phi = 0.060352762
    Label_force.Text = Val(TextBox_weight.Text) * 9.81 * 2.45
    Form2.Label67.Text = Label_t1.Text
    Form2.Label68.Text = Label_t2.Text
    Form2.Label69.Text = Label_t3.Text
    Form2.Label70.Text = Label_t4.Text
    Form2.Label71.Text = Label_t5.Text
    Form2.Label72.Text = Label_t6.Text
    Form2.Label220.Text = Label_time.Text
End If
If Label_time.Text < 458 Then
    th = 0.25713941
    phi = 0.07
    Label_force.Text = Val(TextBox_weight.Text) * 9.81 * 2.6
    Form2.Label61.Text = Label_t1.Text
    Form2.Label62.Text = Label_t2.Text
    Form2.Label63.Text = Label_t3.Text
    Form2.Label64.Text = Label_t4.Text
    Form2.Label65.Text = Label_t5.Text
    Form2.Label66.Text = Label_t6.Text
    Form2.Label221.Text = Label_time.Text
End If
If Label_time.Text < 417 Then
    th = 0.227234404
    phi = 0.078284271
    Label_force.Text = Val(TextBox_weight.Text) * 9.81 * 2.7
    Form2.Label55.Text = Label_t1.Text
    Form2.Label56.Text = Label_t2.Text
    Form2.Label57.Text = Label_t3.Text
    Form2.Label58.Text = Label_t4.Text
    Form2.Label59.Text = Label_t5.Text
    Form2.Label60.Text = Label_t6.Text
    Form2.Label222.Text = Label_time.Text
End If
If Label_time.Text < 375 Then
    th = 0.179018287
    phi = 0.084641016
    Label_force.Text = Val(TextBox_weight.Text) * 9.81 * 2.8
    Form2.Label49.Text = Label_t1.Text
    Form2.Label50.Text = Label_t2.Text
    Form2.Label51.Text = Label_t3.Text
    Form2.Label52.Text = Label_t4.Text
    Form2.Label53.Text = Label_t5.Text
    Form2.Label54.Text = Label_t6.Text
    Form2.Label223.Text = Label_time.Text
End If
If Label_time.Text < 333 Then
    th = 0.11576559
```

```
        phi = 0.088637033
        Label_force.Text = Val(TextBox_weight.Text) * 9.81 * 2.7
        Form2.Label43.Text = Label_t1.Text
        Form2.Label44.Text = Label_t2.Text
        Form2.Label45.Text = Label_t3.Text
        Form2.Label46.Text = Label_t4.Text
        Form2.Label47.Text = Label_t5.Text
        Form2.Label48.Text = Label_t6.Text
        Form2.Label224.Text = Label_time.Text
    End If
    If Label_time.Text < 292 Then
        th = 0.04697097
        phi = 0.09
        Label_force.Text = Val(TextBox_weight.Text) * 9.81 * 2.6
        Form2.Label37.Text = Label_t1.Text
        Form2.Label38.Text = Label_t2.Text
        Form2.Label39.Text = Label_t3.Text
        Form2.Label40.Text = Label_t4.Text
        Form2.Label41.Text = Label_t5.Text
        Form2.Label42.Text = Label_t6.Text
        Form2.Label225.Text = Label_time.Text
    End If
    If Label_time.Text < 250 Then
        th = -0.022247224
        phi = 0.088637033
        Label_force.Text = Val(TextBox_weight.Text) * 9.81 * 1.65
        Form2.Label31.Text = Label_t1.Text
        Form2.Label32.Text = Label_t2.Text
        Form2.Label33.Text = Label_t3.Text
        Form2.Label34.Text = Label_t4.Text
        Form2.Label35.Text = Label_t5.Text
        Form2.Label36.Text = Label_t6.Text
        Form2.Label226.Text = Label_time.Text
    End If
    If Label_time.Text < 208 Then
        th = -0.088429088
        phi = 0.084641016
        Label_force.Text = Val(TextBox_weight.Text) * 9.81 * 0.7
        Form2.Label25.Text = Label_t1.Text
        Form2.Label26.Text = Label_t2.Text
        Form2.Label27.Text = Label_t3.Text
        Form2.Label28.Text = Label_t4.Text
        Form2.Label29.Text = Label_t5.Text
        Form2.Label30.Text = Label_t6.Text
        Form2.Label227.Text = Label_time.Text
    End If
    If Label_time.Text < 167 Then
        th = -0.15127787
        phi = 0.078284271
        Label_force.Text = Val(TextBox_weight.Text) * 9.81 * 0.55
        Form2.Label19.Text = Label_t1.Text
        Form2.Label20.Text = Label_t2.Text
        Form2.Label21.Text = Label_t3.Text
        Form2.Label22.Text = Label_t4.Text
        Form2.Label23.Text = Label_t5.Text
        Form2.Label24.Text = Label_t6.Text
        Form2.Label228.Text = Label_time.Text
```



```
End If
If Label_time.Text < 125 Then
    th = -0.204703472
    phi = 0.07
    Label_force.Text = Val(TextBox_weight.Text) * 9.81 * 0.4
    Form2.Label113.Text = Label_t1.Text
    Form2.Label114.Text = Label_t2.Text
    Form2.Label115.Text = Label_t3.Text
    Form2.Label116.Text = Label_t4.Text
    Form2.Label117.Text = Label_t5.Text
    Form2.Label118.Text = Label_t6.Text
    Form2.Label229.Text = Label_time.Text
End If
If Label_time.Text < 83 Then
    th = -0.244033249
    phi = 0.060352762
    Label_force.Text = Val(TextBox_weight.Text) * 9.81 * 0.35
    Form2.Label7.Text = Label_t1.Text
    Form2.Label8.Text = Label_t2.Text
    Form2.Label9.Text = Label_t3.Text
    Form2.Label10.Text = Label_t4.Text
    Form2.Label11.Text = Label_t5.Text
    Form2.Label12.Text = Label_t6.Text
    Form2.Label230.Text = Label_time.Text
End If
If Label_time.Text < 42 Then
    th = -0.273524679
    phi = 0.05
    Label_force.Text = Val(TextBox_weight.Text) * 9.81 * 0.3
    Form2.Label11.Text = Label_t1.Text
    Form2.Label12.Text = Label_t2.Text
    Form2.Label13.Text = Label_t3.Text
    Form2.Label14.Text = Label_t4.Text
    Form2.Label15.Text = Label_t5.Text
    Form2.Label16.Text = Label_t6.Text
    Form2.Label231.Text = Label_time.Text
End If
TextBox_th2.Text = th
TextBox_phi2.Text = phi
a = Val(TextBox_a.Text)
b = Val(Label_b.Text)
l(2) = Val(TextBox_l2.Text)
x(1) = Val(Label_x1.Text)
x(2) = Val(Label_x2.Text)
x(3) = Val(Label_x3.Text)
x(4) = Val(Label_x4.Text)
x(5) = Val(Label_x5.Text)
x(6) = Val(Label_x6.Text)
y(1) = Val(Label_y1.Text)
y(2) = Val(Label_y2.Text)
y(3) = Val(Label_y3.Text)
y(4) = Val(Label_y4.Text)
y(5) = Val(Label_y5.Text)
y(6) = Val(Label_y6.Text)
z(1) = Val(Label_z1.Text)
z(2) = Val(Label_z2.Text)
z(3) = Val(Label_z3.Text)
```

```

z(4) = Val(Label_z4.Text)
z(5) = Val(Label_z5.Text)
z(6) = Val(Label_z6.Text)
z(1) = 0
z(2) = 0
z(3) = 0
z(4) = 0
z(5) = 0
z(6) = 0
th = Val(TextBox_th2.Text)
phi = Val(TextBox_phi2.Text)
If phi ^ 2 > th ^ 2 Then psi = (System.Math.PI / 4) *
System.Math.Atan(System.Math.Tan(th) / System.Math.Tan(phi))
If phi ^ 2 > th ^ 2 Then
    TextBox_psi2.Text = psi
    If th > 0 And phi > 0 Then
        x(13) = x(14) + 1(2) / System.Math.Sqrt(1 + (1 /
(System.Math.Tan(th) ^ 2)) + (1 / (System.Math.Tan(psi) ^ 2)))
        y(13) = y(14) - 1(2) /
System.Math.Sqrt(((System.Math.Tan(psi) ^ 2)) + 1 + (1 /
(System.Math.Tan(phi) ^ 2)))
        z(13) = z(14) - 1(2) /
System.Math.Sqrt((System.Math.Tan(th) ^ 2) + (System.Math.Tan(phi) ^
2) + 1)
    End If
    If th < 0 And phi < 0 Then
        x(13) = x(14) - 1(2) / System.Math.Sqrt(1 + (1 /
System.Math.Tan(th) ^ 2) + (1 / System.Math.Tan(psi) ^ 2))
        y(13) = y(14) + 1(2) /
System.Math.Sqrt((System.Math.Tan(psi) ^ 2) + 1 + (1 /
System.Math.Tan(phi) ^ 2))
        z(13) = z(14) - 1(2) /
System.Math.Sqrt((System.Math.Tan(th) ^ 2) + (System.Math.Tan(phi) ^
2) + 1)
    End If
    If th < 0 And phi > 0 Then
        x(13) = x(14) - 1(2) / System.Math.Sqrt(1 + (1 /
(System.Math.Tan(th) ^ 2)) + (1 / (System.Math.Tan(psi) ^ 2)))
        y(13) = y(14) - 1(2) /
System.Math.Sqrt(((System.Math.Tan(psi) ^ 2)) + 1 + (1 /
(System.Math.Tan(phi) ^ 2)))
        z(13) = z(14) - 1(2) /
System.Math.Sqrt((System.Math.Tan(th) ^ 2) + (System.Math.Tan(phi) ^
2) + 1)
    End If
    If th > 0 And phi < 0 Then
        x(13) = x(14) + 1(2) / System.Math.Sqrt(1 + (1 /
(System.Math.Tan(th) ^ 2)) + (1 / (System.Math.Tan(psi) ^ 2)))
        y(13) = y(14) + 1(2) /
System.Math.Sqrt(((System.Math.Tan(psi) ^ 2)) + 1 + (1 /
(System.Math.Tan(phi) ^ 2)))
        z(13) = z(14) - 1(2) /
System.Math.Sqrt((System.Math.Tan(th) ^ 2) + (System.Math.Tan(phi) ^
2) + 1)
    End If
End If
End If

```

```

        If th ^ 2 > phi ^ 2 Then psi = (System.Math.PI / 4) *
System.Math.Atan(System.Math.Tan(phi) / System.Math.Tan(th))
        If th ^ 2 > phi ^ 2 Then
            TextBox_psi2.Text = psi
            If th > 0 And phi > 0 Then
                x(13) = x(14) + l(2) / System.Math.Sqrt(1 + (1 /
(System.Math.Tan(th) ^ 2)) + ((System.Math.Tan(psi) ^ 2)))
                y(13) = y(14) - l(2) /
System.Math.Sqrt(((System.Math.Tan(psi) ^ 2)) + 1 + (1 /
(System.Math.Tan(phi) ^ 2)))
                z(13) = z(14) - l(2) /
System.Math.Sqrt((System.Math.Tan(th) ^ 2) + (System.Math.Tan(phi) ^
2) + 1)
            End If
            If th < 0 And phi < 0 Then
                x(13) = x(14) - l(2) / System.Math.Sqrt(1 + (1 /
(System.Math.Tan(th) ^ 2)) + ((System.Math.Tan(psi) ^ 2)))
                y(13) = y(14) + l(2) /
System.Math.Sqrt((System.Math.Tan(psi) ^ 2) + 1 + (1 /
System.Math.Tan(phi) ^ 2))
                z(13) = z(14) - l(2) /
System.Math.Sqrt((System.Math.Tan(th) ^ 2) + (System.Math.Tan(phi) ^
2) + 1)
            End If
            If th < 0 And phi > 0 Then
                x(13) = x(14) - l(2) / System.Math.Sqrt(1 + (1 /
(System.Math.Tan(th) ^ 2)) + ((System.Math.Tan(psi) ^ 2)))
                y(13) = y(14) - l(2) /
System.Math.Sqrt(((System.Math.Tan(psi) ^ 2)) + 1 + (1 /
(System.Math.Tan(phi) ^ 2)))
                z(13) = z(14) - l(2) /
System.Math.Sqrt((System.Math.Tan(th) ^ 2) + (System.Math.Tan(phi) ^
2) + 1)
            End If
            If th > 0 And phi < 0 Then
                x(13) = x(14) + l(2) / System.Math.Sqrt(1 + (1 /
(System.Math.Tan(th) ^ 2)) + ((System.Math.Tan(psi) ^ 2)))
                y(13) = y(14) + l(2) /
System.Math.Sqrt(((System.Math.Tan(psi) ^ 2)) + 1 + (1 /
(System.Math.Tan(phi) ^ 2)))
                z(13) = z(14) - l(2) /
System.Math.Sqrt((System.Math.Tan(th) ^ 2) + (System.Math.Tan(phi) ^
2) + 1)
            End If
        End If
        Label_x.Text = x(13)
        Label_y.Text = y(13)
        Label_z.Text = z(13)
        scx(1) = (a / 1.414213562) * -0.965925826 + x(13) + (a /
1.414213562) * 0.47140452 * System.Math.Cos(psi) * System.Math.Cos(th)
- (a / 1.414213562) * 0.47140452 * System.Math.Cos(phi) *
System.Math.Sin(psi) + (a / 1.414213562) * 0.47140452 *
System.Math.Cos(psi) * System.Math.Sin(th) * System.Math.Sin(phi)
        scy(1) = (a / 1.414213562) * -0.258819045 + y(13) + (a /
1.414213562) * 0.47140452 * System.Math.Cos(th) * System.Math.Sin(psi)
+ (a / 1.414213562) * 0.47140452 * System.Math.Cos(phi) *

```

```

System.Math.Cos(psi) + (a / 1.414213562) * 0.47140452 *
System.Math.Sin(psi) * System.Math.Sin(th) * System.Math.Sin(phi)
    scz(1) = z(13) + (a / 1.414213562) * 0.47140452 *
System.Math.Sin(th) - (a / 1.414213562) * 0.47140452 *
System.Math.Cos(th) * System.Math.Sin(phi)
    scx(6) = (a / 1.414213562) * -0.965925826 + x(13) + (a /
1.414213562) * 0.47140452 * System.Math.Cos(psi) * System.Math.Cos(th)
+ (a / 1.414213562) * 0.47140452 * System.Math.Cos(phi) *
System.Math.Sin(psi) - (a / 1.414213562) * 0.47140452 *
System.Math.Cos(psi) * System.Math.Sin(th) * System.Math.Sin(phi)
    scy(6) = (a / 1.414213562) * 0.258819045 + y(13) + (a /
1.414213562) * 0.47140452 * System.Math.Cos(th) * System.Math.Sin(psi)
- (a / 1.414213562) * 0.47140452 * System.Math.Cos(phi) *
System.Math.Cos(psi) - (a / 1.414213562) * 0.47140452 *
System.Math.Sin(psi) * System.Math.Sin(th) * System.Math.Sin(phi)
    scz(6) = z(13) + (a / 1.414213562) * 0.47140452 *
System.Math.Sin(th) + (a / 1.414213562) * 0.47140452 *
System.Math.Cos(th) * System.Math.Sin(phi)
    scx(5) = (a / 1.414213562) * 0.25519045 + x(13) + (a /
1.414213562) * 0.17254603 * System.Math.Cos(psi) * System.Math.Cos(th)
+ (a / 1.414213562) * 0.64395055 * System.Math.Cos(phi) *
System.Math.Sin(psi) - (a / 1.414213562) * 0.64395055 *
System.Math.Cos(psi) * System.Math.Sin(th) * System.Math.Sin(phi)
    scy(5) = (a / 1.414213562) * 0.965925826 + y(13) + (a /
1.414213562) * 0.17254603 * System.Math.Cos(th) * System.Math.Sin(psi)
- (a / 1.414213562) * 0.64395055 * System.Math.Cos(psi) *
System.Math.Cos(phi) - (a / 1.414213562) * 0.64395055 *
System.Math.Sin(psi) * System.Math.Sin(th) * System.Math.Sin(phi)
    scz(5) = z(13) + (a / 1.414213562) * 0.17254603 *
System.Math.Sin(th) + (a / 1.414213562) * 0.64395055 *
System.Math.Cos(th) * System.Math.Sin(phi)
    scx(4) = (a / 1.414213562) * 0.707106781 + x(13) - (a /
1.414213562) * 0.64395055 * System.Math.Cos(psi) * System.Math.Cos(th)
+ (a / 1.414213562) * 0.17254603 * System.Math.Cos(phi) *
System.Math.Sin(psi) - (a / 1.414213562) * 0.17254603 *
System.Math.Cos(psi) * System.Math.Sin(th) * System.Math.Sin(phi)
    scy(4) = (a / 1.414213562) * 0.707106781 + y(13) - (a /
1.414213562) * 0.64395055 * System.Math.Cos(th) * System.Math.Sin(psi)
- (a / 1.414213562) * 0.17254603 * System.Math.Cos(psi) *
System.Math.Cos(phi) - (a / 1.414213562) * 0.17254603 *
System.Math.Sin(psi) * System.Math.Sin(th) * System.Math.Sin(phi)
    scz(4) = z(13) - (a / 1.414213562) * 0.64395055 *
System.Math.Sin(th) + (a / 1.414213562) * 0.17254603 *
System.Math.Cos(th) * System.Math.Sin(phi)
    scx(3) = (a / 1.414213562) * 0.707106781 + x(13) - (a /
1.414213562) * 0.64395055 * System.Math.Cos(psi) * System.Math.Cos(th)
- (a / 1.414213562) * 0.17254603 * System.Math.Cos(phi) *
System.Math.Sin(psi) + (a / 1.414213562) * 0.17254603 *
System.Math.Cos(psi) * System.Math.Sin(th) * System.Math.Sin(phi)
    scy(3) = (a / 1.414213562) * -0.707106781 + y(13) - (a /
1.414213562) * 0.64395055 * System.Math.Cos(th) * System.Math.Sin(psi)
+ (a / 1.414213562) * 0.17254603 * System.Math.Cos(psi) *
System.Math.Cos(phi) + (a / 1.414213562) * 0.17254603 *
System.Math.Sin(psi) * System.Math.Sin(th) * System.Math.Sin(phi)
    scz(3) = z(13) - (a / 1.414213562) * 0.64395055 *
System.Math.Sin(th) - (a / 1.414213562) * 0.17254603 *
System.Math.Cos(th) * System.Math.Sin(phi)

```

```
scx(2) = (a / 1.414213562) * 0.25519045 + x(13) + (a /
1.414213562) * 0.17254603 * System.Math.Cos(psi) * System.Math.Cos(th)
- (a / 1.414213562) * 0.64395055 * System.Math.Cos(phi) *
System.Math.Sin(psi) + (a / 1.414213562) * 0.64395055 *
System.Math.Cos(psi) * System.Math.Sin(th) * System.Math.Sin(phi)
scy(2) = (a / 1.414213562) * -0.965925826 + y(13) + (a /
1.414213562) * 0.17254603 * System.Math.Cos(th) * System.Math.Sin(psi)
+ (a / 1.414213562) * 0.64395055 * System.Math.Cos(psi) *
System.Math.Cos(phi) + (a / 1.414213562) * 0.64395055 *
System.Math.Sin(psi) * System.Math.Sin(th) * System.Math.Sin(phi)
scz(2) = z(13) + (a / 1.414213562) * 0.17254603 *
System.Math.Sin(th) - (a / 1.414213562) * 0.64395055 *
System.Math.Cos(th) * System.Math.Sin(phi)
x(7) = x(1) + scx(1)
x(8) = x(2) + scx(2)
x(9) = x(3) + scx(3)
x(10) = x(4) + scx(4)
x(11) = x(5) + scx(5)
x(12) = x(6) + scx(6)
y(7) = y(1) + scy(1)
y(8) = y(2) + scy(2)
y(9) = y(3) + scy(3)
y(10) = y(4) + scy(4)
y(11) = y(5) + scy(5)
y(12) = y(6) + scy(6)
z(7) = z(1) + scz(1)
z(8) = z(2) + scz(2)
z(9) = z(3) + scz(3)
z(10) = z(4) + scz(4)
z(11) = z(5) + scz(5)
z(12) = z(6) + scz(6)
Label_x1.Text = x(1)
Label_x2.Text = x(2)
Label_x3.Text = x(3)
Label_x4.Text = x(4)
Label_x5.Text = x(5)
Label_x6.Text = x(6)
Label_x7.Text = x(7)
Label_x8.Text = x(8)
Label_x9.Text = x(9)
Label_x10.Text = x(10)
Label_x11.Text = x(11)
Label_x12.Text = x(12)
Label_x13.Text = x(13)
Label_x14.Text = x(14)
Label_x15.Text = x(15)
Label_x16.Text = x(16)
Label_y1.Text = y(1)
Label_y2.Text = y(2)
Label_y3.Text = y(3)
Label_y4.Text = y(4)
Label_y5.Text = y(5)
Label_y6.Text = y(6)
Label_y7.Text = y(7)
Label_y8.Text = y(8)
Label_y9.Text = y(9)
Label_y10.Text = y(10)
```

```

Label_y11.Text = y(11)
Label_y12.Text = y(12)
Label_y13.Text = y(13)
Label_y14.Text = y(14)
Label_y15.Text = y(15)
Label_y16.Text = y(16)
Label_z1.Text = z(1)
Label_z2.Text = z(2)
Label_z3.Text = z(3)
Label_z4.Text = z(4)
Label_z5.Text = z(5)
Label_z6.Text = z(6)
Label_z7.Text = z(7)
Label_z8.Text = z(8)
Label_z9.Text = z(9)
Label_z10.Text = z(10)
Label_z11.Text = z(11)
Label_z12.Text = z(12)
Label_z13.Text = z(13)
Label_z14.Text = z(14)
Label_z15.Text = z(15)
Label_z16.Text = z(16)
s(1) = System.Math.Sqrt((x(1) - x(7)) ^ 2 + (y(1) - y(7)) ^ 2
+ (z(1) - z(7)) ^ 2)
s(2) = System.Math.Sqrt((x(2) - x(8)) ^ 2 + (y(2) - y(8)) ^ 2
+ (z(2) - z(8)) ^ 2)
s(3) = System.Math.Sqrt((x(3) - x(9)) ^ 2 + (y(3) - y(9)) ^ 2
+ (z(3) - z(9)) ^ 2)
s(4) = System.Math.Sqrt((x(4) - x(10)) ^ 2 + (y(4) - y(10)) ^
2 + (z(4) - z(10)) ^ 2)
s(5) = System.Math.Sqrt((x(5) - x(11)) ^ 2 + (y(5) - y(11)) ^
2 + (z(5) - z(11)) ^ 2)
s(6) = System.Math.Sqrt((x(6) - x(12)) ^ 2 + (y(6) - y(12)) ^
2 + (z(6) - z(12)) ^ 2)
Label_t1.Text = (s(1) - 43.7) * 10
Label_t2.Text = (s(2) - 43.7) * 10
Label_t3.Text = (s(3) - 43.7) * 10
Label_t4.Text = (s(4) - 43.7) * 10
Label_t5.Text = (s(5) - 43.7) * 10
Label_t6.Text = (s(6) - 43.7) * 10
Label_s1.Text = s(1)
Label_s2.Text = s(2)
Label_s3.Text = s(3)
Label_s4.Text = s(4)
Label_s5.Text = s(5)
Label_s6.Text = s(6)
Label39.Text = System.Math.Sqrt((x(13) - x(14)) ^ 2 + (y(13) -
y(14)) ^ 2 + (z(13) - z(14)) ^ 2)

PictureBox1.CreateGraphics.Clear(System.Drawing.Color.LightBlue)

PictureBox1.CreateGraphics.DrawLine(System.Drawing.Pens.Yellow, CInt(2
* y(1) + 180), CInt(2 * x(1) + 330), CInt(2 * y(2) + 180), CInt(2 *
x(2) + 330))

PictureBox1.CreateGraphics.DrawLine(System.Drawing.Pens.Yellow, CInt(2

```

## Appendix

---

```
* y(2) + 180), CInt(2 * x(2) + 330), CInt(2 * y(3) + 180), CInt(2 *
x(3) + 330))

PictureBox1.CreateGraphics.DrawLine(System.Drawing.Pens.Yellow, CInt(2
* y(3) + 180), CInt(2 * x(3) + 330), CInt(2 * y(4) + 180), CInt(2 *
x(4) + 330))

PictureBox1.CreateGraphics.DrawLine(System.Drawing.Pens.Yellow, CInt(2
* y(4) + 180), CInt(2 * x(4) + 330), CInt(2 * y(5) + 180), CInt(2 *
x(5) + 330))

PictureBox1.CreateGraphics.DrawLine(System.Drawing.Pens.Yellow, CInt(2
* y(5) + 180), CInt(2 * x(5) + 330), CInt(2 * y(6) + 180), CInt(2 *
x(6) + 330))

PictureBox1.CreateGraphics.DrawLine(System.Drawing.Pens.Yellow, CInt(2
* y(6) + 180), CInt(2 * x(6) + 330), CInt(2 * y(1) + 180), CInt(2 *
x(1) + 330))
    PictureBox1.CreateGraphics.DrawLine(System.Drawing.Pens.Green,
CInt(2 * y(7) + 180), CInt(2 * x(7) + 330), CInt(2 * y(8) + 180),
CInt(2 * x(8) + 330))
    PictureBox1.CreateGraphics.DrawLine(System.Drawing.Pens.Green,
CInt(2 * y(8) + 180), CInt(2 * x(8) + 330), CInt(2 * y(9) + 180),
CInt(2 * x(9) + 330))
    PictureBox1.CreateGraphics.DrawLine(System.Drawing.Pens.Green,
CInt(2 * y(9) + 180), CInt(2 * x(9) + 330), CInt(2 * y(10) + 180),
CInt(2 * x(10) + 330))
    PictureBox1.CreateGraphics.DrawLine(System.Drawing.Pens.Green,
CInt(2 * y(10) + 180), CInt(2 * x(10) + 330), CInt(2 * y(11) + 180),
CInt(2 * x(11) + 330))
    PictureBox1.CreateGraphics.DrawLine(System.Drawing.Pens.Green,
CInt(2 * y(11) + 180), CInt(2 * x(11) + 330), CInt(2 * y(12) + 180),
CInt(2 * x(12) + 330))
    PictureBox1.CreateGraphics.DrawLine(System.Drawing.Pens.Green,
CInt(2 * y(12) + 180), CInt(2 * x(12) + 330), CInt(2 * y(7) + 180),
CInt(2 * x(7) + 330))
    PictureBox1.CreateGraphics.DrawLine(System.Drawing.Pens.Green,
CInt(2 * y(13) + 180), CInt(2 * x(13) + 330), CInt(2 * y(14) + 180),
CInt(2 * x(14) + 330))
    PictureBox1.CreateGraphics.DrawLine(System.Drawing.Pens.Pink,
CInt(2 * y(1) + 180), CInt(2 * x(1) + 330), CInt(2 * y(7) + 180),
CInt(2 * x(7) + 330))
    PictureBox1.CreateGraphics.DrawLine(System.Drawing.Pens.White,
CInt(2 * y(2) + 180), CInt(2 * x(2) + 330), CInt(2 * y(8) + 180),
CInt(2 * x(8) + 330))

PictureBox1.CreateGraphics.DrawLine(System.Drawing.Pens.Purple, CInt(2
* y(3) + 180), CInt(2 * x(3) + 330), CInt(2 * y(9) + 180), CInt(2 *
x(9) + 330))
    PictureBox1.CreateGraphics.DrawLine(System.Drawing.Pens.Black,
CInt(2 * y(4) + 180), CInt(2 * x(4) + 330), CInt(2 * y(10) + 180),
CInt(2 * x(10) + 330))
    PictureBox1.CreateGraphics.DrawLine(System.Drawing.Pens.Blue,
CInt(2 * y(6) + 180), CInt(2 * x(6) + 330), CInt(2 * y(12) + 180),
CInt(2 * x(12) + 330))

PictureBox1.CreateGraphics.DrawLine(System.Drawing.Pens.Orange, CInt(2
```

## Appendix

---

```
* y(5) + 180), CInt(2 * x(5) + 330), CInt(2 * y(11) + 180), CInt(2 *
x(11) + 330))

PictureBox2.CreateGraphics.Clear(System.Drawing.Color.LightBlue)

PictureBox2.CreateGraphics.DrawLine(System.Drawing.Pens.Yellow, CInt(2
* y(1) + 180), CInt(-2 * z(1) + 500), CInt(2 * y(2) + 180), CInt(-2 *
z(2) + 500))

PictureBox2.CreateGraphics.DrawLine(System.Drawing.Pens.Yellow, CInt(2
* y(2) + 180), CInt(-2 * z(2) + 500), CInt(2 * y(3) + 180), CInt(-2 *
z(3) + 500))

PictureBox2.CreateGraphics.DrawLine(System.Drawing.Pens.Yellow, CInt(2
* y(3) + 180), CInt(-2 * z(3) + 500), CInt(2 * y(4) + 180), CInt(-2 *
z(4) + 500))

PictureBox2.CreateGraphics.DrawLine(System.Drawing.Pens.Yellow, CInt(2
* y(4) + 180), CInt(-2 * z(4) + 500), CInt(2 * y(5) + 180), CInt(-2 *
z(5) + 500))

PictureBox2.CreateGraphics.DrawLine(System.Drawing.Pens.Yellow, CInt(2
* y(5) + 180), CInt(-2 * z(5) + 500), CInt(2 * y(6) + 180), CInt(-2 *
z(6) + 500))

PictureBox2.CreateGraphics.DrawLine(System.Drawing.Pens.Yellow, CInt(2
* y(6) + 180), CInt(-2 * z(6) + 500), CInt(2 * y(1) + 180), CInt(-2 *
z(1) + 500))
    PictureBox2.CreateGraphics.DrawLine(System.Drawing.Pens.Green,
CInt(2 * y(7) + 180), CInt(-2 * z(7) + 500), CInt(2 * y(8) + 180),
CInt(-2 * z(8) + 500))
    PictureBox2.CreateGraphics.DrawLine(System.Drawing.Pens.Green,
CInt(2 * y(8) + 180), CInt(-2 * z(8) + 500), CInt(2 * y(9) + 180),
CInt(-2 * z(9) + 500))
    PictureBox2.CreateGraphics.DrawLine(System.Drawing.Pens.Green,
CInt(2 * y(9) + 180), CInt(-2 * z(9) + 500), CInt(2 * y(10) + 180),
CInt(-2 * z(10) + 500))
    PictureBox2.CreateGraphics.DrawLine(System.Drawing.Pens.Green,
CInt(2 * y(10) + 180), CInt(-2 * z(10) + 500), CInt(2 * y(11) + 180),
CInt(-2 * z(11) + 500))
    PictureBox2.CreateGraphics.DrawLine(System.Drawing.Pens.Green,
CInt(2 * y(11) + 180), CInt(-2 * z(11) + 500), CInt(2 * y(12) + 180),
CInt(-2 * z(12) + 500))
    PictureBox2.CreateGraphics.DrawLine(System.Drawing.Pens.Green,
CInt(2 * y(12) + 180), CInt(-2 * z(12) + 500), CInt(2 * y(7) + 180),
CInt(-2 * z(7) + 500))
    PictureBox2.CreateGraphics.DrawLine(System.Drawing.Pens.Green,
CInt(2 * y(13) + 180), CInt(-2 * z(13) + 500), CInt(2 * y(14) + 180),
CInt(-2 * z(14) + 500))
    PictureBox2.CreateGraphics.DrawLine(System.Drawing.Pens.Pink,
CInt(2 * y(1) + 180), CInt(-2 * z(1) + 500), CInt(2 * y(7) + 180),
CInt(-2 * z(7) + 500))
    PictureBox2.CreateGraphics.DrawLine(System.Drawing.Pens.White,
CInt(2 * y(2) + 180), CInt(-2 * z(2) + 500), CInt(2 * y(8) + 180),
CInt(-2 * z(8) + 500))

PictureBox2.CreateGraphics.DrawLine(System.Drawing.Pens.Purple, CInt(2
```



```
* y(3) + 180), CInt(-2 * z(3) + 500), CInt(2 * y(9) + 180), CInt(-2 *
z(9) + 500))
    PictureBox2.CreateGraphics.DrawLine(System.Drawing.Pens.Black,
CInt(2 * y(4) + 180), CInt(-2 * z(4) + 500), CInt(2 * y(10) + 180),
CInt(-2 * z(10) + 500))
    PictureBox2.CreateGraphics.DrawLine(System.Drawing.Pens.Blue,
CInt(2 * y(6) + 180), CInt(-2 * z(6) + 500), CInt(2 * y(12) + 180),
CInt(-2 * z(12) + 500))

PictureBox2.CreateGraphics.DrawLine(System.Drawing.Pens.Orange, CInt(2
* y(5) + 180), CInt(-2 * z(5) + 500), CInt(2 * y(11) + 180), CInt(-2 *
z(11) + 500))

PictureBox3.CreateGraphics.Clear(System.Drawing.Color.LightBlue)

PictureBox3.CreateGraphics.DrawLine(System.Drawing.Pens.Yellow, CInt(2
* x(1) + 200), CInt(-2 * z(1) + 500), CInt(2 * x(2) + 200), CInt(-2 *
z(2) + 500))

PictureBox3.CreateGraphics.DrawLine(System.Drawing.Pens.Yellow, CInt(2
* x(2) + 200), CInt(-2 * z(2) + 500), CInt(2 * x(3) + 200), CInt(-2 *
z(3) + 500))

PictureBox3.CreateGraphics.DrawLine(System.Drawing.Pens.Yellow, CInt(2
* x(3) + 200), CInt(-2 * z(3) + 500), CInt(2 * x(4) + 200), CInt(-2 *
z(4) + 500))

PictureBox3.CreateGraphics.DrawLine(System.Drawing.Pens.Yellow, CInt(2
* x(4) + 200), CInt(-2 * z(4) + 500), CInt(2 * x(5) + 200), CInt(-2 *
z(5) + 500))

PictureBox3.CreateGraphics.DrawLine(System.Drawing.Pens.Yellow, CInt(2
* x(5) + 200), CInt(-2 * z(5) + 500), CInt(2 * x(6) + 200), CInt(-2 *
z(6) + 500))

PictureBox3.CreateGraphics.DrawLine(System.Drawing.Pens.Yellow, CInt(2
* x(6) + 200), CInt(-2 * z(6) + 500), CInt(2 * x(1) + 200), CInt(-2 *
z(1) + 500))
    PictureBox3.CreateGraphics.DrawLine(System.Drawing.Pens.Green,
CInt(2 * x(7) + 200), CInt(-2 * z(7) + 500), CInt(2 * x(8) + 200),
CInt(-2 * z(8) + 500))
    PictureBox3.CreateGraphics.DrawLine(System.Drawing.Pens.Green,
CInt(2 * x(8) + 200), CInt(-2 * z(8) + 500), CInt(2 * x(9) + 200),
CInt(-2 * z(9) + 500))
    PictureBox3.CreateGraphics.DrawLine(System.Drawing.Pens.Green,
CInt(2 * x(9) + 200), CInt(-2 * z(9) + 500), CInt(2 * x(10) + 200),
CInt(-2 * z(10) + 500))
    PictureBox3.CreateGraphics.DrawLine(System.Drawing.Pens.Green,
CInt(2 * x(10) + 200), CInt(-2 * z(10) + 500), CInt(2 * x(11) + 200),
CInt(-2 * z(11) + 500))
    PictureBox3.CreateGraphics.DrawLine(System.Drawing.Pens.Green,
CInt(2 * x(11) + 200), CInt(-2 * z(11) + 500), CInt(2 * x(12) + 200),
CInt(-2 * z(12) + 500))
    PictureBox3.CreateGraphics.DrawLine(System.Drawing.Pens.Green,
CInt(2 * x(12) + 200), CInt(-2 * z(12) + 500), CInt(2 * x(7) + 200),
CInt(-2 * z(7) + 500))
```

```
        PictureBox3.CreateGraphics.DrawLine(System.Drawing.Pens.Green,
CInt(2 * x(13) + 200), CInt(-2 * z(13) + 500), CInt(2 * x(14) + 200),
CInt(-2 * z(14) + 500))
        PictureBox3.CreateGraphics.DrawLine(System.Drawing.Pens.Pink,
CInt(2 * x(1) + 200), CInt(-2 * z(1) + 500), CInt(2 * x(8) + 200),
CInt(-2 * z(8) + 500))
        PictureBox3.CreateGraphics.DrawLine(System.Drawing.Pens.White,
CInt(2 * x(2) + 200), CInt(-2 * z(2) + 500), CInt(2 * x(9) + 200),
CInt(-2 * z(9) + 500))

PictureBox3.CreateGraphics.DrawLine(System.Drawing.Pens.Purple, CInt(2
* x(3) + 200), CInt(-2 * z(3) + 500), CInt(2 * x(10) + 200), CInt(-2 *
z(10) + 500))
        PictureBox3.CreateGraphics.DrawLine(System.Drawing.Pens.Black,
CInt(2 * x(4) + 200), CInt(-2 * z(4) + 500), CInt(2 * x(11) + 200),
CInt(-2 * z(11) + 500))
        PictureBox3.CreateGraphics.DrawLine(System.Drawing.Pens.Blue,
CInt(2 * x(6) + 200), CInt(-2 * z(6) + 500), CInt(2 * x(12) + 200),
CInt(-2 * z(12) + 500))

PictureBox3.CreateGraphics.DrawLine(System.Drawing.Pens.Orange, CInt(2
* x(5) + 200), CInt(-2 * z(5) + 500), CInt(2 * x(11) + 200), CInt(-2 *
z(11) + 500))
        ExportRegion6Data()
    End Sub
```